

eScholarship@UMassChan

Acute Modulation of Endothelial Cell Glucose Transport: A Dissertation

Item Type	Doctoral Dissertation
Authors	Cura, Anthony J.
DOI	10.13028/jgzc-7722
Publisher	University of Massachusetts Medical School
Rights	Copyright is held by the author, with all rights reserved.
Download date	2026-03-07 18:00:14
Link to Item	https://hdl.handle.net/20.500.14038/31843

Acute Modulation of Endothelial Cell Glucose Transport

A Dissertation Presented

By

Anthony J. Cura

Submitted to the Faculty of the
University of Massachusetts Graduate School of Biomedical Sciences, Worcester
in partial fulfillment of the requirements for the degree of

DOCTOR OF PHILOSOPHY

October 15, 2010

Biochemistry and Molecular Pharmacology

ACUTE MODULATION OF ENDOTHELIAL CELL GLUCOSE TRANSPORT

A Dissertation Presented

By

Anthony J. Cura

The signatures of the Dissertation Defense Committee signifies completion and approval as to style and content of the Dissertation

Dr. Anthony Carruthers, Thesis Advisor

Dr. Silvia Corvera, Member of Committee

Dr. Ian Simpson, Member of Committee

Dr. William Kobertz, Member of Committee

The signature of the Chair of the Committee signifies that the written dissertation meets the requirements of the Dissertation Committee

Dr. Reid Gilmore, Chair of Committee

The signature of the Dean of the Graduate School of Biomedical Sciences signifies that the student has met all graduation requirements of the school.

Anthony Carruthers, Ph.D.,
Dean of the Graduate School of Biomedical Sciences

Biochemistry and Molecular Pharmacology

October 15, 2010

This work is dedicated to my family: my dad Joe, my mom Marie, my sisters Lisa and Gina, my brother-in-law Tim, and my grandmother Mary Nicosia, as well as to the memory of Mario Nicosia. None of this would have been possible without your love and support and I love you all very much.

COPYRIGHT NOTICE

Parts of this dissertation have appeared in the following:

Cura, A. J. and Carruthers, A. (2010) Acute modulation of sugar transport in brain capillary endothelial cell cultures during activation of the metabolic stress pathway. *J Biol Chem*, 285 (20), 15430-9

Cura, A. J. and Carruthers, A. (2010) AMP kinase regulation of sugar transport in brain capillary endothelial cells during acute metabolic stress. *J Biol Chem*, (*submitted*)

ACKNOWLEDGEMENTS

I would like to first and foremost thank Dr. Anthony Carruthers, my mentor, for allowing and encouraging me the freedom to develop my own project that was off the beaten path tread by our lab. His patience, insight, support, and excitement for the work even when things weren't working so well made the production of this thesis possible, and I can say I've learned a lot from him over the years. I would also like to thank Dr. Reid Gilmore, Dr. William Kobertz, and Dr. Silvia Corvera, my thesis committee, for providing much appreciated guidance and support throughout the course of my project. Their suggestions and comments really helped drive and shape this work into something cohesive. I would also like to thank Dr. Ian Simpson for taking time out of his schedule to sit on my dissertation committee.

I need to thank Dr. Otto Gildemeister and Dr. Elisabet Mandon for their input and aid from the time I went through my qualifying exam until now. Their friendly support and willingness to offer suggestions and help has been very much appreciated over the years. I would like to acknowledge Jennifer Broderick for her technical assistance with the luminometer, which made ATP measurements much easier to do. I would also like to thank Elizabeth Hoyt, Annette Stratton, Denise Silva, Tiffanie Covello, and Karen Welch for always being willing to help with scheduling meetings, booking rooms, managing lab finances, and helping me coordinate ordering to make sure I had everything I needed to do my research.

I must thank my friends Joe, Mandy, Phil, Martine, Carla, Gayle, Conor, and Laura for supporting my move from industry to grad school and keeping me grounded and as sane as possible over the years. Their support has made even the toughest times bearable. To my friends Sabrina, Jay, and Siobhan I also give my heartfelt thanks. Not only have they taught me a lot scientifically (like qPCR), but they have made daily lab life unbelievably fun while keeping the crazy at bay. I wish each of them the best of luck as they continue towards their degrees.

Finally, I must once again thank my family for their overwhelming support and encouragement during the transition from having a job to being a student. My parents Joe and Marie have supported me in all possible aspects over the years, and my sisters Lisa and Gina and brother-in-law Tim have been a source of great strength throughout graduate school, I am forever indebted to them. My grandmother Mary has been an inspiration and guiding force in all areas of my life, and I am ever grateful to her for her support.

ABSTRACT

Studies have demonstrated that under conditions of chronic metabolic stress, GLUT1-mediated sugar transport is upregulated at the blood-brain barrier by a number of mechanisms. Although acute metabolic stress has also been shown to increase GLUT1-mediated transport, the mechanisms underlying this regulation remain unclear. This work attempts to explain how GLUT1-mediated sugar uptake is increased during acute metabolic stress, as well as explore the factors involved in this modulation of sugar transport in blood-brain barrier endothelial cells. Glucose depletion, KCN and FCCP were applied to brain microvascular endothelial cell line bEnd.3 in order to induce acute metabolic stress by ATP depletion. Kinetic sugar uptake measurements in combination with qPCR, whole cell lysate western blots, and cell-surface biotinylation were employed to probe for changes in GLUT1-mediated sugar uptake, GLUT1 expression levels, and GLUT1 localization during metabolic stress. Finally, the role of AMP-activated kinase (AMPK) in the bEnd.3 cell response to acute stress was examined using the specific AMPK activator AICAR and inhibitor Compound C.

The data presented in this thesis supports the following two conclusions: 1. GLUT1-mediated sugar transport in bEnd.3 cells during acute metabolic stress is increased 3-7 fold due to translocation of intracellular GLUT1 to the plasma membrane, with no change in expression of total GLUT1 protein, and 2. AMPK plays a direct role in modulating increases in GLUT1-mediated sugar transport in bEnd.3 cells during acute metabolic stress by regulating trafficking of GLUT1 to the plasma membrane

TABLE OF CONTENTS

COPYRIGHT NOTICE	iii
ACKNOWLEDGEMENTS	iv
ABSTRACT	vi
TABLE OF CONTENTS	vii
List of Figures	ix
List of Tables	x
List of Abbreviations	xi
CHAPTER I	1
INTRODUCTION AND LITERATURE REVIEW	1
The Brain	1
Brain Metabolism	1
The Blood-Brain Barrier	3
Facilitative Transporters	4
The GLUT Family of Facilitative Transporters	6
Class 1 Glucose Transporters	8
Class 2 Glucose Transporters	12
Class 3 Glucose Transporters	14
GLUT1 Structural Characteristics	17
GLUT1 Secondary Structure	19
GLUT1 Tertiary Structure	20
GLUT1 Quaternary Structure	20
GLUT1-Mediated Transport	22
Kinetics of GLUT1 Transport: The Simple Carrier	23
Kinetics of GLUT1 Transport: The Fixed Site Carrier	25
ATP and GLUT1 Transport	28
Other Suppressors of GLUT1-Mediated Transport	30
GLUT1 Transport Upregulation by Signaling Molecules	31
GLUT1 and Cancer	32
GLUT1 Regulation and Metabolic Stress	33
GLUT1-Mediated Transport at the Blood-Brain Barrier	34

GLUT1 Deficiency Syndrome: Blood-Brain Barrier Transport Dysfunction	35
Blood-Brain Barrier Transport and Metabolic Stress	36
Remaining Questions	37
CHAPTER II.....	39
EVALUATION OF THE BRAIN MICROVASCULAR ENDOTHELIAL CELL LINE bEnd.3 AS A MODEL SYSTEM FOR BLOOD-BRAIN BARRIER GLUCOSE TRANSPORT STUDIES	39
Abstract.....	39
Introduction.....	40
Experimental Procedures	43
Results.....	50
Discussion.....	65
CHAPTER III	70
ACUTE MODULATION OF SUGAR TRANSPORT IN BRAIN CAPILLARY ENDOTHELIAL CELL CULTURES DURING ACTIVATION OF THE METABOLIC STRESS PATHWAY	70
Abstract.....	70
Introduction.....	71
Experimental Procedures	73
Results.....	79
Discussion.....	92
CHAPTER IV	100
AMP KINASE REGULATION OF SUGAR TRANSPORT IN BRAIN CAPILLARY ENDOTHELIAL CELLS DURING ACUTE METABOLIC STRESS	100
Abstract.....	100
Introduction.....	101
Experimental Procedures	102
Results.....	105
Discussion.....	117
CHAPTER V	122
CONCLUSIONS AND FUTURE DIRECTIONS.....	122
BBLIOGRAPHY	132

List of Figures

Figure 1.1: Structural Homology of GLUT Proteins	9
Figure 1.2: Putative Topology of GLUT1	18
Figure 1.3: The Simple Carrier	24
Figure 1.4: The Modified Fixed Site Carrier	27
Figure 2.1: Sequence Alignment of Human and Mouse GLUT1	51
Figure 2.2: Western blot of bEnd.3 Cells.....	54
Figure 2.3: RT-PCR Screen for GLUT Family Members	55
Figure 2.4: Time Course of 2-DOG Uptake	58
Figure 2.5: bEnd.3 Zero-Trans 2-DOG and 3-OMG Uptake.....	60
Figure 2.6: 2-DOG Dose Response to 3-OMG.....	62
Figure 2.7: bend.3 Equilibrium Exchange Transport.....	62
Figure 2.8: Dose Response to CCB	64
Figure 3.1: ATP Depletion in bEnd.3 Cells.....	80
Figure 3.2: bEnd.3 Dose Dependent ATP Depletion.....	80
Figure 3.3: ATP Depletion and Recovery in bEnd.3 Cells.....	81
Figure 3.4: Sugar uptake at 4 °C in bEnd.3 cells.	83
Figure 3.5: Time Course of Recovery from KCN Poisoning.....	86
Figure 3.6: bEnd.3 Equilibrium Exchange Transport	86
Figure 3.7: Concentration Dependence of Transport Stimulation by Poison	88
Figure 3.8: RT-PCR of bEnd.3 Cells	89
Figure 3.9: Western Blot of bEnd3 Cells During Poisoning.....	91
Figure 3.10: Surface Biotinylation of bEnd.3 GLUT1	93
Figure 3.11: AMPK Phosphorylation During Metabolic Stress	94
Figure 4.1: Inhibition of AMPK Phosphorylation by Compound C.....	106
Figure 4.2: Inhibition of ACC Phosphorylation by Compound C	107
Figure 4.3: Inhibition of Stimulation of Sugar Uptake by Compound C.....	109
Figure 4.4: Inhibition of AMPK Phosphorylation During Stress	111
Figure 4.5: Inhibition of Metabolic Stress-Stimulated Transport	112
Figure 4.6: Inhibition of AMPK Induced GLUT1 Recruitment By Compound C	114
Figure 4.7: Inhibition of GLUT1 Recruitment Upon Glucose Depletion.....	115
Figure 4.8: Inhibition of KCN Recruitment of GLUT1 by Compound C	116

List of Tables

Table 1.1: Properties of GLUT Proteins.....	11
Table 2.1: Sequence Difference Between Human and Mouse GLUT1.....	52
Table 2.2: Summary of GLUT's Expressed in bEnd.3 Cells.....	56
Table 2.3: Summary of 2-DOG and 3-OMG Kinetics in bEnd.3 and Red Cells.....	62
Table 3.1: Summary of bEnd.3 3-OMG Transport.....	84

List of Abbreviations

2-DOG	2-deoxy-D-glucose
3-OMG	3-O-methyl-D-glucose
ADP	adenosine-5'-diphosphate
AICAR	aminoimidazole carboxamide ribonucleotide
AMP	adenosine-5'-monophosphate
AMPK	5'- adenosine-monophosphate-dependent kinase
ATP	adenosine-5'-triphosphate
BBB	blood-brain barrier
bEnd.3	murine brain microvascular endothelial cell line
CCB	cytochalasin B
DHA	dehydroascorbic acid
DPBS	Dulbecco's phosphate buffered saline
DTT	dithiothreitol
EDTA	ethylenediaminetetraacetic acid
FCCP	carbonyl cyanide 4-(trifluoromethoxy)phenylhydrazone
GLUT	major facilitator superfamily glucose transport protein
HEPES	(N-[2-Hydroxyethyl]piperazine-N'-[2-ethanesulfonic acid])
KCN	potassium cyanide
MFS	major facilitator superfamily
NaCl	sodium chloride
PNGase F	N-linked glycosidase F

qPCR	quantitative reverse-transcriptase polymerase chain reaction
RT-PCR	reverse transcriptase polymerase chain reaction
SDS-PAGE	sodium dodecyl sulfate-polyacrylamide gel electrophoresis
SLC2	solute-linked carrier protein 2
TBS	tris buffered saline
TBST	tris buffered saline containing 0.2% Tween 20
Tris-HCl	tris(hydroxymethyl)aminomethane hydrochloride
Tris Base	2-amino-2-(hydroxymethyl)-1,3-propanediol
ZMP	5-amino-1- β -D-ribofuranosylimidazole-4-carboxamide-5'-monophosphate

CHAPTER I

INTRODUCTION AND LITERATURE REVIEW

The Brain

In mammals, the brain is responsible for integrating and maintaining a variety of systemic processes that are required to sustain the life of the organism. Whether coordinating basic organ function, regulating hormone levels, integrating external stimuli, or executing higher order behavioral responses in order to promote survival (1-6), healthy brain function is essential in order to maintain system-wide bodily homeostasis in all living mammals. Although the majority of the details of exactly how the brain works remain elusive, modern research is making progress in uncovering how the brain operates and promotes its own survival. One of the most basic, yet most important requirements for proper brain function is a constant supply of energy. By attempting to understand how the brain is able to manage its energy needs, it may be possible to gain more insight into how different areas of the brain operate locally, as well as how the brain communicate with other systems on a global scale in order to maintain a healthy mammalian system.

Brain Metabolism

The brain primarily uses glucose as the preferred substrate for its energetic needs (7-10). It has been stated that although the brain only accounts for a small percentage of total body mass (approximately 2%), it requires 25% of the body's glucose supply in order to maintain function (11). Glucose consumption by the brain occurs in both neurons

and astrocytes, and appears to be a highly complex process (9,11,12). The supply of glucose from the blood is thought to barely meet the brain's demand for energy under normal conditions (13); therefore it is important that the brain be able to control not only its metabolism, but access to a steady supply of glucose. In fact, it has been shown that increased activity in the brain is often met with increased blood flow to the active area, presumably to ensure the supply of glucose is sufficient to support increased brain function (14-16).

Although originally it was thought that direct oxidative phosphorylation of glucose was the preferred means of generating energy in neurons and astrocytes (7,8), there have been a number of studies that have shown that this is not always the case. The presence of monocarboxylate transporters in brain cells is well documented (12,17), and studies show increased consumption of lactate is used for energy generation in both neurons and astrocytes (18-21). The picture of brain metabolism becomes more complex upon considering the proposal that release of neuronal glutamate increases lactate production by astrocyte glycolysis. This lactate is then exported and taken up by active neurons for energy production in a process called the astrocyte to neuron lactate shuttle (22). To even further complicate the issue, a conflicting model has also been proposed where neuronal lactate produced by both basal and stimulated metabolism is shuttled into astrocytes for energy consumption in a process named the neuron to astrocyte lactate shuttle (23).

While there is currently no consensus on the precise model of integrated brain metabolism, what is fundamentally clear is that glucose is the essential substrate of brain

energy production, regardless of which glycolytic products are favored by brain cells. Neurons contain no appreciable stores of glycogen, and astrocytes contain a limited amount of glycogen at any given time, certainly not enough to sustain long-term brain function. Therefore, a steady supply of glucose must be maintained at all times. In order for the brain to utilize glucose, it must have access to it from the circulating bloodstream. While most mammalian organ systems allow for free exchange of nutrients between blood and tissue, glucose destined for the brain must overcome a significant hurdle before utilization: the blood-brain barrier.

The Blood-Brain Barrier

The blood-brain barrier is a structure formed by endothelial cells that line the blood vessels throughout the majority of the brain (24). While endothelial cells are a key structural component of all blood vessels throughout the circulatory system, there are stark differences between endothelial cells comprising the blood-brain barrier (and other blood tissue barriers) and those of the peripheral circulatory system. First, blood-brain barrier endothelial cells contain significantly more mitochondria than peripheral endothelial cells (25). Second, it has also been shown that blood-brain barrier capillary walls are approximately 40% thinner than those of the peripheral endothelium (24). Finally, in most cases, the endothelium that lines the inside of blood vessels in the peripheral circulatory system is patterned with fenestrations, or gaps, between the interconnected cells. These fenestrations allow free diffusion of circulating nutrients between blood and surrounding tissues (26). However, the endothelial cells of the blood-brain barrier are joined together by tight junctions (27,28), thus denying most large,

charged, and polar molecules, such as proteins (29), ions (30-32), and sugars (33-35), free passage from the bloodstream into the brain.

While the structure of the blood-brain barrier protects the delicate neurons of the brain from damage from a variety of toxic agents and pathogens, it also imposes a major hurdle to delivery of essential nutrients to the brain that are required for proper function, especially its primary energetic substrate, glucose (7,8,10). Since glucose cannot freely diffuse into the brain at a rate sufficient to meet energy demand, its movement across the blood-brain barrier, as with other nutrients, requires specialized carrier proteins (33-38), which must be present on both the luminal (blood-facing) and abluminal (brain-facing) membranes of the endothelial cell in order to efficiently deliver substrate to brain cells. The primary carrier protein responsible for glucose uptake across the blood-brain barrier has been identified as the facilitative glucose transport protein SLC2A1, or GLUT1 (39).

Facilitative Transporters

Diffusion of molecules across the plasma membrane can be classified as either passive or active. Passive diffusion can be mediated by pores, channels, and carrier proteins (or transporters). Pores present simultaneous substrate binding sites on the inside and outside of the cell, and facilitate selective diffusion of molecules in a single-file motion through the protein down a concentration gradient. The water pore aquaporin is an example of a pore protein (40). Channels mediate the selective passage of ions across the plasma membrane down their electrochemical gradient. Unlike pores, channels are regulated by a number of factors such as membrane potential, ion concentration, and second messenger

molecules. Channels are often gated by a C-terminal portion of the protein which allows for the blocking of the channel once a certain threshold is reached. An example of this phenomenon is seen in voltage gated Kv K⁺ channels, which are responsible for modulating muscle contractions, especially in the heart (41). Neither pores nor channels require the direct use of energy to mediate substrate transport. The free energy driving net transport comes from the electrochemical gradient of the transported substrate.

Carrier proteins differ from pores and channels in a number of ways. First, carriers have been proposed to present a single substrate binding site on one side of the plasma membrane at a time, not simultaneously at both sides of the membrane like pores and channels (42,43). Second, upon binding substrate, carrier proteins undergo a conformational change which translocates substrate through the protein and across the plasma membrane, whereas pores and channels remain relatively fixed in the membrane (42). Finally, carriers can facilitate either passive or active transport of molecules, while pores and channels are strictly passive transport proteins. Passive carriers such as GLUT1 demonstrate selectivity of substrate like pores and channels, and move molecules down their concentration gradient without energy expenditure (42). Active carriers fall into one of two categories, primary and secondary. Primary active carriers require ATP hydrolysis to induce a conformational change in the protein and allow transport a substrate against its concentration gradient. A good example of an active carrier is the Na⁺K⁺ATPase, which requires ATP to pump three sodium molecules out of the cell, at the same time importing two potassium molecules (44). Secondary active carriers do not require ATP hydrolysis, and can be divided into two sub-groups: antiporters and

symporters. Antiporters catalyze active transport by exchanging one molecule down its concentration gradient for another against its concentration gradient via conformational change of the protein. The NCX sodium calcium exchanger proteins, which import three sodium ions for every calcium ion exported out of the cell, are classic antiporters (45). Symporters catalyze the co-transport of two molecules in the same direction by using the energy of an electrochemical gradient of one of the molecules to drive the transport of another molecule against its concentration gradient. An example of a symport protein is the SGLT family of glucose transporters, which mediate glucose reabsorption in the kidney by using the energy of transporting sodium down its concentration gradient to co-transport and take up glucose into the cell, where concentrations are high (46).

In order to understand the mechanisms of carrier mediated transport, it is important to examine some of the structural characteristics that define each class of proteins. The human facilitative glucose transport family of proteins contains fourteen members, each of which differs slightly in structure and function. However, there are key structural similarities between the members that help define the family and give some insight into the functional role each carrier plays in the body.

The GLUT Family of Facilitative Transporters

GLUT1 is a member of the major facilitator superfamily (MFS) of carrier proteins, one of the largest membrane protein families found in living organisms (47,48). The MFS superfamily currently consists of 29 established families of transport proteins, including sugar, ion, and drug transporters, hexose proton symporters, and sugar ion symporters

found ubiquitously in all species including bacteria, plants, and mammals (49). To date, only three of the over 5,000 MFS superfamily members have been crystallized: the glycerol-3-phosphate transporter GlpT (50), the lactose permease LacY (51), and the multi-drug transporter EmrD (52), all from *Escherichia coli*. In addition, the structure of the oxalate-formate exchange protein OxIT from *Oxalobacter formigenes* has been visualized by cryo-electron microscopy, but not crystallized (53). While these proteins may provide some general structural insights into the organization of MFS superfamily proteins, the lack of sequence identity between members makes drawing sweeping conclusions about structure difficult. As a result, many of the properties of protein structure, function, and substrate binding for the majority of MFS members have yet to be elucidated. A subset of the MFS superfamily, the facilitative sugar transporter (or GLUT) family of proteins, currently contains 14 identified members in mammals, all members of the SLC2A (Solute Linked Carrier 2A) gene family: GLUT1-GLUT12, GLUT14, and HMIT (GLUT13) (54-56). The GLUT proteins share between 25-68% amino acid sequence identity with one another (54,57), and also share several signature structural and functional features. To date, none of the GLUT proteins have been visualized three-dimensionally by crystallography, although GLUT1 and GLUT3 virtual structures have been predicted using homology modeling (58,59).

GLUT proteins contain 12 hydrophobic transmembrane (TM) spanning α -helical domains threaded together by hydrophilic loops of varying length, with a large intracellular loop between TM domains 6 and 7 of the protein (54,57). There is also a highly conserved 5 amino acid motif, RXGRR/K, which is located in the loop between

TM domains 2 and 3 and duplicated in the loop between TM's 8 and 9 (54,57). This sequence is found not just in the GLUTs, but in the majority of MFS superfamily proteins as well (60,61), and is thought to aid in determining proper membrane topology (62). In addition, there are certain sugar transport signatures that are commonly found in all GLUTs that are thought to be essential for substrate and inhibitor selectivity and sensitivity. Among them are a PMY domain in TM 4, a PESPRY/FLL domain in the large intracellular loop 6, a QQLSGIN domain in TM7 thought to aid in glucose binding, a GXXXXP motif in TM10 which potentially determines inhibitor and substrate binding, a single W in TM 11 which has been shown to be critical for transporter function in GLUT1, and a VPETKG in the C-terminus of the protein (Figure 1.1) (63). GLUT proteins also feature N- and C-termini that are intracellular, and a single glycosylation site on the exofacial side of the protein, either in the loop between TMs 1 and 2, or 9 and 10 (54,57). The GLUT family can be sub-divided into three classes based on substrate transport and structural variations, and some of their key features are summarized in Table 1.1.

Class 1 Glucose Transporters

The class 1 transporters, GLUT1-4 and GLUT14, are the most well characterized of the group, since (with the exception of GLUT14) they were discovered relatively early and have been studied extensively. Loop 1-2 of class 1 GLUTs is longer than the other five extracellular loops, and contains a single N-linked glycosylation site; and they also share a QL motif in TM5, and a STSIF motif found in extracellular loop 7-8 (57). In addition, there is a tryptophan after the GXXXXP motif in class 1 GLUTs that is thought

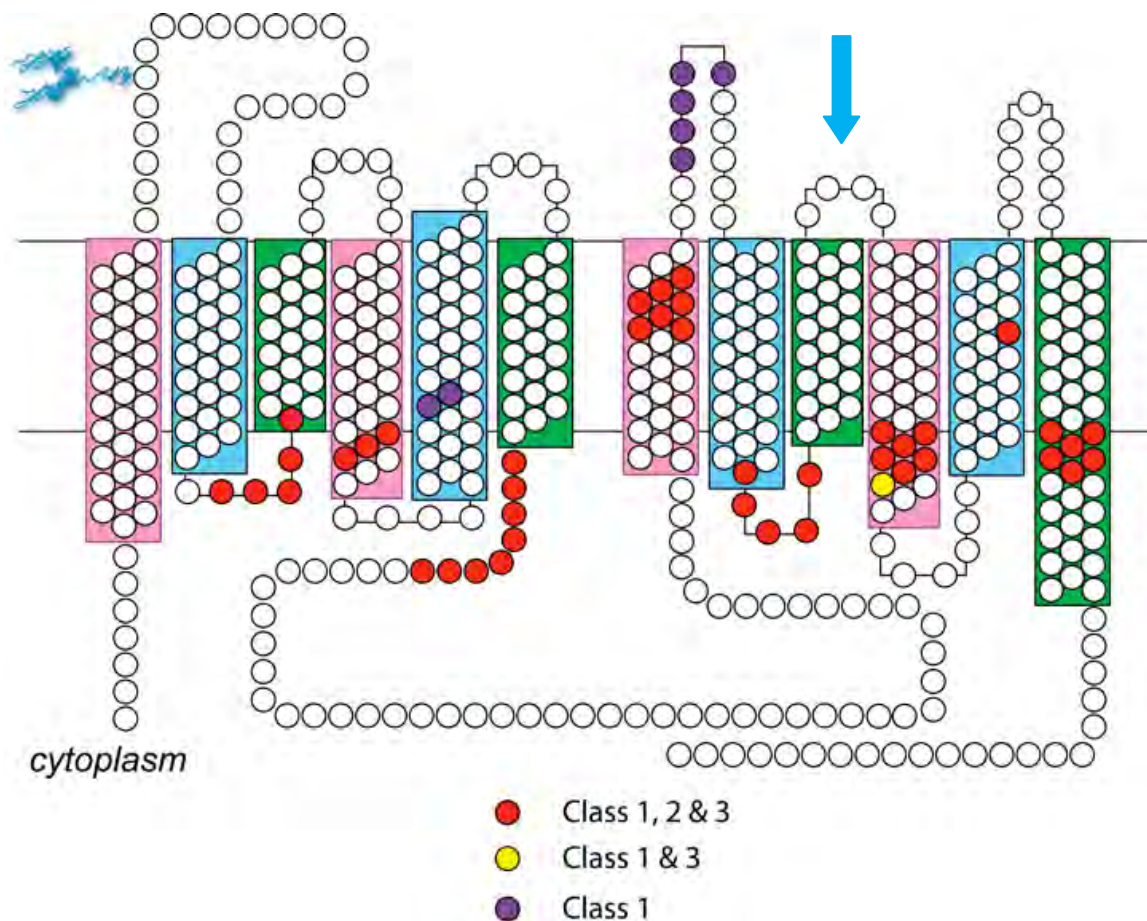


Figure 1.1: Structural Homology of GLUT Proteins

Representative schematic of the generic GLUT family structure. Circles in red represent the structural motifs and residues present in all GLUTs: RXGRR (loop 2 and 8), PMY (TM4), PESPRY/FLL (loop 6), QQLSGIN (TM7), GXXXXP (TM10), W (TM11), and VPETKG (C-terminus). Circles in yellow represent residues found in class 1 and 3 GLUTs: W (TM10). Circles in purple represent motifs found in class 1 GLUTs only: QL (TM5), STSIF (loop 7). Blue arrow represents the N-linked glycosylation site for Class 3 GLUTs at loop 9, which is longer than in Class 1 and 2 GLUT proteins.

to confer substrate specificity as well as sensitivity to the competitive inhibitor cytochalasin B (57,64-66). Class 1 GLUT's are typically glucose transporters, though GLUT1, GLUT3, and GLUT4 are also able to transport dehydroascorbic acid (DHA), an oxidized form of vitamin C (67-69). With the exception of GLUT1, GLUT proteins demonstrate highly tissue-specific expression patterns. GLUT1, the first of the GLUT proteins to be cloned, was originally isolated from liver HepG2 cells (70), but has since been shown to be expressed ubiquitously throughout the body, with highest expression levels in erythrocytes, cardiac muscle cells, blood-tissue barrier cells, astrocytes, and in developing embryos (71-73). GLUT1 has often been termed a high-affinity glucose transporter and serves to maintain basal glucose uptake throughout the body, but is critical for blood-brain barrier glucose uptake (34,38,74,75). The properties of GLUT1-mediated transport will be described in greater detail in this introduction. GLUT2 expression is localized to pancreatic β -cells, the liver, the hepatic portal vein, intestine, and kidney (76). Of the class 1 GLUTs, GLUT2 has the lowest reported affinity for glucose and cytochalasin B; and it has been shown to transport fructose, but not dehydroascorbic acid (65,66). Originally, GLUT2's low affinity for glucose was thought to allow it to function as a high capacity transporter, but it has been shown that high expression and catalytic turnover are more important factors (77). However, in the context of where it is expressed, GLUT2 is thought to act as a glucose sensor protein in the intestine, liver and pancreas (66). GLUT3 is a glucose transporter primarily found in neurons, making it the major transporter responsible for neuronal glucose uptake, but is also expressed in white blood cells, pre-implantation embryos, the

Name	Class	Primary Substrates	CCB Sensitive?	Tissue Distribution
GLUT 1	1	Glucose, DHA	Yes	Ubiquitous expression in human/murine tissue, mostly red cells, endothelial cells, astrocytes
GLUT 2	1	Glucose, Fructose	Yes	Liver, pancreas (b-cells), but also in kidney and small intestine absorptive cells
GLUT 3	1	Glucose, DHA	Yes	Neurons, also in sperm, embryo, white blood cells, and carcinomas
GLUT 4	1	Glucose, DHA	Yes	Fat and skeletal muscle, insulin responsive
GLUT 5	2	Fructose	No	Intestine, testis, and kidney, also in skeletal muscle, fat cells, and brain
GLUT 6	3	Glucose*	Yes	Brain cells and spleen cells
GLUT 7	2	Glucose,* Fructose,*	No	Small intestine and colon (apical membranes)
GLUT 8	3	Glucose, Fructose**	Yes	Testis, brain, fat, liver, and spleen
GLUT 9	2	Urate, Glucose, Fructose	No	Kidney and liver, but also in the placenta, lung, small intestine
GLUT 10	3	Glucose	Yes	Heart, lung, brain, liver, skeletal muscle, pancreas, placenta and kidney"
GLUT 11	2	Glucose, Fructose	Yes	Heart (A, C) skeletal muscle (A, C), kidney (A, B), adipose tissue (B, C), placenta (B), pancreas (C)
GLUT 12	3	Glucose, Fructose	Yes	Heart, skeletal muscle, brown adipose tissue, prostate
GLUT 14	1	Glucose**, DHA**	Yes**	Testis
HMIT	3	H ⁺ myoinositol	No	Brain

Table 1.1: Properties of GLUT Proteins

* indicates substrates tested may not be primary substrate, more data needed

** indicates unconfirmed substrate transport/affinity, no data available

testes, spermatozoa, and some carcinomas (64,78). Like GLUT1, GLUT3 has been shown to transport DHA, thus allowing neurons to potentially take up and metabolize vitamin C (67,68) in addition to mannose, xylose, and galactose (78). The presence of both GLUT3 and GLUT1 in the brain are critical for maintaining proper glucose uptake, and therefore energy supply in the brain. GLUT4, the insulin-sensitive glucose transporter, is expressed mostly in cardiac and skeletal muscle, as well as adipocytes (79). Unlike the other class 1 GLUT proteins, GLUT4 is targeted primarily to specialized intracellular pools under non-insulin stimulated conditions due to the presence of an FQQ motif in the N-terminus and both a dileucine motif and an endosomal targeting TELEYLGP in the C-terminus (80). Exposure to insulin causes massive increases in GLUT4 at the plasma membrane, allowing it to act as a key modulator of blood glucose levels in the body. GLUT4 can also transport DHA in addition to glucose (68) and works in concert with GLUT2 to modulate glucose homeostasis in the blood. GLUT14, the most recently cloned class 1 transporter, is thought to be a gene duplication of GLUT3, since it shares 95% sequence identity to the protein (55). Unlike GLUT3, GLUT14 is only expressed in the testes. Although the characterization of GLUT14 is not complete, it can be assumed that it is both a glucose and DHA transporter like GLUT3, with similar transport characteristics.

Class 2 Glucose Transporters

Unlike class 1 GLUTs, the class 2 transporters (GLUT5, GLUT7, GLUT9, and GLUT11) are primarily fructose transporters, although they have been shown to transport glucose as well as other substrates, such as uric acid (81-85). Another notable difference

that distinguishes class 2 GLUTs is the absence of the tryptophan residue the GXXXXP motif in TM10 (57). This lack of tryptophan renders class 2 GLUTs insensitive to cytochalasin B and aids in selectivity for fructose as opposed to glucose (57). Like their class 1 counterparts, tissue-specific expression is a hallmark of class 2 GLUT proteins. GLUT5 was the first of the class 2 GLUTs to be discovered, and is the major fructose transporter in the intestines, kidney, and spermatozoa, though it has also been shown to be expressed at the blood-brain barrier, in skeletal muscle, and in fat (82,86,87). GLUT7 is expressed mainly in the colon and small intestine, but may also be found in the testes and prostate (83). It is possible that GLUT7's role is to transport a different substrate besides sugars, but as of yet, such a substrate has not been found. GLUT7 is also hypothesized to aid in the uptake of fructose and glucose in the gut when sugar levels are low (87). GLUT9 is expressed primarily in liver, kidney, and developing embryo, but is also found to be expressed in the heart, lung, and leukocytes (81,88). GLUT9 contains a dileucine motif in the N-terminus, but the motif does not sequester GLUT9 to intracellular pools, unlike most other GLUT family members (81). Interestingly, GLUT9 exists as two splice variants, dubbed GLUT9a and GLUT9b, that demonstrate differential localization in the proximal tubules of the kidney, with GLUT9a localizing to the basolateral membrane, and GLUT9b localizing to the apical membrane (81,89). Studies show that GLUT9 appears to play an important role in mediating glucose uptake in the very early stages of embryonic development (88). However, the main role for GLUT9 appears to be urate transport as evidenced by genetic and functional studies (89-91). Kinetic analysis indicates that GLUT9-mediated urate transport is stimulated by the

presence of glucose and fructose on the opposite side of the membrane, suggesting that GLUT9 plays a role in sugar reabsorption from the urine as well as urate clearance from the bloodstream (92). The final member of the class 2 glucose transporters, GLUT11, exists as three known splice variants, two of which have different expression patterns. The full length form (GLUT11L) is expressed in the brain, lung, leukocytes, small intestine, placenta, and liver (93), while the shorter form GLUT11S is expressed almost exclusively in the heart and muscle (84). The third splice variant encodes a severely truncated version of the protein that has yet to be characterized (93). Both the long and short forms of GLUT11 have been shown to transport glucose and fructose; and unlike the other class 2 GLUTs, GLUT11 shows a low affinity for cytochalasin B (84,93). The true role GLUT11 plays in physiology still remains to be determined.

Class 3 Glucose Transporters

The class 3 GLUTs comprise GLUT6, GLUT8, GLUT10, GLUT12, and HMIT and are the least characterized of the GLUT proteins to date. Structurally, this class of proteins has some notable differences from the other two classes. Most strikingly, class 3 GLUT proteins contain a single glycosylation site on loop 9-10 of the protein, as opposed to loop 1-2 for classes 1 and 2. Also, all class 3 GLUTs contain signal sequence motifs in either the N- or C-terminus of the protein which direct the protein to intracellular compartments rather than directly to the plasma membrane (57). However, despite these differences, class 3 GLUT proteins appear to contain the conserved tryptophan after the GXXXXP motif in TM 10 like class 1 transporters, as well as demonstrate tissue-specific expression like the other GLUT proteins. GLUT6, the first family member identified but

the second cloned, appears to be prevalent in the brain, spleen and leukocytes; and preliminary analysis shows transport activity for glucose and sensitivity to cytochalasin B, with low affinity for both (94). GLUT6 also contains a dileucine motif in the N-terminus which sequesters it to intracellular pools; and to date, stimulation by a number of factors such as insulin, phorbol esters, and osmotic shock does not significantly recruit it to the plasma membrane (95). It would appear the true physiological role GLUT6 plays has yet to be determined. GLUT8, which was the first of the class 3 transporters to be cloned, is predominantly expressed in the brain, testes, liver, spleen, adipose, and lung, and may also be expressed in muscle, heart, and kidney (96). GLUT8 is a high-affinity glucose transporter that is inhibitable by cytochalasin b, but is also shown to be inhibited by fructose and galactose, which indicates both sugars as potential substrates for the transporter (96,97). Like GLUT6, GLUT8 contains a dileucine motif in the N-terminus of the protein that localizes it to intracellular stores. In blastocysts, GLUT8 has been shown to translocate to the plasma membrane in response to insulin, since GLUT4 is absent at this stage of development (98). Interestingly, in fully developed mammals, GLUT8 recruitment to the plasma membrane has not been seen, even in the presence of insulin and a number of known recruitment stimulants (95,99,100). While the function of GLUT8 still requires further study, it is thought that GLUT8 acts as an intracellular glucose transporter responsible for moving glucose between organelles (99). GLUT10 expression is localized to the heart, lung, brain, placenta, liver, kidney, pancreas, and skeletal muscle (101). Although initial characterization shows GLUT10 to be a high-affinity glucose transporter that is sensitive to cytochalasin B, but not fructose (102), the

exact role of GLUT10 in mammals is unclear. It has been hypothesized, based on recent studies, that GLUT10 plays a role in vascular changes occurring in Type 2 diabetes, since mutations in the GLUT10 gene alter angiogenesis and cause arterial tortuosity syndrome (103). However, the role GLUT10 plays in both vascularization and diabetes requires more study. GLUT12 is localized to the heart, muscle, brain, placenta, pancreas, kidney, and adipose tissue (104,105). It has been shown to localize to intracellular stores, and has similar targeting motifs to the other class 3 GLUTs, as well as GLUT4 (104,105).

GLUT12 is responsive to insulin, and translocates to the plasma membrane upon insulin stimulation as well as during hyperglycemia (106,107). GLUT12 has been identified as a glucose, fructose, and galactose transporter that is sensitive to cytochalasin b (104), and it is hypothesized to compensate for insulin-sensitive glucose transport when GLUT4 is knocked out in mice (108). The full role GLUT12 plays in Type 2 diabetes and insulin-regulated glucose uptake, as well as its substrate preference remain to be seen. The last member of the class 3 GLUTs, HMIT or GLUT13, is a H⁺-myoinositol symporter, a secondary active carrier that shows no transport capability for hexoses even though it retains many signatures of glucose transport in its structure. While it is able to transport myoinositol on its own, the presence of protons increases its rate of transport. HMIT is expressed in the brain, predominantly in astrocytes, but may also be expressed in neurons, adipose and kidney. HMIT is localized to intracellular stores, but translocates to the plasma membrane upon membrane depolarization and may play an important role in brain myoinositol metabolism, but the physiological role it plays requires further characterization (109).

While the GLUT family of proteins is diverse, tissue specific, and varied in function, the primary focus of our studies revolves around the class 1 transporter GLUT1 and its role in modulating glucose uptake across the blood-brain barrier. In order to understand how GLUT1 mediates transport in blood-brain barrier endothelial cells, it is important to understand GLUT1 structure and the characteristics of sugar uptake it exhibits.

GLUT1 Structural Characteristics

GLUT1 is a 492 amino acid protein with a calculated molecular weight of 54,117 Daltons. The sequence NQT at amino acids 45-47 in exofacial loop 1 comprises the single N-linked glycosylation sequence found in GLUT1 (Figure 1.1). It has been shown that glycosylation of GLUT1 is heterogeneous, causing the protein to run as a smeared band from 45-65 kDa when visualized by SDS-PAGE or Western blot (110); and that this smeared band collapses to a single band of approximately 38 kDa upon deglycosylation (111). In addition, unlike some of the other GLUT proteins, deglycosylation of GLUT1 causes a 50% decrease in sugar uptake and a 2.5-fold decrease in affinity for glucose, though targeting to the plasma membrane remains unaffected (111). These data seems to suggest that the glycan plays a role in maintaining GLUT1 structure, and its affinity for substrate. The sequence GRRTLHLIGLAG, which corresponds to amino acids 332-343 in loop 8 and TM9 of GLUT1, is a Walker B nucleotide-binding domain(112-114). GLUT1 has been shown to bind ATP, which plays

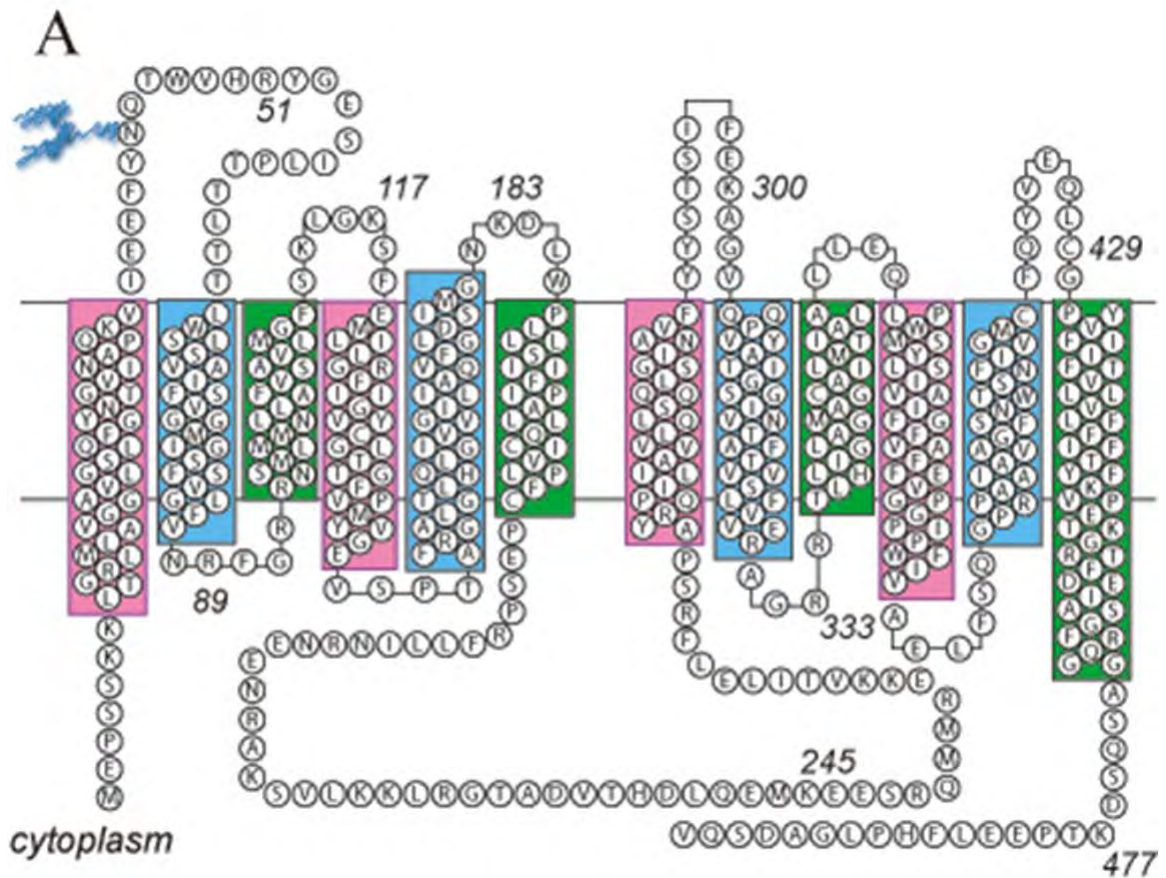


Figure 1.2: Putative Topology of GLUT1

Representative schematic of human GLUT1 topology showing purported transmembrane spanning domains (TMs), loops, and intracellular N- and C-termini. Horizontal parallel lines represent the plasma membrane, colored boxes represent potential symmetry of the TMs, and blue graphic at Asn 45 represents the glycan.

an important role in regulation of transport (115-117). The truncation of the last 37 amino acids of GLUT1's C-terminus has also been shown to ablate transport activity and lock GLUT1 into an inward facing conformation that cannot bind substrate. However, GLUT1 trafficking to the plasma membrane remains unaffected, indicating that this region is required to maintain the structural integrity of GLUT1 upon substrate transport (118).

GLUT1 Secondary Structure

Approximately 60% of GLUT1's amino acid sequence contains hydrophobic residues, leading to the prediction of twelve plasma membrane spanning α -helical domains by hydropathy analysis upon cloning (70). Further studies using Fourier transform infrared spectroscopy confirm the α -helical nature of GLUT1 (119); and circular dichroism spectroscopy analysis indicate that GLUT1 structure is approximately 82% α -helical, 10% β -turn, and 8% random coil structure (120). GLUT1 α -helices were shown to be perpendicular to the plasma membrane, confirming the hypothesized transmembrane-spanning structure of the protein (121). When incubated with D-glucose, the secondary structure of purified GLUT1 increases in a saturable manner when measured by circular dichroism, while cytochalasin B appears to have no effect on structure (122). This demonstrates the conformational change GLUT1 undergoes upon substrate binding, and also shows that cytochalasin B is not transported, but seems to lock the protein in a single conformation.

GLUT1 Tertiary Structure

The amphipathic nature of the α -helices is thought to promote arrangement of a water-accessible sugar binding site and translocation pathway, which has been confirmed by scanning mutagenesis, as well as accessibility to biotinylated bis-mannose, membrane-impermeant NHS-biotin and proteolytic enzymes (123-125). In addition, the solved crystal structures of the MFS family members GlpT and LacY, two of the MFS superfamily members, have been used as a scaffold to predict GLUT1 tertiary structure based on homology of helical packing and secondary structure (59,126). These models suggest that the first and second halves of GLUT1 exist in a symmetrical antiparallel 3-dimensional structure, with TMs 2, 4, 5, 7, 8, and 10 forming a funnel-like translocation channel, and TMs 3, 6, 9, and 12 acting as structural stabilizers around the outer edges of the protein. In contrast, the large intracellular loop 6 and the N- and C-termini of GLUT1 appear as disordered random coil structures. The symmetry of the three-dimensional model, combined with some of the conserved sequence symmetry in the first and second halves of the protein (i.e. the GRR/K motif in TM2 and 8), has led to the hypothesis that GLUT1, and indeed the GLUT family of transporters, arose as a result of a gene duplication event (127). However, it should be noted, that while the two halves of GLUT1 can self associate and transport sugar when expressed separately, each half of the protein is unable to mediate glucose uptake individually (128).

GLUT1 Quaternary Structure

The initial analysis of GLUT1 transport and structure seemed to indicate the presence of a higher order oligomeric structure to the protein. Initial ligand binding studies

indicated the presence of two binding sites per GLUT1 transporter, one facing the cytosol, and one facing the extracellular space (129). Since carriers cannot present both endofacial and exofacial binding sites at once, this suggests the formation of GLUT1 dimers. When GLUT1 is purified from erythrocytes, reconstitution in cholerae yields two species of approximately 104 and 226 kDa, respectively, when resolved by SDS-PAGE and size exclusion chromatography (130,131), which suggests the presence of both GLUT1 dimer and tetramer. The addition of reductant to the purified protein yields a single 104 kDa species, indicating that tetramer formation, but not dimer formation, may be associated with disulfide formation (131). Studies using GLUT1-GLUT4 chimeras expressed in CHO cells and 3T3-L1 adipocytes also suggest oligomer formation, since immunoprecipitation of chimeras with GLUT4 C-terminal antibody were able to pull down native GLUT1, but not GLUT4 (132). Finally, freeze-fracture electron microscopy and light scattering studies of GLUT1 in different detergents indicate the presence of homodimeric or homotetrameric protein structure (133).

Until the crystal structure of GLUT1 is solved, many details of how GLUT1 is arranged in the plasma membrane remain elusive. Visualizing GLUT1 in three dimensions may ultimately lead to clearer answers as to how it functions as a glucose transporter, and how it is inhibited. However, there are certain structural elements that have been shown to play a critical role in the mediation and regulation of glucose transport, such as the C-terminus, ATP-binding domain, and its quaternary structure. While still incomplete, many of the details of GLUT1-mediated transport have been well

characterized in the two systems where its expression is the highest: the erythrocyte and the blood-brain barrier.

GLUT1-Mediated Transport

GLUT1 is primarily responsible for D-glucose transport in cells; while it recognizes both α and β D-glucose equally (134,135), it does not bind or transport L-glucose. In addition to D-glucose and DHA, GLUT1 is able to transport 2-deoxyglucose and 3-O-methylglucose, which have been key molecules for measuring its transport properties. The sugar analog 2-deoxy-D-glucose (2-DOG) is a semi-metabolizable substrate that can be transported by GLUT1 into the cell, where it is phosphorylated by hexokinase. 2-DOG phosphorylation traps it inside the cell, since its phosphorylated form is not transported by GLUT1, and it cannot be further metabolized (136). In contrast, 3-O-methyl-D-glucose is a sugar analog that cannot be metabolized, but can be transported by GLUT1. Thus, it is transported into and out of cells, mimicking D-glucose under physiological conditions (137). The use of these sugar analogs is preferred to D-glucose in kinetic sugar transport kinetics because they ensure that only protein-mediated sugar uptake, and not glucose metabolism, is being measured.

In addition, GLUT1 activity is competitively inhibited by a number of molecules such as cytochalasin B, phloretin, forskolin, and maltose. Cytochalasin B and forskolin bind at the cytosolic sugar binding site with high affinity, while maltose binds GLUT1 extracellularly with lower affinity. Phloretin is thought to bind GLUT1 both intra- and extracellularly with lower affinity than cytochalasin B, though the exact binding sites for

all of these molecules have yet to be resolved (65,138-140). The use of radiolabeled (^{14}C or ^3H) and cold versions of these sugar analogs and inhibitors have been critical tools for studying the parameters of GLUT1-mediated transport.

There are four traditional assays that have been employed when performing GLUT1 sugar uptake measurements: *zero-trans* entry and exit, *infinite-cis* entry and exit, *infinite-trans* entry and exit, and equilibrium exchange transport. In these assays, *cis* refers to the side of the membrane where transport is initiated, and *trans* refers to the opposite side of the membrane. Entry refers to uptake into the cell, and exit refers to efflux out of the cell, when sugar is pre-loaded before measuring transport. Therefore, *zero-trans* measures transport of variable concentrations of sugar into sugar-free medium; *infinite-cis* measures transport of a fixed, saturating amount of sugar into an environment of variable sugar levels; and *infinite-trans* measures transport of variable concentrations of sugar into an environment of a fixed, saturating sugar concentration. Equilibrium exchange is unique, in that the *cis* and *trans* concentrations of sugar are identical, and transport measures the movement of a trace amount of radiolabeled sugar across the plasma membrane (42,141). The combination of these assays has been used extensively to elucidate the kinetics of GLUT1-mediated transport in a variety of systems, with the most detailed analysis performed in the red blood cell.

Kinetics of GLUT1 Transport: The Simple Carrier

GLUT1-mediated transport was first characterized before the protein itself had been discovered. Since simple diffusion of glucose was unable to account for the rate of

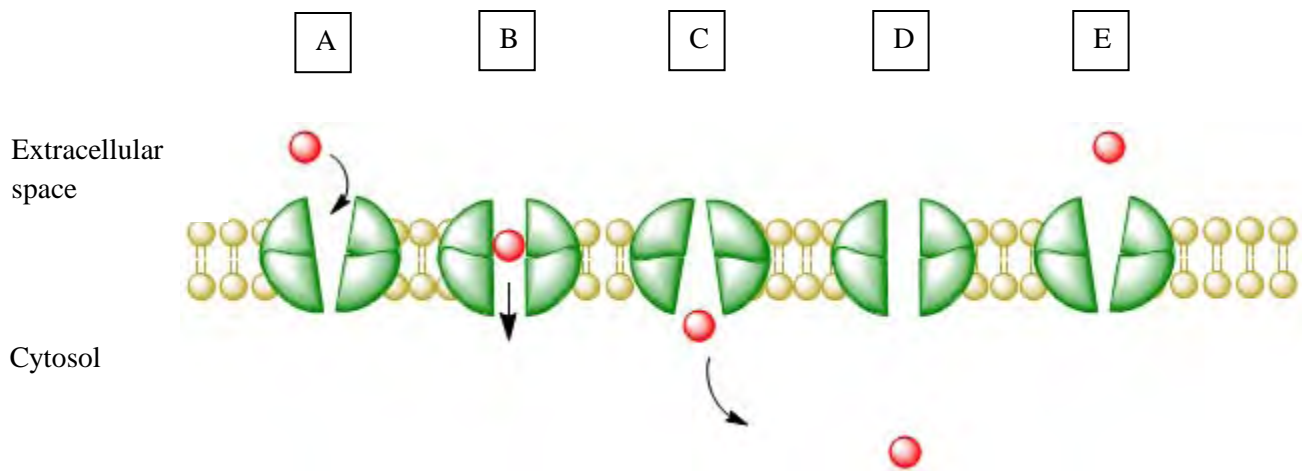


Figure 1.2: The Simple Carrier

Schematic representation of GLUT1-mediated transport of glucose according to the simple carrier model. GLUT1 is represented in green residing in the plasma membrane (yellow), and glucose in red. In *A*, a single exofacial glucose binding site is exposed, and binding causes a conformational change that allows translocation through GLUT1 (*B*) while occluding additional glucose binding. Glucose is released into the cytosol in *C*, exposing an endofacial binding site. Intracellular glucose can either bind to be exported, or, in the absence of substrate (*D*), GLUT1 can relax to the exofacial conformation, regenerating the binding site and allowing another round of uptake to occur, seen in *E*.

transport across the blood-placental barrier of sheep, the simple carrier hypothesis was proposed to describe glucose uptake (43). The main assumptions developed from this study stated the following: 1. the carrier protein was selective for glucose, 2. the carrier presented a single binding site on one side of the membrane at a time, and alternated between each side regardless of whether glucose was bound, and 3. transport of glucose was both a saturable and equilibrative process following Michaelis-Menten kinetics (43,141). A schematic of simple carrier transport is represented in Figure 1.2. While this was able to partially describe the kinetics of GLUT1 glucose uptake, studies using inhibitors such as ethylidene glucose, isopropylidene glucose, and trimethylglucose, demonstrated an asymmetrical inhibition of transport when glucose entry and exit were measured (137). Similar results were also seen with cytochalasin B, phloretin, and maltose (139). In addition, further cytochalasin B binding studies demonstrated that affinity for exofacial ligand was reduced in a complex manner when cytochalasin B was bound internally (129,142). These studies led to the rejection of the simple carrier model for GLUT1 transport, instead favoring another model where GLUT1 presents two simultaneous sugar binding sites intra- and extracellularly. This model is known as the fixed site carrier.

Kinetics of GLUT1 Transport: The Fixed Site Carrier

The fixed site carrier model of transport states that the carrier presents simultaneous entry and exit sites for substrate binding; and the availability of two substrate binding sites allows for simultaneous bidirectional transport. Originally, this model proposed that a monomer of GLUT1 presented simultaneous binding sites at both sides of the plasma

membrane with different affinities for glucose and inhibitors; and that sugar bound inside and outside the cell passed one another through the same translocation channel during transport. (143). While this model partially explains the asymmetry seen in GLUT1 transport and inhibition, it does little to explain how binding of substrate on one side of the membrane changes the affinity for substrate on the other side (129); or how low concentrations of inhibitor on one side of the membrane are able to increase the affinity for inhibitor on the opposite side of the membrane. In an analogous fashion, sugar or inhibitor on one side of the membrane can stimulate uptake of sugar on the other side of the membrane (called *trans* acceleration) (143,144). However, taking into account the oligomeric structure of GLUT1, a modified fixed site carrier model could explain such kinetic phenomena. GLUT1 is thought to exist as a tetramer, with each complex presenting two cytosolic sugar binding sites and two exofacial sugar binding sites. The monomers are thought to be arranged in an anti-parallel manner, meaning that if one subunit is presenting a sugar binding site, the adjacent subunits must present a sugar exit site. While each subunit is able to form a glucose translocation pathway and function as a simple carrier independently, the movement of one subunit during sugar transport allosterically affects the movements of the other subunits, thus allowing bidirectional transport to take place (Figure 1.3). Inter-subunit interaction also allows binding of substrate at one site to cooperatively alter the affinity for substrate at the other sites (144,145). While transport in most cell types expressing GLUT1 fits the modified fixed site model, special considerations must be made when measuring red cell transport, due to its complexity (146).

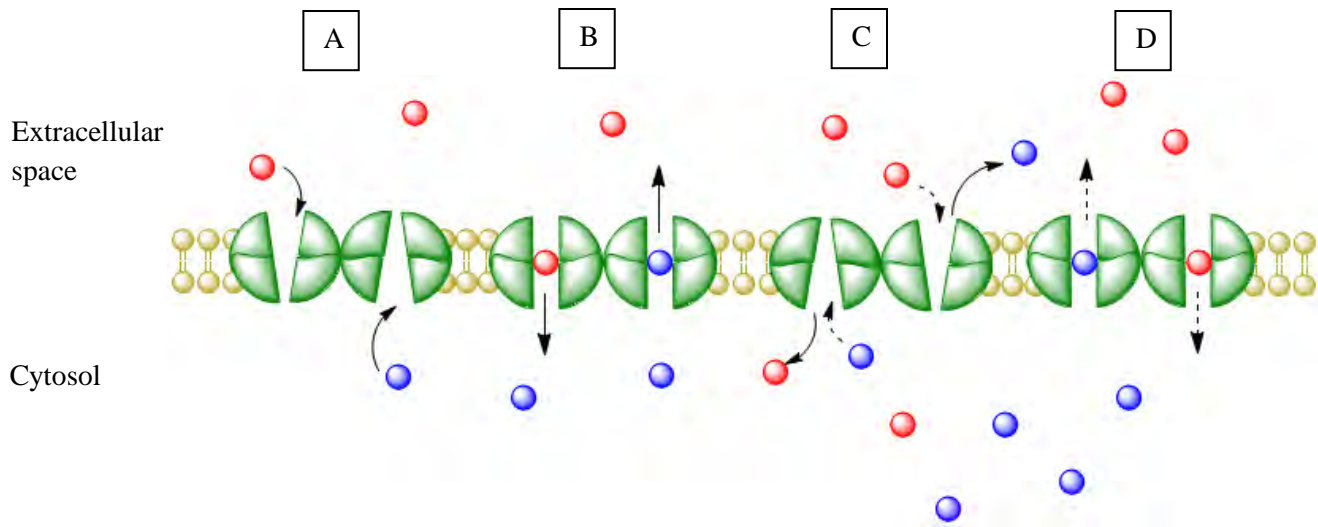


Figure 1.3: The Modified Fixed Site Carrier

Schematic representation of GLUT1-mediated transport according to the modified fixed-site carrier model. One half of a GLUT1 tetramer is represented in green residing in the plasma membrane (yellow), extracellular glucose is represented in red, and cytosolic glucose in blue. In *A*, endofacial and exofacial glucose binding sites are simultaneously presented at both sides of the plasma membrane. Glucose is able to bind both sites simultaneously, inducing a conformational change in both subunits and bidirectional transport, seen in *B*. Upon glucose release from GLUT1, binding sites are regenerated in the opposite configuration from *A*, allowing glucose transport to once again occur at either side of the plasma membrane, shown in *C* and *D*, with dashed lines representing a second round of transport. Presumably, the surrounding subunits adjacent to the two represented here would present binding sites in opposition to their neighbor, allowing transport of up to four glucose molecules, two into the cell, and two out. Binding of glucose at one site is sufficient to induce conformational change in the surrounding subunits, regardless of whether all glucose binding sites are filled.

GLUT1-mediated transport in human erythrocytes cells is unique in that it has been shown to be a multiphasic process. At low concentrations of 3-OMG, transport appears to be biphasic with fast and slow components of uptake corresponding to sugar translocation and release into the cytosol, respectively (147,148). Quench-flow analysis at very short time points reveals the presence of a third, rapid phase of transport which corresponds to glucose binding to GLUT1 in a temperature-sensitive manner (149). All three phases of transport have been shown to be protein-mediated, though the exact mechanism of how glucose is moving through GLUT1 at each phase remains unclear (148,149). The complexity seen while measuring transport in erythrocytes has led to the hypothesis that GLUT1 has non-catalytic sugar binding sites that interact with glucose and can form a cage for sugar, preventing free diffusion into the cytosol after transport (147). Similarly, it has been proposed that an unstirred layer exists within the cytosol of erythrocytes, slowing glucose diffusion upon release by GLUT1 (141). While the true mechanism of red cell transport has yet to be revealed, the presence of such complex kinetics must be considered when using erythrocyte GLUT1 transport measurements as a benchmark since traditional assays tend to over- or underestimate the true kinetics involved (148,149). Adding further to the complexity of GLUT1-mediated transport is its regulation by the nucleotide ATP.

ATP and GLUT1 Transport

The effect of ATP on GLUT-mediated sugar uptake was first observed in studies measuring both glucose uptake and tryptophan fluorescence. ATP was shown to increase the affinity for glucose and decrease the V_{\max} for glucose transport in GLUT1 residing in

inside-out vesicles. Further studies demonstrated that ATP decreases V_{\max} and decreases K_m (increasing affinity) for sugar uptake into red cells, while decreasing V_{\max} and increasing K_m (decreasing affinity) for sugar exit (150). In addition, ATP enhances the ability of glucose to quench intrinsic tryptophan fluorescence of GLUT1 through conformational change upon substrate binding both in vesicles and stripped ghosts (151,152). While fluorescence quenching with ADP and AMP was also observed, there was no change to the rate of glucose uptake or affinity for glucose in the presence of either nucleotide (151,152). In addition, the nucleotides GTP, UTP, and ITP also show no effect on GLUT1 function (153). It has since been demonstrated that ATP, ADP, and AMP can all directly bind to GLUT1 and competitively displace one another from the protein, but that GLUT1 itself has no detectable ATPase activity (113,115). ATP has also been shown to bind GLUT1 in a cooperative manner (154). Taken together, these data indicate that the rate of GLUT1-mediated uptake and its affinity for glucose are directly related to the amount of ATP/AMP present in the cytosol, allowing both nucleotides to modulate sugar uptake in direct response to cellular energy levels.

While the mechanism of how ATP controls GLUT1 sugar uptake is not clearly defined, the available data offers several clues as to how this process may occur. ATP binding to GLUT1 reduces reactivity of the C-terminus of the protein with specific antibodies raised against it (115); and studies using sulfo-NHS-biotin to modify lysines in both intracellular loop 6 and the C-terminus suggest interaction between these regions upon ATP binding (155). Thus, ATP binding to GLUT1 induces conformational changes in the protein that have two consequences: 1. an increase in the affinity for extracellular

glucose, which slows down uptake into the cell; and 2. an interaction between the C-terminus and loop 6, that could potentially form a “cage” structure on the cytosolic face of the protein. This cage structure is thought to occlude glucose diffusion into the cytosol, either physically or through the presence of additional glucose binding sites. Occluded glucose can either be transported back out of the cell, interact with additional glucose binding sites within the cage, or eventually be released into the cytosol (117).

Other Suppressors of GLUT1-Mediated Transport

In addition to ATP, there are other molecules that are able to down regulate GLUT1-mediated glucose uptake in cells, usually through direct interaction. The membrane protein stomatin, which was first identified as band 7.2 when GLUT1 was first purified from red blood cells, has been shown to play a possible role in suppressing glucose uptake. It was observed that stomatin co-immunoprecipitates with GLUT1 using GLUT1 antibodies; however, direct interaction between stomatin and GLUT1 has not yet been proven, only speculated (156). Further studies show that during erythropoiesis, GLUT1-mediated sugar uptake is suppressed and DHA uptake increased in human erythroblasts and erythrocytes. This conversion from transport of glucose to DHA is thought to be modulated by stomatin through its interaction with GLUT1 (157). However, since it is expressed in a wide variety of cells and little is known about its function, the role stomatin plays in red blood cell and other mammalian cells requires further study.

Barbiturates, which are frequently used as anesthetics, have been shown to suppress the V_{\max} of GLUT1-mediated transport by approximately 50% in red blood cells, blood-

brain barrier endothelial cells, and other cell types in addition to reducing cerebral blood flow and metabolism (158,159). Fluorescence studies have shown that barbiturates directly interact with GLUT1, quenching intrinsic fluorescence in a dose-dependent manner regardless of the presence of D-glucose. This indicates a direct interaction with GLUT1 that is dose-dependent and not competitive with substrate binding. Unlike ATP, barbiturate treatment does not alter the K_m for D-glucose, and the suppression of glucose uptake appears to be isoform-specific, with little effect seen in GLUT4-containing cells (159).

GLUT1 Transport Upregulation by Signaling Molecules

Control of energy homeostasis is critical for maintaining cell viability; and there are a number of mechanisms that control GLUT1-mediated glucose uptake based on metabolic demand. While red blood cells contain the highest concentration of GLUT1 of all cell types, they lack the regulatory machinery to control GLUT1 expression and translocation (129). Consequently, GLUT1 regulation has been most studied in cells where it is the primary glucose transporter, such as the endothelium comprising blood-tissue barriers, as well as in cells where GLUT1 and GLUT4 are co-expressed, such as insulin-sensitive tissues. While not normally insulin-sensitive, GLUT1 translocation to the plasma membrane is increased approximately twofold in insulin-sensitive cells along with other proteins in the constitutive recycling pathway, including transferrin (160). Activation of the phosphatidylinositol-3-kinase (PI3K) pathway has been shown to mediate this increase in GLUT1 translocation (161,162) during insulin stimulation.

Since growth factors are responsible for activating energetically demanding cellular processes, GLUT1 is an ideal target to supply much needed glucose to meet cellular metabolic requirements. Molecules such as platelet-derived growth factor (PDGF), vascular endothelial growth factor (VEGF), fibroblast growth factor (FGF), and epidermal growth factor (EGF) play a key role in modulating GLUT1 expression and localization in a variety of cell types. In 3T3-L1 adipocytes, treatment with PDGF for 10 minutes increases GLUT1 translocation to the plasma membrane and doubles 2-DOG uptake via PI3K activity (163). VEGF treatment of bovine retinal endothelial cells for 24 hours increases plasma membrane GLUT1 1.7-fold, while increasing 3-OMG uptake approximately 1.6-fold with no change to GLUT1 mRNA expression or total GLUT1 protein. In contrast to insulin-sensitive cells, this translocation appears to be mediated by protein kinase C activity (164). Chronic exposure of 3T3-L1 adipocytes to FGF-21 increases GLUT1 expression and 2-DOG uptake, and this effect is further enhanced upon activation of PPAR γ , an anti-diabetes target (165). Finally, mouse embryonic cells exposed to EGF for 12-24 hours demonstrate increased GLUT1 expression and 2-DOG uptake that appears to be modulated by PKC and p38/MAPK (166).

GLUT1 and Cancer

GLUT1 expression has been shown to be upregulated by inflammatory oncogenic signaling molecules, such as the cytokines transforming growth factor beta (TGF β) and tumor necrosis factor alpha (TNF α) (167). As a result, high levels of GLUT1 have been observed in a number of cancers (168). Overexpression of GLUT1 and increased glucose uptake have been observed in carcinomas of the lung, breast, colon, kidney, brain, ovary

and squamous cell, among others (169-175). For the most part, detection of GLUT1 in tumor tissue is associated with poor prognosis, tumor angiogenesis, and metastasis; and it is often used as a marker protein to flag patients who may need more aggressive treatment. Tumor cells are noted for their high metabolic demand and low oxygen consumption as compared to healthy cells. Their switch from relying on oxidative metabolism to anaerobic glycolysis for energy has been deemed the Warburg effect, and upregulation of GLUT1 plays a critical role in supplying tumors with much needed glucose (176). As a result, GLUT1's role as the energy supplier in tumor cells has made it a desirable target for anti-cancer therapy in recent years.

GLUT1 Regulation and Metabolic Stress

Since GLUT1 is responsible for delivering glucose to cells for energy metabolism, its activity is tightly bound to the cell's metabolic state. When conditions exist that cause decreases in intracellular ATP, GLUT1 transport is upregulated in order to maintain adequate energy supplies. Chronic hypoxia has been shown to increase GLUT1 expression through the activity of hypoxia inducible factor 1 alpha (HIF1 α), which regulates expression of the GLUT1 gene in addition to other glycolytic targets (177,178). In addition, the AMP-dependent kinase (AMPK) can directly modulate GLUT1 expression and trafficking during chronic hypoxia and hypoglycemia through HIF1 α -dependent and independent mechanisms (179-181). Similarly, when cells are subjected to acute hyperosmotic shock, both GLUT1 trafficking to the plasma membrane and intrinsic activity have been shown to increase (182). Inhibition of oxidative metabolism with reagents such as cyanide and carbonyl cyanide-p-trifluoromethoxyphenylhydrazone

(FCCP) also acutely increase GLUT1-mediated transport without increasing GLUT1 expression, localization, or total GLUT1 protein through de-repression of plasma membrane GLUT1 transport activity (183,184).

While the sources and length of metabolic stress may vary greatly in these studies, the common theme is that ATP depletion increases GLUT1-mediated transport in a variety of cell types. In the context of brain metabolism and its dependence on blood-brain barrier glucose transport, it is important to consider these regulatory mechanisms for insight into how GLUT1 mediates glucose uptake under normal and metabolically stressed conditions.

GLUT1-Mediated Transport at the Blood-Brain Barrier

GLUT1-mediated transport at the blood-brain barrier is, as with red cells, a saturable, equilibrative process that follows Michaelis-Menten kinetics (34,36). However, there are some notable differences between the roles of red cells and endothelial cells in regards to glucose transport. First, the red blood cell primarily acts as a glucose carrier, as the high GLUT1 content allows for rapid equilibration of glucose between serum and red cell cytoplasm, which increases the glucose carrying capacity of the blood. Blood-brain barrier endothelial cells, on the other hand, mediate transcellular glucose uptake that is primarily unidirectional in nature, with uptake occurring at the luminal side of the cell, and efflux taking place at the abluminal surface. Second, healthy red cells are thought to have uniform distribution of GLUT1 throughout the plasma membrane (135), while blood-brain barrier endothelial cells demonstrate polarization with unequal distribution of

GLUT1 between the luminal and abluminal faces of the cell (26,185). In addition, approximately 50% of GLUT1 is sequestered in intracellular stores in endothelial cells, unlike red blood cells (186). Finally, as previously mentioned, red cell glucose transport is unique in its kinetic complexity (146); and for reasons that remain unclear, this complexity may be lacking in blood-brain barrier endothelial cells (187).

GLUT1 Deficiency Syndrome: Blood-Brain Barrier Transport Dysfunction

Impairment of blood-brain barrier glucose transport has dire consequences on brain function. A rare pathological condition called GLUT1-deficiency syndrome (GLUT1-DS) has been shown to cause a number of detrimental symptoms in young children which result from reduced endothelial glucose uptake. GLUT1-DS causes seizures, delayed development and head growth, impaired motor skills, learning disabilities, and mental handicap if left untreated (188,189). GLUT1-DS can result from a number of point mutations, truncations, deletions, or insertions in the GLUT1 gene that cause alteration of GLUT1 structure and ablation of glucose and DHA transport function (188,190,191). While homozygous mutations are lethal, heterozygous mutations are autosomal dominant, and result in an approximately 50% reduction in GLUT1-mediated transport across the blood-brain barrier (192). While there is no cure, a high fat ketogenic diet has been shown to alleviate the symptoms of GLUT-DS and allow for more normal brain metabolism and development (193). The damaging effects of impaired blood-brain barrier transport underscore both the critical role GLUT1 plays in supplying fuel for the brain, and the need for proper regulation of blood-brain barrier glucose transport. Understanding how the blood-brain barrier regulates GLUT1-mediated glucose uptake,

especially during stress conditions, is therefore critical to gaining insight into both brain metabolism and whole organism development and homeostasis.

Blood-Brain Barrier Transport and Metabolic Stress

As in other cell types, the effects of both chronic and acute metabolic stress have been studied in blood-brain barrier endothelial cells. Chronic hypoxia has been shown to increase both brain vascularization, total GLUT1 protein, and glucose uptake in the blood-brain barriers of rats (194). Similarly, GLUT1 mRNA and protein expression are both increased in cultured endothelial cells subjected to hypoxic conditions for several hours (195). The blood-brain barrier of rats subjected to hypoglycemia for 5-14 days shows increases in GLUT1 mRNA, total protein, and glucose uptake, while chronic hyperglycemia has no effect on GLUT1 expression or transport activity (196,197). Brain injury caused by trauma increases GLUT1 expression in the vasculature around the site of injury; while unilateral ischemia-hypoxia, which causes developmental brain damage, has also been shown to upregulate GLUT1 gene expression and total protein in rat brain (198,199). These results indicate that, as in other cell types, GLUT1 expression, localization, and transport are all increased in blood-brain barrier endothelial cells exposed to chronic metabolic stresses.

Acute metabolic stress has been shown to upregulate GLUT1-mediated transport at the blood-brain barrier. However, the mechanisms underlying this regulation are not as well defined as those of the chronic stress response. Acute metabolic stress induced by seizures has demonstrated that the glucose transport capacity of the blood-brain barrier

doubles in rat brains with no apparent change to the K_m for glucose (200). Interestingly, immunogold labeling of blood-brain barrier GLUT1 during seizures does not indicate increased total plasma membrane protein, but in some cases shows decreased GLUT1 presence (200). These findings lead to several questions about how GLUT1 activity is modulated at the blood-brain barrier during acute metabolic stress.

Remaining Questions

Analysis of blood-brain barrier endothelial cell responses to metabolic stress seems to indicate two distinct mechanisms of regulation. While chronic responses mirror those seen in other cell types, i.e. increased GLUT1 gene expression, protein levels, and eventual trafficking to the plasma membrane, the acute response data raise some questions. First, what are the effects of acute glucose deprivation on blood-brain barrier endothelial cells? There is little data demonstrating the effect of acute hypoglycemia at the blood-brain barrier. Since blood-tissue barrier endothelial cells have a higher mitochondrial content than those of the peripheral endothelium, they may be able to sense rapid changes in glucose more easily than their less energetically demanding counterparts (26). On a similar note, how does inhibition of oxidative phosphorylation affect endothelial cell glucose uptake? Since mitochondria are abundant in blood-tissue barrier endothelial cells, inhibition of oxidative phosphorylation would likely have a profound effect on energy metabolism and by extension glucose uptake, but again, there is little data to demonstrate this in endothelial cells.

Perhaps the most glaring question is this: how is the increase in glucose uptake mediated during acute stress in blood-brain barrier endothelial cells? Since the increases in transport were seen during seizures (where brain energy demand rapidly increases), this seems to imply communication between the brain cells and the blood-brain barrier (200,201). Are neurons and astrocytes required to modulate increased blood-brain barrier glucose uptake, or can the endothelium sense changes in energy availability and compensate on its own? Are GLUT1 expression, trafficking, or intrinsic activity affected during acute stress, or is the effect a combination of these events? Finally, what signaling factors, if any, play a role in modulating glucose transport at the blood-brain barrier? GLUT1 is subject to regulation by a number of different pathways, including the AMPK, HIF1 α , PKC, and PI3K signaling cascades (161,166,177,202,203). Are these pathways involved in the acute stress response, or are there others that may play a role?

The data presented in this thesis attempt to answer some of the questions above by defining the time course, kinetics, and mechanism of GLUT1-mediated transport during a variety of acute metabolic stresses in cultured blood-brain barrier endothelial cells as well as by examining the signaling cascades that may play a role in modulating transport under normal and acute stress conditions.

CHAPTER II

EVALUATION OF THE BRAIN MICROVASCULAR ENDOTHELIAL CELL LINE bEnd.3 AS A MODEL SYSTEM FOR BLOOD-BRAIN BARRIER GLUCOSE TRANSPORT STUDIES

Abstract

Studies of the effects of acute metabolic stress on blood-brain barrier endothelial cell glucose transport are difficult *in vivo* due to temporal resolution and substrate delivery required to accurately measure transport. Primary cultures of endothelial cells are notoriously difficult to isolate and sustain for long periods without compromising their integrity. Therefore cultured cell systems are ideal for their flexibility and resilience in the face of such studies. Here we evaluate the murine brain microvascular endothelial cell line bEnd.3 as a model system for studying blood-brain barrier endothelial cell transport during acute metabolic stress. Sequence alignment of human and mouse GLUT1 protein shows approximately 97% sequence homology between the proteins, with 100% homology in the purported ATP binding domain, 88% in the N-terminus, 100% in the C-terminus, and 97% in loop 6 of the protein. A combination of Western blot, qPCR, and pharmacological analysis shows that GLUT1 is the primary transporter responsible for glucose uptake in these cells. Sugar uptake measurements using 2-DOG and 3-OMG demonstrate that GLUT1-mediated transport is detectable and inhibitable by cytochalasin B in bEnd.3 cells. Analysis of kinetic data shows that zero-trans entry and equilibrium exchange sugar uptake data for both 2-DOG and 3-OMG are mostly comparable to

published values seen in human red blood cells. These results taken together indicate that bEnd.3 cells are an adequate model system for studying the effects of acute metabolic stress on GLUT1-mediated glucose transport.

Introduction

Understanding how nutrient transport across the blood-brain barrier is affected is important for studying regulation of brain metabolism. However, the mechanics of undertaking transport studies have proven difficult for a number of reasons. While *in vivo* systems are ideal for transport studies, they present significant obstacles for data collection. First, there are severe restrictions placed on human studies, limiting the types of assays that can be performed. Second, specific isolation and delivery of the substrate of interest to the blood-brain barrier is very difficult to achieve in a repeatable manner. Finally, the complexity of a whole organism prevents the ability to specifically knock down, inhibit, or stimulate a target without inducing system wide effects on the organism. As a result, *in vitro* studies are preferred when studying blood-brain barrier nutrient uptake since the system is more isolated, and therefore better able to be controlled than an *in vivo* model.

There are two main sources of *in vitro* systems for studying blood-brain barrier nutrient transport: primary cell lines and immortalized cell lines. Primary cells offer many advantages, such as retention of *in vivo* endothelial cell characteristics and the formation of monolayers of cells that form tight junctions in culture, which can be quite useful in simulating the blood-brain barrier (204). However, there are a number of

drawbacks to using primary cell systems, such as large amounts of time and biological material needed to generate a cell line, the variability of cell quality from sample to sample, and the limited passages that can be performed before cells senesce or die (204) that may make them undesirable for long term studies. Immortalized cells, on the other hand, offer a number of advantages over primary cells, such as rapid growth, the ability to passage many times, consistency of sample, and retention of many blood-brain barrier endothelial characteristics (205). However, in order to choose the correct system, an analysis must be done of that system's characteristics to determine if it is a good choice.

Glucose transport at the blood-brain barrier, which is mediated by the facilitative transporter GLUT1, is upregulated during acute metabolic stress (200,201). However, there are limited studies elucidating the details of how GLUT1 is modulating the increase in sugar transport under these conditions. Therefore, we sought to examine how GLUT1-mediated sugar transport is regulated during acute metabolic stress. However, in order to study blood-brain barrier transport, an appropriate system was necessary. The inability to induce acute stress *in vivo* without causing either irreparable harm to the organism or compensatory reactions to stress throughout the body made an animal system a poor choice. Primary cultured *in vitro* models, though desirable for their close resemblance of *in vivo* blood-brain barrier mechanics, were not ideal due to time and biological material constraints. As a result, we sought to use the immortalized *in vitro* tissue culture system bEnd.3 as a model for our studies.

The murine microvascular endothelial cell line bEnd.3 is a polyoma virus middle T-antigen transformed cell line isolated from brain microvessels. Like low passage primary endothelial cells, bEnd.3 cells demonstrate a spindle-shaped morphology, express tight junction proteins, can be induced to form tight junctions, and have been shown to express GLUT1 by reverse-transcriptase (RT) PCR (205). Therefore, we sought to establish the feasibility of the bEnd.3 cell line as a system for studying regulation of glucose transport during acute metabolic stress. We compared the sequences of human and mouse GLUT1 for differences in regulatory regions of the protein. We screened whole-cell lysates for the presence of GLUT1, and probed for GLUT family expression using RT and quantitative PCR. Using the glucose analogs 2-deoxyglucose (2-DOG) and 3-O-methylglucose (3-OMG) we examined the time courses and kinetics of GLUT1-mediated sugar uptake in bEnd.3 cells and compared the values to published red blood cell data. Our results show that GLUT1 is the primary transporter responsible for sodium-independent glucose uptake in bEnd.3 cells. Transport is inhibitable by cytochalasin B (CCB) and, for the most part, comparable to established erythrocyte kinetic data. We also detected GLUT8 and GLUT9 mRNA in bEnd.3 cells, though expression is very low compared to GLUT1. No other class 1 glucose transporters were detected in these cells based on our analysis. Although not a primary cell line or an *in vivo* animal model, our data suggests that bEnd.3 cells are an adequate cell line that provide an opportunity to study sugar transport in cells derived from the endothelium.

Experimental Procedures

Tissue Culture

bEnd.3 cells were obtained from ATCC and maintained in Dulbecco's Modified Eagle Medium (DMEM) from Gibco supplemented with 10% fetal bovine serum (FBS) from Hyclone and 1% Penicillin/Streptomycin (Pen/Strep) solution (Gibco) at 37°C in a humidified 5% CO₂ incubator. All experiments were performed at cell confluence. Plates were subcultured at a ratio of 1:2-1:3 by washing with sterile Dulbecco's phosphate buffered saline (DPBS) and treating with 0.5% Trypsin-EDTA (Gibco) for 5-7 minutes at 37°C. Passages 3-16 were used in all experiments.

Antibodies

A custom, affinity-purified rabbit polyclonal antibody raised against a synthetic peptide corresponding to GLUT1 amino acids 480-492 was produced by New England Peptide. HRP conjugated Goat anti-rabbit secondary antibodies were obtained from Bio Rad and Jackson Labs.

Buffers

Cell lysis buffer consisted of 5 mM HEPES, 5 mM MgCl₂, 150 mM NaCl, 50 μM EDTA, and 1% SDS. Uptake stop solution included 10μM cytochalasin B (CCB, Sigma) and 100 μM phloretin (Sigma) in DPBS. TAE buffer consisted of 40 mM Tris base, 1 mM EDTA, and 20 mM acetic acid. TBS was composed of 20 mM Tris base and 135 mM NaCl, pH 7.6. TBST comprised TBS buffer with 0.2% Tween-20.

Sequence Alignment of Human and Mouse GLUT1 Protein

The amino acid sequence for human GLUT1 (GenPept number NP_006507.2) and mouse GLUT1 (GenPept number NP_035530.2) were obtained from NCBI. Sequences were aligned and compared using the ClustalW algorithm.

Western Blotting of bEnd.3 Cells

Confluent 100 mm dishes of bEnd.3 cells were washed twice with DPBS, lysed, and analyzed for total protein concentration using a micro BCA kit (Pierce). Lysates were normalized for total protein and run on either 4-12% Bis-Tris or 10% Bis-Tris gels in MES buffer (Invitrogen), transferred to PVDF membranes (ThermoFisher), blocked with either 5 or 10% bovine serum albumin (BSA), and probed with a 1:5,000 dilution of C-terminal antibody, a 1:20,000 dilution of HRP-conjugated goat anti-rabbit was also used. Chemiluminescence was visualized either on film, or using the Fujifilm LAS-3000 with SuperSignal Reagent (Pierce).

Endpoint Reverse Transcriptase PCR

Confluent bEnd.3 cells were washed twice with ice cold DPBS, and total RNA was isolated using the RNeasy Mini Kit and Qias shredder (Qiagen). Reverse transcriptase PCR was carried out on bEnd.3 RNA samples using Qiagen's One-Step RT-PCR Kit as per kit instructions using the following primers (IDT): GLUT1: 5'-GAACCTGTTGGCCTTTGTGGC-3' and 5'-GCTGGCGGTAGGCCGGGTGAGCG-3' which produced a DNA fragment of 515 bp, GLUT2: 5'-AAGAGGAGACTGAAGGATCTGC -3' and 5'-GTAGCAGAC ACTGCAGAAGAGC-

3' which produced a DNA fragment of 461 bp (206), GLUT3: 5'-
CGCCGTGACTGTTGCCACG ATC-3' and 5'-CCACAGTTCTTCAGAGCCC AGA-3'
which produced a DNA fragment of 517 bp, GLUT4: 5'-
TGCAACGTGGCTGGGTAGGC AA-3' and 5'-AGGGAGTACTGTGAGAGCCAG A-
3' which produced a DNA fragment of 444 bp, GLUT5: 5'-
CTAACTGGAGTCCCCGCAGGCC-3' and 5'-GACACAGACAATGCTGATATAG-3'
which produced a DNA fragment of 548 bp, GLUT6: 5'-
ACCCCCTGATGTTTCGTGGGGCC-3' and 5'-CGTAGAGCCCCAGTGTCAGGTT-3'
which produced a DNA fragment of 592 bp, GLUT7: 5'-
CCCATGTACCTGGGAGAACTGG-3' and 5'-ATCAGCTGCCAGCGCAGGGGCC-3'
which produced a DNA fragment of 390 bp, GLUT8: 5'-
TGGCTGGCCGTGCTGGGCTGTG-3' and 5'-AGTAGGTACCAAAGGCACTCAT-3'
which produced a DNA fragment of 464 bp, GLUT9: 5'-
TTGAGCGCTTAGGAAGGAGACC-3' and 5'-ACCGCTGCAGAACGAGGCAATG-3'
which produced a DNA fragment of 163 bp, GLUT10: 5'-
AATGCCAGCCAGCAGGTGGAT C-3' and 5'-AGGACAGCGGTCAGCCCATAG A-
3' which produced a DNA fragment of 526 bp, GLUT12: 5'-
GTGCTTAGTGAGATCTTTCCC-3' and 5'-CCTTTGCTAGCTCCACTGATAT-3'
which produced a DNA fragment of 244 bp, and HMIT: 5'-
CTGAAATCTATCCTCTCTGGGC-3' and 5'-CAATGTACCTCCCTTCATCCGA-3'
which produced a DNA fragment of 284 bp. Analysis of DNA fragments was performed
using agarose gel electrophoresis (1.5% agarose in TAE buffer). Bands were visualized

with ethidium bromide staining under UV light on a Fujifilm LAS-3000 and gels were analyzed using Fujifilm Multigauge 3.0 software.

Quantitative Reverse Transcriptase PCR

Total RNA was isolated from bEnd.3 cells as described above, and quantitative RT-PCR was performed using an iScript One-Step RT-PCR Kit with SYBR Green (Bio-Rad). Each reaction was run in duplicate using the following primers (IDT): GLUT1: 5'-AGCCCTGCTACAGTGTAT-3' and 5'-AGGTCTCGGGTCACATC-3' which generated a DNA fragment of 135 bp; GLUT8: 5'-TGTGGGCATAATCCAGGT-3' and 5'-GGGT CAGTTTGAAGTAGGTAC-3' which produced a DNA fragment of 140 bp, GLUT9: 5'-CTCAT TGTGGGACGGTT-3' and 5'-CAGATGAAGAT GGCAGT-3' which produced a DNA fragment of 132 bp, and as a mouse expression control, EIF1 α : 5'-CAACATCGTCGTAATCGGACA-3' and 5'-GCTTAAGACCCAGGCGTACTT-3' which was used to normalize PCR data (207). Samples were run on an MJ-Research PTC-200 Peltier Thermal Cycler with a Chromo4 Real Time PCR detector using Opticon Monitor 3 software (Bio-Rad). Relative RNA expression was quantitated using the $\Delta\Delta CT$ method and results graphed using Synergy Software's Kaleidagraph Version 4.0. All primers were verified using Qiagen's One-Step RT-PCR Kit and run on a 2% agarose gel in TAE. Bands were visualized by ethidium bromide staining under UV light on a Fujifilm LAS-3000 and gels were analyzed using Fujifilm Multigauge 3.0 software.

Time Course of 2-DOG Uptake

Confluent 150 mm² dishes of bEnd.3 cells were split into 12-well plates the afternoon before each experiment. On the day of the assay, cells were placed in serum-free DMEM for 2 hours at 37°C. Cells were washed with 1 ml of DPBS, incubated in 0.5 ml wash media for 10 minutes at 37°C. Wash medium was drained, and cells were treated with 400 µl of 100 µM 2-deoxy-D-glucose (2-DOG) with 2.5 µCi [³H]-2-deoxyglucose ([³H]-2-DOG) in DPBS in the absence or presence of 10 µM CCB or 10 µM CCB plus 50 µM phlorizin (Sigma) at 37°C. Uptake was measured at various time points from 0 to 15 minutes and was stopped by adding 1 ml of uptake stop solution followed immediately by media aspiration. Each well was washed twice more with 1 ml of stop solution and treated with 0.5 ml of cell lysis buffer. Samples were counted in duplicate by liquid scintillation spectrometry (Beckman). Each measurement was performed in triplicate. Protein concentrations for each sample were determined using Pierce's BCA protein assay kit.

Time Course of 3-OMG Uptake

Uptake was measured as described above, with the following modifications: After the wash step was performed and cells were incubated for 10 minutes at 37°C, plates were immediately placed on ice and cooled to 4°C prior to uptake measurement. Wash medium was drained, and cells were treated with 400 µl of 5 mM 3-O-methylglucose (3-OMG) containing 2.5 µCi/ml [³H]-3-O-methylglucose ([³H]-3-OMG) in DPBS in the absence or presence of 10 µM CCB. Uptake proceeded for various time points from 0 to 15 minutes,

plus a 100 minute equilibrium point, and was stopped by adding 1 ml of uptake stop solution and the media immediately aspirated. Samples were processed as described above.

Zero-Trans 2-DOG Dose Response Sugar Uptake Measurements

Confluent 150 mm² dishes of bEnd.3 cells were prepared as described. After wash medium was drained, cells were treated with 400 μ l of increasing concentrations of 2-deoxy-D-glucose (2-DOG) with 2.5 μ Ci [³H]-2-deoxyglucose ([³H]-2-DOG) in DPBS at 37°C. Uptake proceeded for 5 minutes, and was stopped by adding 1 ml of uptake stop solution and the media immediately aspirated. Each well was washed twice more with 1 ml of stop solution and treated with 0.5 ml of cell lysis buffer. Samples were then processed as described previously

Zero-Trans 3-OMG Dose Response Sugar Uptake Measurements

Confluent 150 mm² dishes of bEnd.3 cells were prepared as described and cooled to 4°C prior to uptake measurement. After wash medium was drained, cells were treated with 400 μ l of increasing concentrations of 3-O-methylglucose (3-OMG) containing 2.5 μ Ci/ml [³H]-3-O-methylglucose ([³H]-3-OMG) in DPBS. Uptake proceeded for 15 seconds at 5 mM and 10 mM 3-OMG, and for 30 seconds at 20 and 40 mM 3-OMG. Uptake was stopped by adding 1 ml of uptake stop solution and the media immediately aspirated. Each well was washed twice more with 1 ml of stop solution and treated with 0.5 ml of cell lysis buffer and processed as described.

Equilibrium Exchange Sugar Uptake Measurements

In these experiments, intracellular concentrations of 3-OMG are equal to extracellular 3-OMG, therefore transport is measured using [³H]-3-OMG. Transport measurements were similar to zero-trans uptake measurements with the following modifications: Cells were serum-depleted in DMEM containing 5, 10, 20, or 40 mM 3-OMG for 2 hours. Cells were washed and incubated as previously described with wash media containing 5, 10, 20, or 40 mM 3-OMG in DPBS. Uptake was measured and terminated as described previously. Cells were then washed and processed as above.

Cytochalasin B and 3-OMG Inhibition of 2-DOG Uptake Measurements

Transport measurements were performed as above with the following modifications: Cells were serum-depleted in DMEM containing 25 mM glucose for two hours prior to measuring uptake, washed with 1.5 ml DPBS, and allowed to incubate at 37°C for 15 minutes. Plates were maintained at 37°C throughout transport measurements. Uptake solutions consisted of 100 μM 2-deoxy-D-glucose (2-DOG) with 2.5 μCi [³H]-2-deoxyglucose ([³H]-2-DOG) plus increasing concentrations of either CCB from 0.1 μM to 10 μM or 3-OMG from 0.1 mM to 40 mM. Uptake proceeded for 5 minutes, at which time uptake was stopped and the cells were washed and processed as described previously.

Analysis of Sugar Uptake

All data analysis was performed using Synergy Software's Kaleidagraph Version 4.0. For time course experiments, background counts were subtracted and uptake was

normalized to total protein per well. Data was fit using either linear regression (2-DOG) or a single exponential (3-OMG). For zero-trans and equilibrium exchange transport experiments, background counts were subtracted and uptake, v , was normalized to total protein/well. Sugar uptake data was fitted to the Michaelis-Menten equation (Equation 1):

$$v = \frac{V_{max}[S]}{K_m + [S]}$$

by non-linear regression and V_{max} and K_m values were extracted from the fits. For cytochalasin B and 3-OMG inhibition experiments, sugar uptake data was fitted to the equation (Equation 2):

$$v = k[S] + J\left(1 - \frac{[I]}{K_{i(app)} + [I]}\right)$$

where J is the rate of protein-mediated transport and I is the inhibitor used. From this equation, the inhibition constant (K_{iapp}) for CCB inhibition of transport was extracted from the fit.

Results

Sequence Alignment of Human and Mouse GLUT1

In order to compare the structural differences between human and mouse GLUT1, sequence alignments were performed using sequence data from NCBI. The aligned sequences for human and mouse GLUT1 are shown in Figure 2.1, with the key amino acid differences summarized in Table 2.1. Human and mouse GLUT1 share approximately 97% total sequence homology with one another, and differ by 17 amino acids out of 492. The majority of amino acid differences occur in the N-terminal half of

```

GLUT1HUMAN  MEFSSKLTGRLMLAVGGAVLGSLLQFGYNTGVINAPQKVIIEEFYNQTVVHRYGESILPTT 60
GLUT1MOUSE  MDPSSKKVTGRLMLAVGGAVLGSLLQFGYNTGVINAPQKVIIEEFYNQTVNHRIGEPSTT 60
*:*:*:*:*:*:*:*:*:*:*:*:*:*:*:*:*:*:*:*:*:*:*:*:*:*:*:*:*:*:*:*:*:*:*:*

GLUT1HUMAN  LTTLWSLSVAIFSVGGMIGSFSVGLFVNRFGRRNSMLMMNLLAFVSAVLMGFSKLGKSF 120
GLUT1MOUSE  LTTLWSLSVAIFSVGGMIGSFSVGLFVNRFGRRNSMLMMNLLAFVAAVLMGFSKLGKSF 120
*****:*:*:*:*:*:*:*:*:*:*:*:*:*:*:*:*:*:*:*:*:*:*:*

GLUT1HUMAN  MLILGRFIIGVYCGLTTFVPMYVGEVSPALRGALGTLHQLGIVVGILIAQVFGLDSIM 180
GLUT1MOUSE  MLILGRFIIGVYCGLTTFVPMYVGEVSPALRGALGTLHQLGIVVGILIAQVFGLDSIM 180
*****:*:*:*:*:*:*:*:*:*:*:*:*:*:*:*:*:*:*:*:*:*:*

GLUT1HUMAN  GNKDLWPLLSIIFIPALLQCIVLPFCPEsprfLLINrNEENRAKSVLKKLRGTADVTHD 240
GLUT1MOUSE  GNADLWPLLSVVFVPAALLQCILLPFCPEsprfLLINrNEENRAKSVLKKLRGTADVTRD 240
* * * * * : : * * * * * : * * * * * : * * * * * : * * * * * : *

GLUT1HUMAN  LQEMKEESRQMMREKKVTILELFRSPAYRQPILIAVVLQLSQQLSGINAVFYSTSI FEK 300
GLUT1MOUSE  LQEMKEEGRQMMREKKVTILELFRSPAYRQPILIAVVLQLSQQLSGINAVFYSTSI FEK 300
***** * *****

GLUT1HUMAN  AGVQQPVYATIGSGIVNTAFTVVSFLVVERAGRRTLHLIGLAGMAGCAILMTIALALLEQ 360
GLUT1MOUSE  AGVQQPVYATIGSGIVNTAFTVVSFLVVERAGRRTLHLIGLAGMAGCAVLMTIALALLER 360
*****:*:*:*:*:*:*:*:*:*:*:*:*:*:*:*:*:*:*:*:*:*:*

GLUT1HUMAN  LPWMSYLSIVAIFGFVAFFEVGPGPIPWFIVAELFSQGPRPAAIAVAGFSNWTSNFIVGM 420
GLUT1MOUSE  LPWMSYLSIVAIFGFVAFFEVGPGPIPWFIVAELFSQGPRPARIAVAGFSNWTSNFIVGM 420
***** * *****

GLUT1HUMAN  CFQYVEQLCGPYVFIIFTVLLVLFIFITYFKVPETKGRTFDEIASGFRQGGASQSDKTPE 480
GLUT1MOUSE  CFQYVEQLCGPYVFIIFTVLLVLFIFITYFKVPETKGRTFDEIASGFRQGGASQSDKTPE 480
*****

GLUT1HUMAN  ELFHPLGADSQV 492
GLUT1MOUSE  ELFHPLGADSQV 492
*****

```

Figure 2.1: Sequence Alignment of Human and Mouse GLUT1

ClustalW alignment of human and mouse sequences of GLUT1. The colors of each amino acid are representative of the following: nonpolar amino acid (red), polar uncharged amino acid (green), acidic amino acid (blue), basic amino acid (purple). Asterisks represent conserved amino acids, colons represent conserved charge or sidechain size, single dots represent conserved charge, but different sidechain size, and gaps represent nonconserved amino acids.

<i>Amino Acid Number</i>	<i>Human Sequence</i>	<i>Mouse Sequence</i>	<i>Location</i>
2	E	D	N-terminus
8	L	V	N-terminus
49**	V	N	Loop 1
52**	Y	I	Loop 1
55*	S	P	Loop 1
57**	L	P	Loop 1
58*	P	S	Loop 1
106	S	A	TM 3
183**	K	A	Loop 5
192	I	V	TM 6
193	I	V	TM 6
195	I	V	TM 6
203	V	L	TM 6
239	H	R	Loop 6
248*	S	G	Loop 6
349	L	V	TM 9
360	Q	R	Loop 9
403**	A	R	TM 11

Table 2.1 Sequence Difference Between Human and Mouse GLUT1

The colors indicate the following side chain properties: Red, nonpolar; Green, polar uncharged; Blue, acidic; Purple, basic

* indicates moderate amino acid substitution

** indicates significant amino acid substitution

the protein, most notably in loop 1 surrounding the glycosylation site at N45. Comparison of the first 16 amino acids of the N-terminus, the last 30 amino acids of the C-terminus, loop 6, and ATP binding region of GLUT1 comprising loop 8/TM 9 show sequence of 88%, 100%, 97%, and 100% respectively. While most sequence differences are conservative in structure and charge, there are five sites that show significant variation between human and mouse GLUT1: V49N, Y52I, L57P, K183A and A403R. The impact that these differences in sequence have on substrate specificity are unknown at this time. Overall, these results indicate that mouse GLUT1 should be detectable by human GLUT1 C-terminal antibodies. Also, mouse GLUT1 should also undergo regulation by ATP in a similar manner to human GLUT1.

Western Blot of bEnd.3 Cells

In order to evaluate the bEnd.3 cell line as a potential system for studying GLUT1 sugar uptake, we sought to detect the presence of GLUT1 protein by Western blot. Antibodies raised against both the C-terminus and loop 6 of human GLUT1 were used to probe whole cell lysates of bEnd.3 cells, and the results can be seen in Figure 2.2. Western blot data indicates that GLUT1 appears as a single band of approximately 55 kDa when probed with C-terminal antibody. The loop 6 antibody demonstrates a faint GLUT1 band at approximately 55 kDa with higher order bands at approximately 60, 62, and 97 kDa respectively. Results are consistent with the initial characterization of bEnd.3 cells by RT-PCR, which demonstrate expression of GLUT1 mRNA.

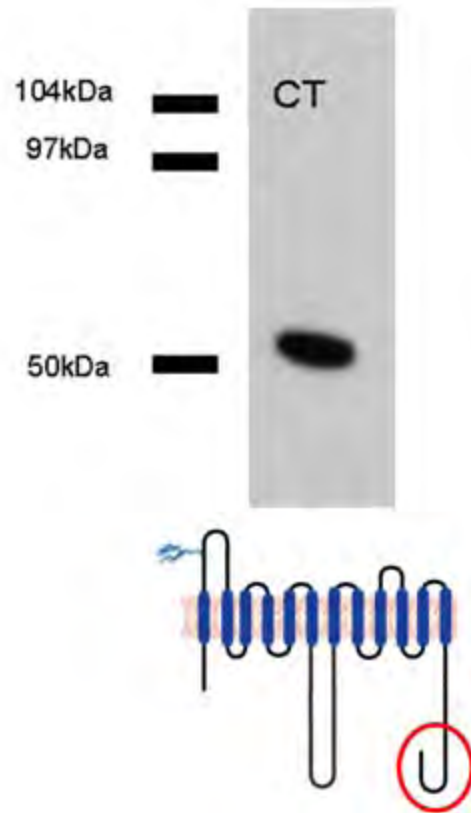


Figure 2.2: Western blot of bEnd.3 Cells

Whole cell lysates of bEnd.3 cells were prepared and analyzed for total protein. 20 μ g of lysate was loaded onto a gel and probed with C-terminal (CT) GLUT1 antibody. A schematic underneath the blot represent GLUT1, with the red circle indicating the region of the protein against which the antibody was raised.

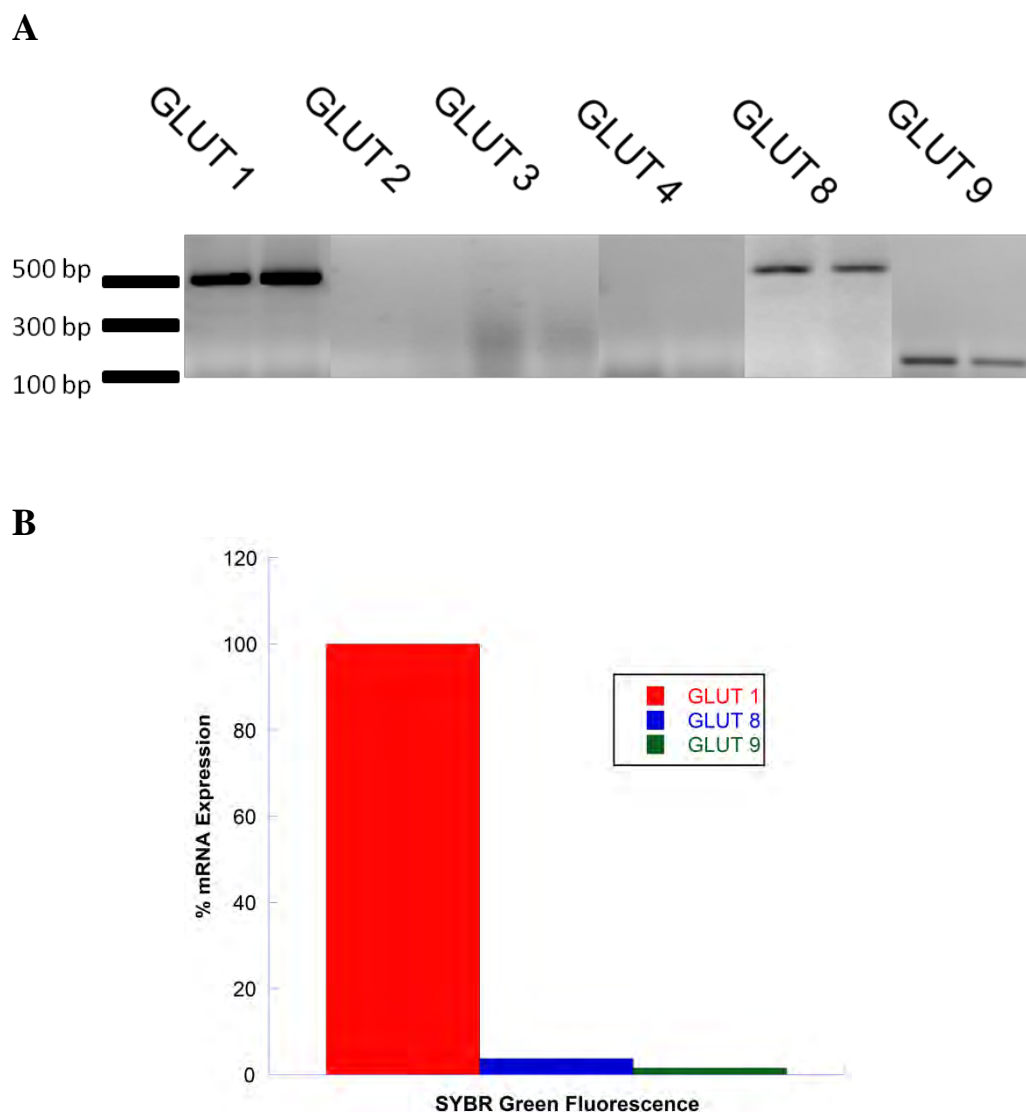


Figure 2.3: RT-PCR Screen for GLUT Family Members

A. Total cellular RNA was isolated from bEnd.3 cells, normalized, and used as a template for RT-PCR. Samples were analyzed on a 1.5% agarose gel in duplicate and visualized with ethidium bromide. Other class 2 and class 3 GLUT family members, which showed no expression, are not shown. *B.* Relative Expression of GLUT1, GLUT8, and GLUT9 in bEnd.3 Cells *Ordinate*, relative expression (%). *Abscissa*: relative SYBR green fluorescence Cells were processed as in *A* and 100 ng of total RNA was used for each reaction. Primers specific to GLUT1, GLUT8, and GLUT9 were used in each reaction, and results are plotted relative to GLUT expression.

Transporter Name	Class	mRNA Detected
GLUT 1	1	Yes
GLUT 2	1	No
GLUT 3	1	No
GLUT 4	1	No
GLUT 5	2	No
GLUT 6	3	No
GLUT 7	2	No
GLUT 8	3	Yes
GLUT 9	2	Yes
GLUT 10	3	No
GLUT 11	2	N/A*
GLUT 12	3	No
HMIT (GLUT 13)	3	No
GLUT 14	1	N/A*

Table 2.2: Summary of GLUTs Expressed in bEnd.3 Cells

** indicates that expression of this GLUT is not known to occur in mice*

Endpoint RT-PCR and qPCR of bEnd.3 Cells

Since the majority of glucose transport in mice is known to be facilitated by 12 of the 14 GLUT proteins, we next sought to identify which family members were present in bEnd.3 cells. The presence of other GLUTs, particularly class 1 family members which are primarily glucose transporters, would impact the feasibility of kinetic studies of bEnd.3 GLUT1. Therefore, using primers specific to each GLUT, we isolated total RNA from bEnd.3 cells, normalized template and primer concentrations, and performed RT-PCR in order to detect the presence of GLUT family member expression. Representative results are seen in Figure 2.3A and summarized in Table 2.2. While no class 1 transporter message was detected other than GLUT1, GLUT8, a class 3 transporter, and GLUT9, a class 2 transporter, were shown to be expressed.

Having detected the presence of GLUT8 and GLUT9, we next sought to determine the relative expression of each transporter. Since RT-PCR is not quantitative, we used quantitative RT-PCR to examine expression of GLUT proteins in bEnd.3 cells using total mRNA as a template. Analysis of the results indicates that while GLUT8 and GLUT9 mRNA are detected, GLUT1 expression is approximately 33-fold higher than either GLUT8 or GLUT9 mRNA. This indicates that GLUT1 is the major GLUT family member responsible for glucose uptake in bEnd.3 cells.

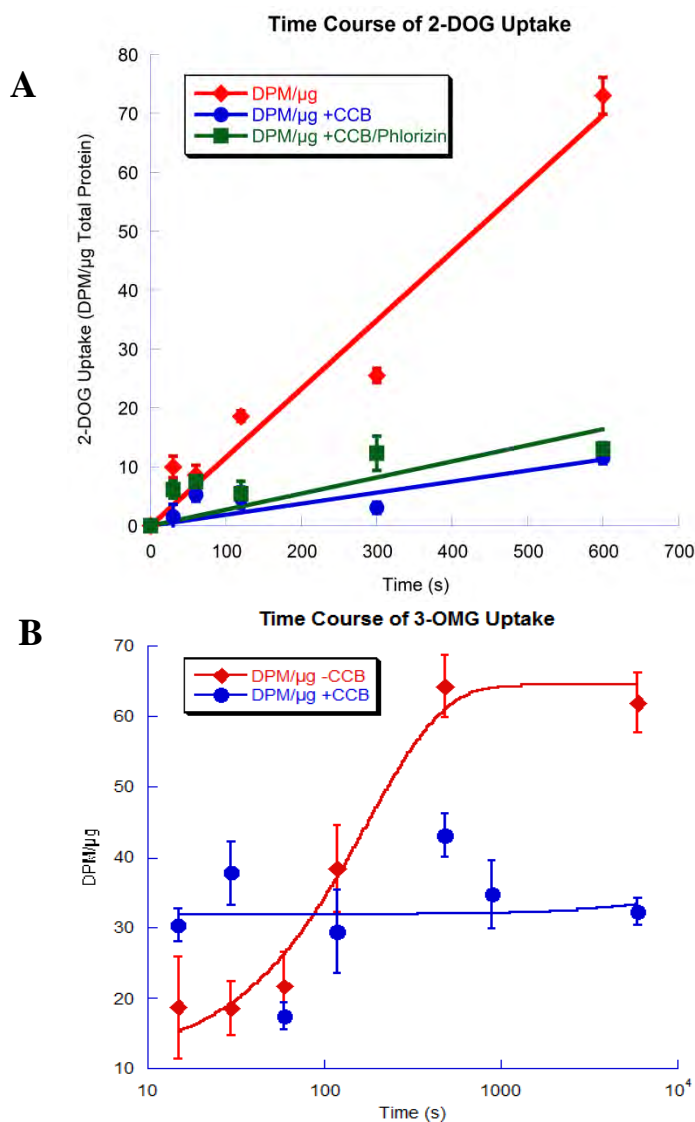


Figure 2.4: Time Course of 2-DOG Uptake

A. Time course of 100 μ M 2-DOG uptake in control cells (\blacklozenge), cells incubated with 10 μ M CCB (\bullet) or 10 μ M CCB + 50 μ M phlorizin (\blacksquare). *Ordinate*, 2-DOG uptake (dpm per μ g total cell protein); *Abscissa*, time in seconds. Data points represent the mean \pm S.E. of three separate determinations. B. Time course of 5 mM 3-OMG uptake in control cells (\blacklozenge) or cells incubated with 10 μ M CCB (\bullet). *Ordinate*, 3-OMG uptake (dpm per μ g total cell protein); *Abscissa*, time in seconds (note log scale). Data points represent the mean \pm S.E. of three separate determinations.

Time Courses of 2-DOG and 3-OMG Uptake

We next sought to determine the properties of GLUT1-mediated uptake in bEnd.3 cells including whether they are able to transport the sugar analogs 2-DOG and 3-OMG. 2-DOG is transported by GLUT1 and phosphorylated by hexokinase, trapping it inside the cell. 3-OMG is a transportable, non-metabolizable substrate of GLUT1. If sugar uptake is protein mediated and GLUT1 specific, then CCB should inhibit uptake regardless of the time transport is measured. In addition, we wanted to determine whether active transport played a role in bEnd.3 sugar uptake. The sodium-glucose co-transporters of the SGLT family are responsible for active uptake of glucose against its concentration gradient, and are sensitive to the compound phlorizin (46). Therefore, we measured sugar uptake using 100 μ M 2-DOG at 37° C over time points ranging from 0-15 minutes in the absence or presence of 10 μ M CCB and 50 μ M phlorizin (Figure 2.4A) Results indicate that 2-DOG uptake progresses in a linear fashion over time, and that uptake is inhibited completely by CCB. The addition of phlorizin had no effect on the background uptake of 2-DOG in the presence of CCB. This result is consistent with sodium independent glucose uptake mediated by GLUT1.

We next sought to determine whether bEnd.3 cells could transport 3-OMG. Therefore, we measured sugar uptake of 5 mM 3-OMG at 4° C over time points ranging from 0-15 minutes, plus a 100 minute equilibrium point in the absence or presence of 10 μ M CCB (Figure 2.4B). Results show that 3-OMG reached equilibration within 3-4 minutes, and as with 2-DOG uptake, was CCB inhibitable, again reinforcing that uptake is protein

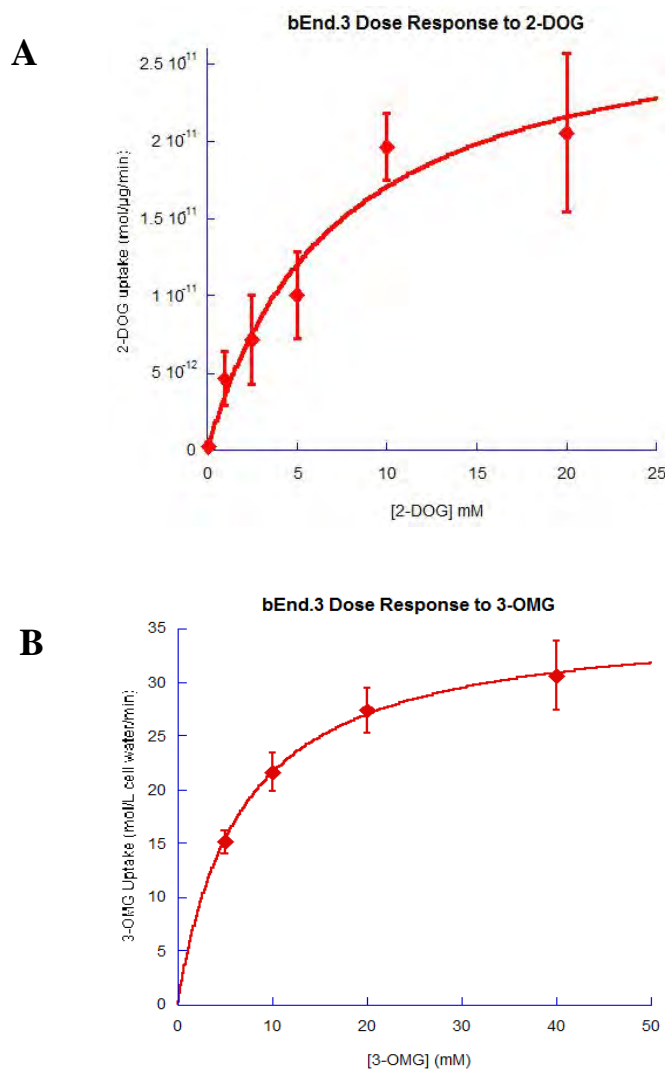


Figure 2.5: bEnd.3 Zero-Trans 2-DOG and 3-OMG Uptake

A. Concentration dependence of zero-trans 2-DOG uptake. *Ordinate*, rate of unidirectional 2-DOG uptake in mol/μg total protein/min; *Abscissa*, [2-DOG] in millimolar. Each point represents the mean ± S.E. of five experiments. *B.* Concentration dependence of zero-trans 3-OMG uptake. *Ordinate*, rate of unidirectional 3-OMG uptake in mol/μg total protein/min; *Abscissa*, [3-OMG] in millimolar. Each point represents the mean ± S.E. of three experiments. Curves were generated from fits to equation 1.

mediated and GLUT1 specific. Time courses of 3-OMG uptake were also performed in the absence and presence of sodium using either potassium or cholate based buffers to confirm the lack of sodium dependent glucose uptake (data not shown). Results indicate no difference in sugar uptake in the absence or presence of sodium, confirming the results seen with phlorizin.

2-DOG and 3-OMG Zero-Trans Uptake Measurements

In order to determine the kinetics of bEnd.3 GLUT1-mediated uptake, we examined the concentration dependence of 2-DOG uptake under *zero-trans* conditions using a 5 minute time point obtained from the time course in Figure 2.4A. Uptake was measured at concentrations from 0.1 to 20 mM 2-DOG at 37° C and results are shown in Figure 2.5A. After fitting to equation 1, a V_{\max} of $2.9 \pm 0.5 \times 10^{-11}$ mol/ μ g/min was obtained, with a K_m of 7 ± 3 mM, indicating that 2-DOG uptake obeys Michaelis-Menten kinetics. Results were converted to mol/cell/min and compared to red cell values in Table 2.3

Due to the rapid equilibration of 3-OMG seen in Figure 2.4B, concentration dependence of 3-OMG uptake was measured at 4° C for 15 seconds at 5 and 10 mM 3-OMG, and 30 seconds at 20 and 40 mM 3-OMG (Figure 2.4B). When the data was fit to equation 1, a V_{\max} of 36 ± 0.6 mol/L/min and a K_m of 6.7 ± 0.4 mM were obtained. The data for 2-DOG and 3-OMG transport were converted into the appropriate units and compared to published values for human red blood cell transport, as seen in Table 2.3. In order to verify the K_m for 3-OMG, we performed a dose response to 3-OMG using 2-DOG as the transportable sugar. Since 2-DOG and 3-OMG compete for the same binding

	2-DOG V_{\max} (mol/cell/min)	2-DOG K_m (mM)	3-OMG V_{\max} (mol/L/min)	3-OMG K_m (mM)	3-OMG V_{\max} (mol/L/min) EE**	3-OMG K_m (mM) EE**
Red Cell*	$4.6 \times 10^{-14} \pm 0.6 \times 10^{-14}$	8 ± 3	1 ± 0.2	0.4 ± 0.1	9 ± 3	23 ± 6
bEnd.3 Cell	$3.4 \pm 1.3 \times 10^{-14}$	7 ± 3	36 ± 0.6	6.7 ± 0.4	114 ± 53	19 ± 19

Table 2.3: Summary of 2-DOG and 3-OMG Kinetics in bEnd.3 and Red Cells

* as referenced in (208)

** denotes equilibrium exchange transport

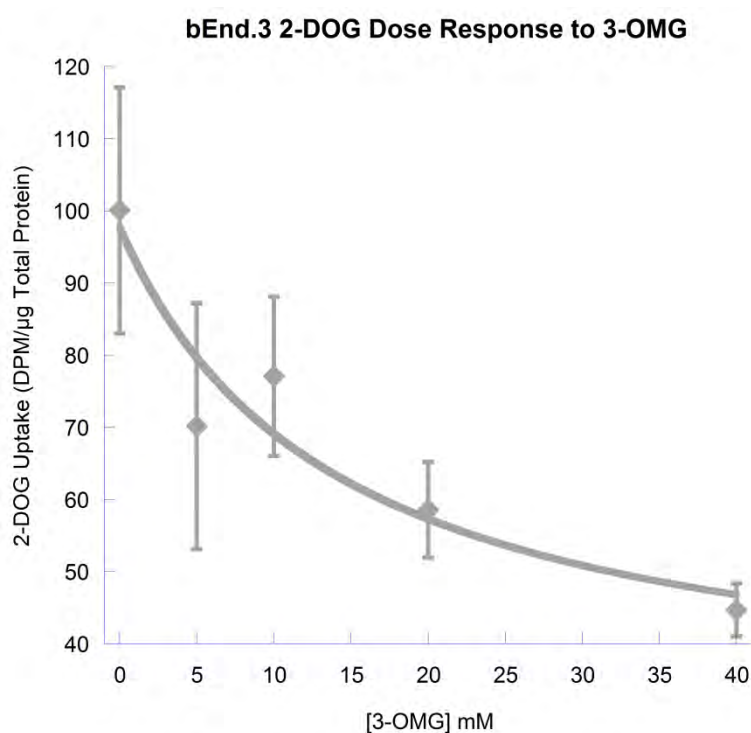


Figure 2.6: 2-DOG Dose Response to 3-OMG

Concentration dependence of zero-trans 2-DOG uptake was measured in the presence of increasing concentration of 3-OMG. *Ordinate*, total 2-DOG uptake/ μg total protein; *Abscissa*, [3-OMG] in millimolar. Each point represents the mean \pm S.E. of two experiments. Curve was generated by fitting data to equation 2, and K_m was determined from the fit.

site, one can be used to inhibit the other. The K_m can be extracted for the inhibiting sugar (3-OMG) when fit to equation 2. Therefore, using a fixed concentration of 2-DOG (100 μ M), we measured inhibition of uptake by 3-OMG over a range of concentrations from 0-40 mM (Figure 2.6). Results were fit to equation 2, and a K_{iapp} of 14 mM was obtained for 3-OMG. Results are summarized in Table 2.3. Based on these experiments, 2-DOG *zero-trans* uptake is in agreement with red cell values, while 3-OMG *zero-trans* uptake appears to have a 35-fold higher V_{max} and 30-fold higher K_m than established values for GLUT1-mediated sugar transport in red blood cells at ice temperature.

Equilibrium Exchange 3-OMG Uptake

Since endothelial cells are rarely depleted of intracellular sugar *in vivo*, we next measured sugar uptake in bEnd.3 cells under equilibrium exchange conditions that more closely resemble those experienced at the blood-brain barrier. Increasing concentrations of 3-OMG were added to bEnd.3 cells prior to uptake so intracellular and extracellular glucose could equilibrate. Cells were then cooled to 4° C, and unidirectional uptake was measured using a trace amount of [³H]-3-OMG in increasing concentrations of cold 3-OMG from 5-20 mM (Figure 2.7). Results were fit to equation 1, yielding a V_{max} of 114 ± 53 mol/L/min with a K_m of 6.7 ± 0.4 mM. Results were compared to known red cell values in Table 2.3. Based on these experiments, equilibrium exchange transport in bEnd.3 cells is approximately 12-fold faster than red cell V_{max} , while K_m values are in agreement with those previously published. Equilibrium exchange transport is also 3-fold

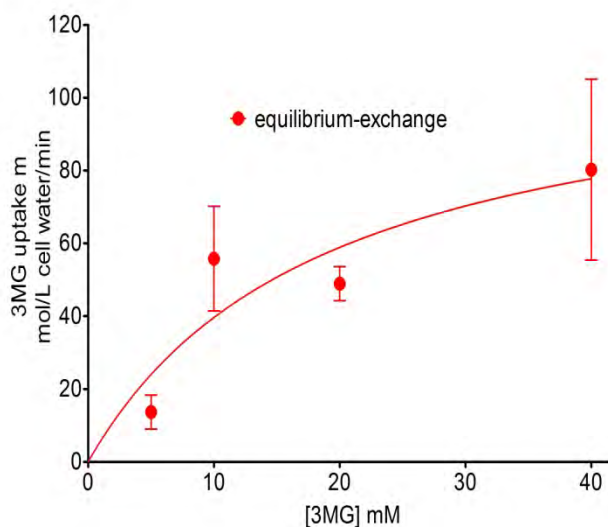


Figure 2.7: bEnd.3 Equilibrium Exchange Transport

Cells were pre-loaded 5-20 mM of 3-OMG and allowed to equilibrate before cooling to 4 °C and measuring unidirectional 3-OMG uptake. *Ordinate* rate of 3-OMG uptake in mol/ μ g total protein/minute. *Abscissa* 3-OMG concentration in mM. Curves were computed using equation 1. Each point represents the mean \pm S.E. for three experiments.

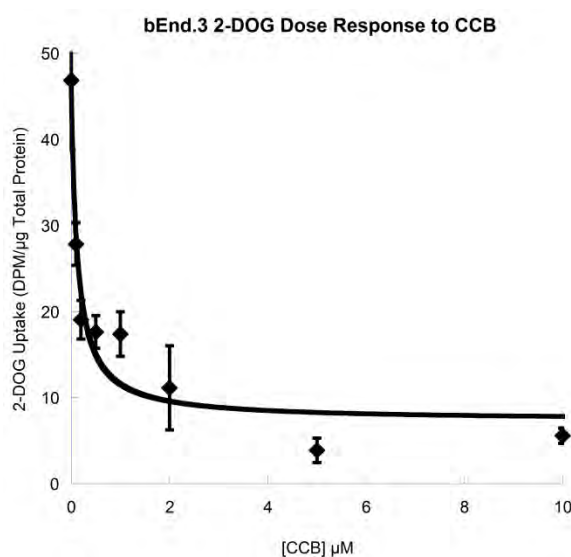


Figure 2.8: Dose Response to CCB

Concentration dependence of zero-trans 2-DOG uptake was measured in the presence of increasing concentration of CCB. *Ordinate*, 2-DOG uptake/ μ g total protein; *Abscissa*, [CCB] in nM. Each point represents the mean \pm S.E. of three experiments. Curve was generated by fitting data to equation 2, and K_i was determined from the fit.

faster than zero-trans uptake in bEnd.3 cells, indicating that trans-acceleration is occurring.

bEnd.3 Dose Response to CCB

CCB is a specific competitive inhibitor of GLUT-mediated transport with a known K_i of 100-200 nM (138). Based on the differences seen between bEnd.3 V_{max} and K_m values from red cells, we wanted to measure the K_i for CCB inhibition of bEnd.3 glucose transport to see if there were differences between murine and human cells. We used 100 μ M 2-DOG to measure sugar uptake with increasing concentrations of CCB and fit the data to equation 2 (Figure 2.8). Based on our analysis, the K_i obtained was 122 ± 47 nM and agrees with red cell values for the K_i of CCB.

Discussion

In this study, we characterized the bEnd.3 cell line as a potential system for studying acute metabolic stress at the blood-brain barrier. We compared sequences for human and mouse GLUT1, and screened bEnd.3 cells for not only GLUT1 expression, but also other GLUT family members by RT and qPCR. We detected GLUT1 protein in bEnd.3 cells by Western blot, and characterized the kinetics of 2-DOG and 3-OMG uptake, as well as CCB inhibition of transport. Finally, we compared the values obtained from transport studies to established values in red blood cells. Detecting GLUT1 mRNA and protein in bEnd.3 cells with anti-human GLUT1 antibodies was unsurprising based on sequence alignment and preliminary characterization of the cell line (205). The absence of other class 1 GLUTs 2, 3, and 4 is beneficial, since each of these proteins is able to transport 2-

DOG and 3-OMG, and each is CCB sensitive. In addition, the varying V_{\max} and K_m values for 2-DOG and 3-OMG uptake by these proteins would complicate the kinetic analysis of bEnd.3 sugar uptake. The presence of GLUT8 and GLUT9 mRNA was an unexpected result, since GLUT8 is traditionally thought to be localized to neurons and astrocytes (97), and GLUT9 is primarily found in digestive tissues (81). However, our data suggest that relative expression of these proteins in comparison to GLUT1 is too low to contribute significantly to sugar uptake in bEnd.3 cells. In addition, GLUT8 is not shown to be expressed at the plasma membrane, so its contribution to glucose uptake would not be a factor, even if protein resides in bEnd.3 cells (100). GLUT9 is CCB insensitive, so its contribution to sugar uptake could be readily accounted for in the presence of CCB and subtracted out of total uptake seen in bEnd.3 cells. However, our observations demonstrate that the majority of sugar transport is CCB inhibitable and sodium insensitive in bEnd.3 cells. In addition, GLUT9 demonstrates slow glucose uptake in the absence of urate, since urate and glucose have been shown to stimulate the uptake of one another when on the opposite sides of the cell membrane (92). As a result, even if GLUT9 protein exists in bEnd.3 cells, it is unlikely that it can contribute significantly to the kinetics of sugar uptake in bEnd.3 cells.

Because of the differences in sequence between human and mouse GLUT1, we wanted to compare the transport data we obtained to kinetics measured in a well established GLUT1-containing system using two known substrates of human GLUT1: 2-DOG and 3-OMG. The red blood cell is the best characterized cell system for studying GLUT1-mediated transport, and for this reason we chose them as a standard. Our results show

that bEnd.3 cells are able to transport 2-DOG in a saturable manner with V_{\max} and K_m values that are almost identical to red blood cells, indicating that the sequence differences between human and mouse GLUT1 don't seem to affect 2-DOG binding. This data is also in agreement with tentative 2-DOG uptake experiments performed in bEnd.3 cells (205). Although the K_m of hexokinase for 2-DOG is approximately the same as the concentration of 2-DOG used to measure uptake (100 μM), our analysis seems to indicate that hexokinase activity is not affecting 2-DOG uptake by GLUT1. Since uptake proceeds in a linear fashion during the time course experiment, the free 2-DOG is very low compared to 2-DOG phosphorylated by hexokinase, therefore free 2-DOG is unlikely to play a role in affecting the kinetics of GLUT1-mediated uptake. When 3-OMG is used as an inhibitor of 2-DOG uptake (Figure 2.6), the measurements become more complex. 3-OMG rapidly equilibrates at 37 °C even at low concentrations, which complicates measurements of 2-DOG uptake in the following ways: 1. 2-DOG and 3-OMG compete for entry into the cell via GLUT1, thus inhibiting 2-DOG uptake; 2. 3-OMG on the inside of the cell will stimulate uptake of 2-DOG outside the cell by *trans-acceleration*; and 3. 3-OMG inside the cell will inhibit 2-DOG exit from the cell, however, 3-OMG will not affect hexokinase activity, therefore 2-DOG is still phosphorylated upon entry into the cell. It could be argued, therefore, that the measurements obtained in Figure 2.6 actually show the V_{\max} for hexokinase activity and the K_m for GLUT1 transport of 2-DOG. Though imperfect, the analysis proves useful for estimating the K_i for 3-OMG in bEnd.3 cells.

There are stark differences between 3-OMG *zero-trans* and equilibrium exchange uptake in red blood cells and bEnd.3 cells. Our results show that GLUT1-mediated *zero-trans* sugar uptake is 33-fold faster, while equilibrium exchange transport is 12-fold faster than red blood cells. In addition, bEnd.3 cells demonstrate a 30-fold lower affinity for 3-OMG than red blood cells in our *zero-trans* measurements. One possible explanation could be the sequence differences that confer altered GLUT1 affinity for 3-OMG in bEnd.3 cells. However, both our 3-OMG equilibrium exchange and CCB dose response data argue against this, since 3-OMG equilibrium V_{\max} and K_m and CCB K_i values are comparable to red blood cells. In addition, both the V_{\max} and K_m for 3-OMG have been confirmed by studies from our lab in the murine fibroblast cell line 3T3-L1, in the 2-DOG dose response experiment, and when comparing known values in blood-brain barrier cells ((209) and unpublished observations). It has long been suspected that due to the complexity of red blood cell sugar transport and its inability to conform to current kinetic models, that measurements of transport, particularly 3-OMG, are underestimated (148,208). Based on our analysis, it would appear that this is the likely explanation for discrepancies between our data and current red-cell data. It is more likely that the red cell *zero-trans* 3-OMG uptake experiments need to be revisited.

Despite the differences in raw kinetic values for 3-OMG uptake, GLUT1-mediated transport in bEnd.3 cells share a signature property with red cells, namely the ability to undergo *trans*-acceleration. Our data shows that bEnd.3 3-OMG uptake is approximately 3-fold faster in cells pre-loaded with 3-OMG versus cells containing no intracellular sugar. Red blood cell equilibrium exchange transport is 9-fold faster than zero-trans

uptake. This data indicates that sequence differences between human and murine GLUT1 do not seem to be involved in conferring the ability to *trans*-accelerate in the presence of intracellular sugar. This data also suggests that murine GLUT1 must exist as at least a dimer, if not a tetramer in the plasma membrane. Since *trans*-acceleration is unable to occur with monomeric GLUT1 based on available kinetic models, it is more likely that bEnd.3 cells contain oligomeric GLUT1 like their red blood cell counterparts. The differences in the amount of *trans*-acceleration seen in bEnd.3 versus red cells could again be attributed to the complexity of red cell transport, and revisiting these measurements might provide clearer insight into red cell kinetics.

In summary, our results indicate that, despite some discrepancies between erythrocyte and bEnd.3 3-OMG uptake, the bEnd.3 cell line appears to be a good model system amenable to studying blood-brain barrier sugar uptake. Further studies will focus on the response of bEnd.3 cell GLUT1-mediated sugar uptake to acute metabolic stress by looking at both the kinetics of sugar transport and the localization of GLUT1 at the plasma membrane.

CHAPTER III

ACUTE MODULATION OF SUGAR TRANSPORT IN BRAIN CAPILLARY ENDOTHELIAL CELL CULTURES DURING ACTIVATION OF THE METABOLIC STRESS PATHWAY

Abstract

GLUT1-catalyzed equilibrative sugar transport across the mammalian blood-brain barrier is stimulated during acute and chronic metabolic stress; however, the mechanism of acute transport regulation is unknown. We have examined acute sugar transport regulation in the murine brain microvasculature endothelial cell line bEnd.3. Acute cellular metabolic stress was induced by glucose-depletion, by potassium cyanide (KCN) or by carbonyl cyanide-p-trifluoromethoxyphenylhydrazone (FCCP), which reduce or deplete intracellular ATP within 15 minutes. This results in a 1.7 to 7-fold increase in V_{\max} for zero-trans 3-O-methylglucose uptake (sugar uptake into sugar-free cells) and a 3-10 fold increase in V_{\max} for equilibrium exchange transport (intracellular [sugar] = extracellular [sugar]). Neither GLUT1 mRNA nor total protein levels are affected by acute metabolic stress. Cell-surface biotinylation reveals that plasma membrane GLUT1 levels are increased 2-3 fold by metabolic depletion while cell surface Na^+, K^+ ATPase levels remain unaffected by ATP-depletion. Treatment with the AMP-activated kinase agonist, AICAR, increases V_{\max} for net 3MG uptake by 2-fold. Glucose depletion and treatment with KCN, FCCP, and AICAR also increase AMP-dependent kinase phosphorylation in bEnd.3 cells. These results suggest that metabolic stress rapidly

stimulates blood-brain barrier endothelial cell sugar transport by acute up-regulation of plasma membrane GLUT1 levels, possibly involving AMPK activity.

Introduction

The cells of the mammalian brain do not contain large stores of glycogen. It is essential, therefore, that glucose uptake by the brain exceeds glucose utilization in order to maintain proper brain function. To enter the brain, serum glucose must cross the blood-brain barrier: an epithelium comprising endothelial cells connected by tight junctions that prevent paracellular diffusion of glucose and other nutrients. Thus, glucose transport into the brain requires trans-endothelial cell transport. This process is catalyzed by the glucose transport protein GLUT1, which is expressed at both luminal and abluminal membranes of the endothelium (39,73,210-212).

Endothelial cells of the blood-brain barrier (bEND) differ from those of the peripheral circulatory system (pEND) in several important ways: 1) bEND cells contain 2 to 5-fold more mitochondria than pEND cells (25); 2) Brain capillary walls (comprising bEND cells) are 40% thinner than capillary walls of the peripheral circulation (24); 3) pEND cells present significantly fewer tight junctions than bEND cells (26); 4) bEND cell tight junction complexes result in polarized cell surface protein expression that is less marked or absent in pEND cells (26). The resulting bEND cell architecture may give rise to behaviors that differ from those of pEND cells but which resemble those of other metabolically active cells and thereby optimally support blood-brain barrier physiology (e.g. transport sensitivity to loss of cellular oxidative metabolic capacity).

Although a simple, equilibrative process, GLUT1-mediated trans-endothelial cell sugar transport appears to be tightly regulated. Sugar transport into the brain only narrowly exceeds brain glucose utilization under normal conditions (13). Under conditions of metabolic stress, such as hypoxia (194), hypoglycemia (196,197,213), and seizures (75,200), the glucose import capacity of the brain is up-regulated. Endothelial cell affinity for transported sugars appears to be unchanged (200). There are three possible explanations for increased V_{\max} for transport: 1) Increased GLUT1 at the plasma membrane, either through increased protein expression or recruitment of intracellular stores; 2) Enhanced intrinsic activity of GLUT1 which catalyzes faster translocation of substrate through the carrier, as seen in the ATP-modulation of GLUT1 in erythrocytes (114,151,153,155,214), or 3) A combination of both effects.

Chronic stress induces transcriptional up-regulation of endothelial GLUT1 levels *in vitro* (215), and *in vivo* (216). While increased protein expression could account for acute stimulation of sugar transport, immunogold staining of cells during seizures has not conclusively demonstrated altered cellular GLUT1 content (217).

Between 30-50% of total cellular GLUT1 resides in cytosolic vesicles in endothelial cells (186). GLUT1 recruitment to the plasma membrane occurs in response to acute metabolic stress in rat liver epithelial cells *in vitro* (182) and in response to growth factor stimulation in bovine retinal endothelial cells (164). We therefore set out to examine whether cultured, brain microvessel endothelial cells respond to acute metabolic stress with increased sugar transport capacity and, if so, to test the hypothesis that increased V_{\max} for sugar uptake results from recruitment of intracellular GLUT1 to the plasma

membrane. Using the mouse brain microvascular endothelial cell line bEnd.3 (205), we have determined the steady-state kinetics of GLUT1-mediated sugar transport in the absence and presence of glucose or the metabolic poisons potassium cyanide (KCN) and carbonyl-cyanide-p-trifluoromethoxyphenylhydrazone (FCCP). We established conditions for bEnd.3 cell ATP-depletion, measured total GLUT1 mRNA and protein levels, and measured changes in plasma membrane levels of GLUT1. We show that ATP depletion of bEnd.3 cells increases V_{\max} for sugar transport and increases plasma membrane GLUT1 levels without changing endothelial cell GLUT1 mRNA or total GLUT1 protein levels. We also show that glucose depletion and treatment with KCN and FCCP increase the phosphorylation of the AMP-activated protein kinase AMPK. Treatment of bEnd.3 cells with the AMPK agonist AICAR increases both the V_{\max} for sugar transport and the phosphorylation of AMPK. Taken together, this data suggests a potential role for AMPK in regulating the acute endothelial cell response to metabolic stress.

Experimental Procedures

Tissue Culture

bEnd.3 cells were obtained from ATCC and maintained in Dulbecco's Modified Eagle Medium (DMEM) from Gibco supplemented with 10% fetal bovine serum (FBS) from Hyclone and 1% Penicillin/Streptomycin (Pen/Strep) solution (Gibco) at 37°C in a humidified 5% CO₂ incubator. All experiments were performed at cell confluence. Plates were subcultured at a ratio of 1:2-1:3 by washing with sterile Dulbecco's phosphate

buffered saline (DPBS) and treating with 0.5% Trypsin-EDTA (Gibco) for 5-7 minutes at 37°C. Passages 3-16 were used in all experiments.

Antibodies

A custom, affinity-purified rabbit polyclonal antibody raised against a synthetic peptide corresponding to GLUT1 amino acids 480-492 was produced by New England Peptide. A mouse monoclonal antibody against Na⁺, K⁺ ATPase was purchased from Abcam. Rabbit polyclonal and monoclonal antibodies against AMPK and phosphorylated AMPK were obtained from Cell Signaling Technology. HRP conjugated Goat anti-rabbit and Goat anti-mouse secondary antibodies were obtained from Jackson Labs.

Buffers

Cell lysis buffer consisted of 5 mM HEPES, 5 mM MgCl₂, 150 mM NaCl, 50 μM EDTA, and 1% SDS. Uptake stop solution included 10 μM cytochalasin B (CCB, Sigma) and 100 μM phloretin (Sigma) in DPBS. TAE Buffer consisted of 40 mM Tris base, 1 mM EDTA, and 20 mM acetic acid. TBS was composed of 20 mM Tris base and 135 mM NaCl, pH 7.6. TBST comprised TBS buffer with 0.2% Tween-20. Biotin Quench solution was composed of 250 mM Tris base. Biotin lysis buffer contained TBS with 0.5% Triton-X-100.

Quantitative Reverse Transcriptase PCR

Confluent 100 mm dishes of bEnd.3 cells were washed with DPBS, then incubated in DPBS, DPBS+ 5 mM KCN or DPBS+ 8 μg/ml FCCP for 10 minutes. Plates were then

washed 2 times in ice cold DPBS, and total RNA was isolated using Qiagen's RNeasy kit and Qiashredder as per kit instructions. Quantitative RT-PCR was performed using an iScript One-Step RT-PCR Kit with SYBR Green (Bio-Rad). Each reaction was run in duplicate using the following primers (IDT): GLUT1: 5'-AGCCCTGCTACAGTGTAT-3' and 5'-AGGTCTCGGGTCACATC-3' which generated a DNA fragment of 135 bp; GLUT8: 5'-TGTGGGCATAATCCAGGT-3' and 5'-GGT CAGTTTGAAGTAGGTAC-3' which produced a DNA fragment of 140 bp, GLUT9: 5'-CTCAT TGTGGGACGGTT-3' and 5'-CAGATGAAGAT GGCAGT-3' which produced a DNA fragment of 132 bp, and as a mouse expression control, EIF1 α : 5'-CAACATCGTCGTAATCGGACA-3' and 5'-GCTTAAGACCCAGGCGTACTT-3' which was used to normalize PCR data (207). Samples were run on an MJ-Research PTC-200 Peltier Thermal Cycler with a Chromo4 Real Time PCR detector using Opticon Monitor 3 software (Bio-Rad). Relative RNA expression was quantitated using the $\Delta\Delta CT$ method. All primers were verified using Qiagen's One-Step RT-PCR Kit and run on a 2% agarose gel in TAE. Bands were visualized by ethidium bromide staining under UV light on a Fujifilm LAS-3000 and gels were analyzed using Fujifilm Multigauge 3.0.

bEnd.3 Cell ATP Depletion

Confluent bEnd.3 cells in 12-well dishes were washed twice with DPBS and incubated with DPBS + 5 mM glucose, DPBS + glucose + 5 mM KCN, or DPBS + glucose + 8 μ g/ml FCCP for various intervals. Cells were processed and assayed using a luciferin-luciferase based ATP assay kit per kit instructions. Luminescence measurements were

made using a Turner Veritas microplate luminometer or a Turner 20/20ⁿ Single Tube Luminometer.

ATP Recovery of bEnd.3 Cells

Confluent bEnd.3 cells in 12-well dishes were washed twice with DPBS and treated with DPBS + 5 mM glucose, DPBS + glucose + 5 mM KCN, or DPBS + glucose + 8 $\mu\text{g/ml}$ FCCP for 10 minutes at 37°. The media were aspirated and replaced with normal cell growth media (DMEM + FBS + Pen-Strep). Cells were placed at 37° in normal growth media and incubated for various times. Cell processing and ATP measurements were performed as per kit instructions.

Zero-Trans Sugar Uptake Measurements

Confluent 150 mm² dishes of bEnd.3 cells were split into 12-well plates the afternoon before each experiment. On the day of the assay, cells were placed in serum-free DMEM for 2 hours at 37°C. Plates for AMPK activation measurements were treated with 2 mM of AICAR (Fisher) in serum-free DMEM for 2 hours at 37°C. Cells were washed with 1 ml of either DPBS, or DPBS containing 5 mM KCN or 8 $\mu\text{g/ml}$ FCCP and containing or lacking 5 mM glucose. Cells were incubated in 0.5 ml wash media for 10 minutes at 37°C, then placed on ice to cool in glucose-free medium. Incubation on ice for 10-15 minutes depletes intracellular sugar levels (via export) without changing cytoplasmic ATP levels. Wash medium was drained, and cells were treated with 400 μl of increasing concentrations of 3-O-methylglucose (3-OMG) containing 2.5 $\mu\text{Ci/ml}$ [³H]-3-O-methylglucose ([³H]-3-OMG) in DPBS in the absence and present of the appropriate

poison (KCN, FCCP, or AICAR). Uptake proceeded for 15 seconds at 5 mM and 10 mM 3-OMG, and for 30 seconds at 20 and 40 mM 3-OMG. Uptake was stopped by adding 1 ml of uptake stop solution and the media immediately aspirated. Each well was washed twice more with 1 ml of stop solution and treated with 0.5 ml of cell lysis buffer. Samples were counted in duplicate by liquid scintillation spectrometry (Beckman). Each measurement was performed in triplicate. Protein concentrations for each sample were determined using Pierce's BCA protein assay kit.

Equilibrium Exchange Sugar Uptake Measurements

In these experiments, intracellular concentrations of 3-OMG are equal to extracellular 3-OMG, therefore transport is measured using [^3H]-3-OMG. Transport measurements were similar to zero-trans uptake measurements with the following modifications: Cells were serum-depleted in DMEM containing 5, 10, 20, or 40 mM 3-OMG for 2 hours. Cells were washed and incubated as previously described with wash media containing 5, 10, 20, or 40 mM 3-OMG in DPBS, DPBS with 5 mM KCN, or DPBS with 8 $\mu\text{g/ml}$ FCCP. Uptake was measured and terminated as described previously. Cells were then washed and processed as above.

Analysis of Sugar Uptake

All data analysis was performed using Synergy Software's Kaleidagraph Version 4.0. For zero-trans and equilibrium exchange transport experiments, background counts were subtracted and uptake, v , was normalized to total protein/well. Sugar uptake data was fitted to the Michaelis-Menten equation (Equation 1):

$$v = \frac{V_{max}[S]}{K_m + [S]}$$

by non-linear regression and V_{max} and K_m values were extracted from the fits.

Western Blotting of bEnd.3 Cells

Confluent 100 mm dishes of bEnd.3 cells were washed with DPBS and incubated in the absence or presence of 5 mM KCN or 8 μ g/ml FCCP for 10 minutes; incubated in the absence of 5mM glucose for 30 minutes; or incubated in the presence of 2 mM AICAR for 2 hours as previously outlined. Cells were then washed twice with DPBS, lysed, and analyzed for total protein concentration using a micro BCA kit (Pierce). Lysates were normalized for total protein and run on either 4-12% Bis-Tris or 10% Bis-Tris gels in MES buffer (Invitrogen), transferred to PVDF membranes (ThermoFisher), blocked with either 5 or 10% bovine serum albumin (BSA), and probed with either 1:10,000 dilution of C-terminal antibody, a 1:5,000 dilution of mouse $\text{Na}^+ \text{K}^+$ ATPase antibody, or a 1:1,000 dilution of rabbit AMPK or AMPK (pThr 172) antibody. A 1:30,000 dilution of either HRP-conjugated goat anti-rabbit or goat anti-mouse secondary antibody was also used (Jackson Labs). Chemiluminescence was visualized either on film, or using the Fujifilm LAS-3000 with SuperSignal Reagent (Pierce). Band densities were quantitated using ImageJ software.

Biotinylation of bEnd.3 cells

150 mm^2 plates of confluent bEnd.3 cells were washed twice with 25 ml of DPBS and incubated with 25 ml of either DPBS alone or DPBS containing 5 mM KCN or 8 μ g/ml

FCCP for 10 minutes at 37°C. Plates were washed twice with ice-cold DPBS, and incubated on ice in 12 ml of DPBS containing 1 mM EZ-Link Sulfo-NHS-SS-Biotin for 30 minutes with gentle rocking. The reaction was quenched with 2 ml biotin quench solution. Cells were gently scraped into solution, washed with TBS, and pelleted. After washing a second time with TBS, cells were resuspended in biotin lysis buffer and biotinylated proteins were incubated with streptavidin beads in the absence or presence of 10,000 units (20 μ L) of PNGase F (New England Biolabs) at 37°C for 1 hour. Biotinylated proteins were then washed and released from streptavidin beads using 150 mM DTT. Protein concentrations were determined using BSA as a standard. Samples were normalized for total protein and analyzed by Western blot.

Results

ATP Depletion of bEnd.3 Cells

ATP levels were measured in bEnd.3 cells treated with PBS containing 5 mM glucose in the absence and presence of either 5 mM KCN or 8 μ g/ml FCCP for up to two hours (Figure 3.1). While ATP depletion occurs within the first 15 minutes of treatment with both poisons, ATP levels in KCN treated cells show a small bounce by 30 minutes and then remain stable. ATP levels in FCCP treated cells are rapidly depleted and remain low throughout the time course. The effects of poisons are dose-dependent with half-maximal effects observed at 3 μ M KCN and 0.25 ng/mL FCCP (Figure 3.2A and 3.2B).

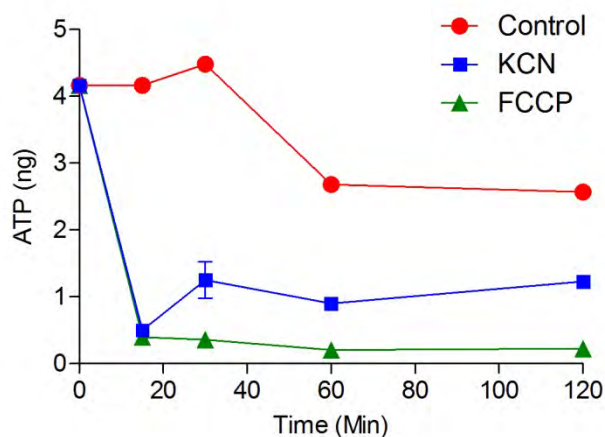


Figure 3.1: ATP Depletion in bEnd.3 Cells

Time course of ATP depletion of bEnd.3 cells incubated with PBS containing 5mM glucose (●), 5mM glucose +5 mM KCN (■), or 5 mM glucose + 8 μ g/ml FCCP (▲). *Ordinate*, ATP levels in ng per 100 μ l of cell extract. *Abscissa*, time of cellular exposure to poison in minutes. Data points represent the mean \pm S.E. for three ATP assays.

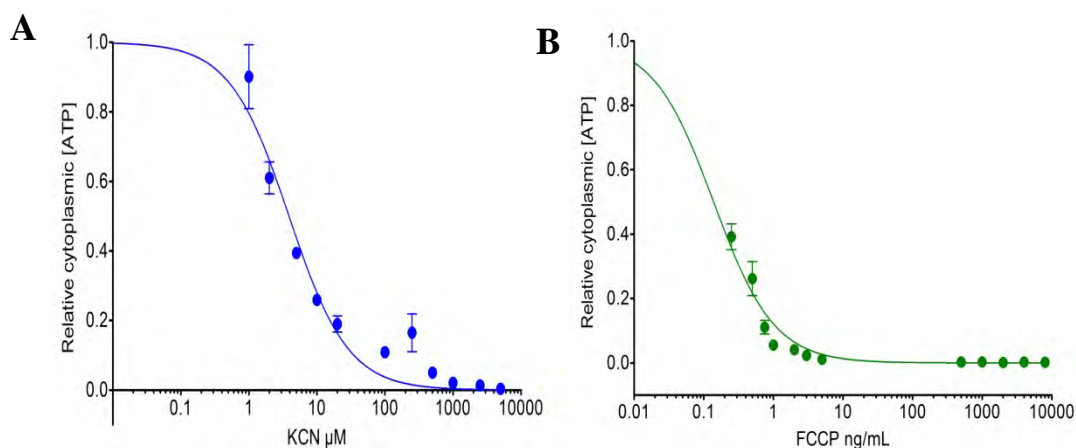


Figure 3.2: bEnd.3 Dose Dependent ATP Depletion

Cells were exposed to varying [poison] for 10 min at 37 $^{\circ}$ C and then cooled, and cellular ATP content was measured as described previously. *Ordinates*, relative to cytoplasmic [ATP] (luminescence per unit of cell protein); *Abscissa*: A. [KCN], B. [FCCP]. Results are shown as mean \pm S.E. for three experiments. Curves were computed assuming that [ATP] decreases in a saturable manner with [poison].

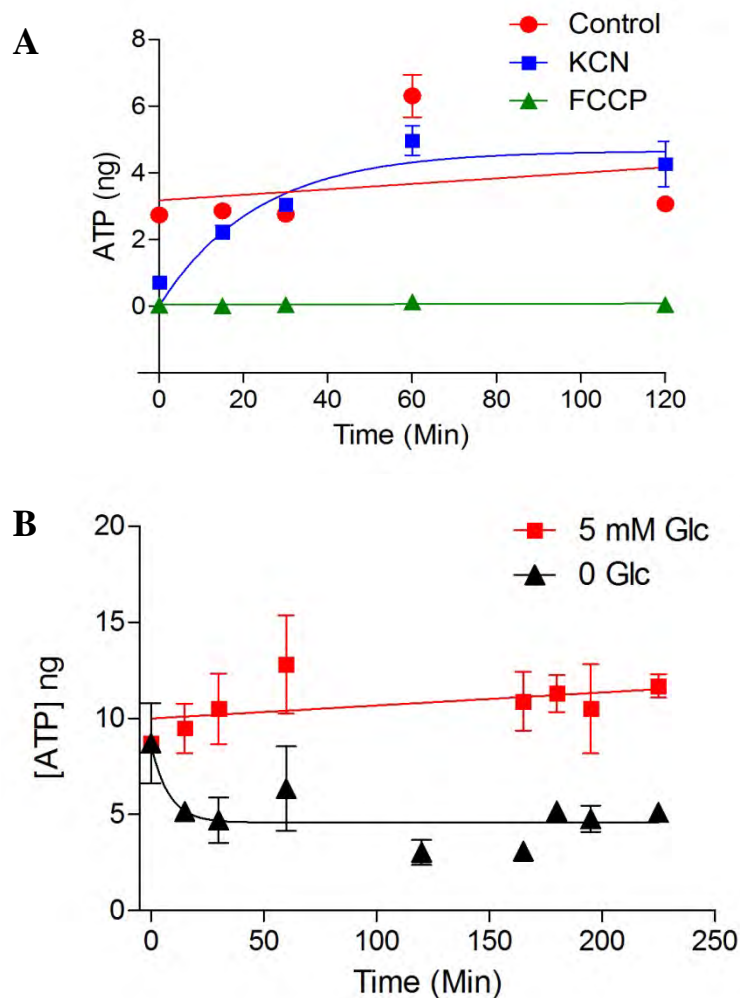


Figure 3.3: ATP Depletion and Recovery in bEnd.3 Cells

A, Time course of ATP recovery following poisoning. Cells were treated with PBS containing 5mM glucose (●), 5mM glucose +5 mM KCN (■), or 5 mM glucose + 8 μg/ml FCCP (▲) for 10 min and then restored to normal growth media (PBS plus 5mM glucose) for the times indicated. *Ordinate*, ATP levels in nanograms per 100 μl of extract. *Abscissa*, time (minutes) that cells were allowed to recover from initial poisoning. Data points represent the mean ± S.E. for three separate ATP assays. *B*, Time course of glucose depletion-induced ATP-depletion in bEnd.3 cells. Cells were treated with PBS containing 5 mM glucose (■) or 0 glucose (▲) for 0–230 min at 37 °C. *Ordinate*, ATP levels in ng. *Abscissa*, time (minutes) that cells were exposed to 0 or 5mM glucose. Data points represent the mean ± S.E. for three separate ATP assays.

We next examined the time course of ATP recovery following treatment with KCN and FCCP (Figure 3.3A). bEnd.3 cells were poisoned for 10 minutes, then the media were replaced with normal cell growth media and cells were sampled for ATP assays for up to two hours post-poisoning. KCN washout allows cells to recover normal ATP levels within 60 minutes. ATP levels in FCCP-treated cells do not recover. Removal of extracellular glucose rapidly decreases cytoplasmic [ATP] by 50% (Figure 3.3B).

Zero-Trans Sugar Uptake

We next asked whether bEnd.3 cell ATP depletion affects sugar uptake. 3-OMG is a nonmetabolizable transport substrate. Sugar uptake at 10 mM 3-OMG and 4 °C shows simple monoexponential kinetics with a half-time of approximately 4 min. ATP-depletion with FCCP (10 min at 8 µg/ml) or KCN (10 min at 5 mM) reduces the half-time for uptake to 2 and 1 minute respectively (Figure 3.4A) and have the following constants: control, equilibrium space = 5.65 ± 0.38 dpm/µg; $k = 0.0032 \pm 0.0005$ /s; FCCP, equilibrium space = 5.60 ± 0.53 dpm/µg, $k = 0.0073 \pm 0.0017$ /s; and KCN, equilibrium space = 6.43 ± 0.58 dpm/µg, $k = 0.0089 \pm 0.0019$ /s. These data indicate that the equilibrium 3-OMG space of the cells is not significantly affected by metabolic depletion indicating that poisons do not alter cell volume. The rate of sugar uptake in control and poisoned cells is inhibited by $84 \pm 16\%$ by the sugar transport inhibitor CCB with $K_i = 122 \pm 47$ nM ($n = 3$) indicating that sugar import is protein-mediated.

V_{\max} and K_m for 3-OMG transport were obtained by nonlinear regression analysis of the concentration dependence of sugar uptake assuming that uptake is described by the

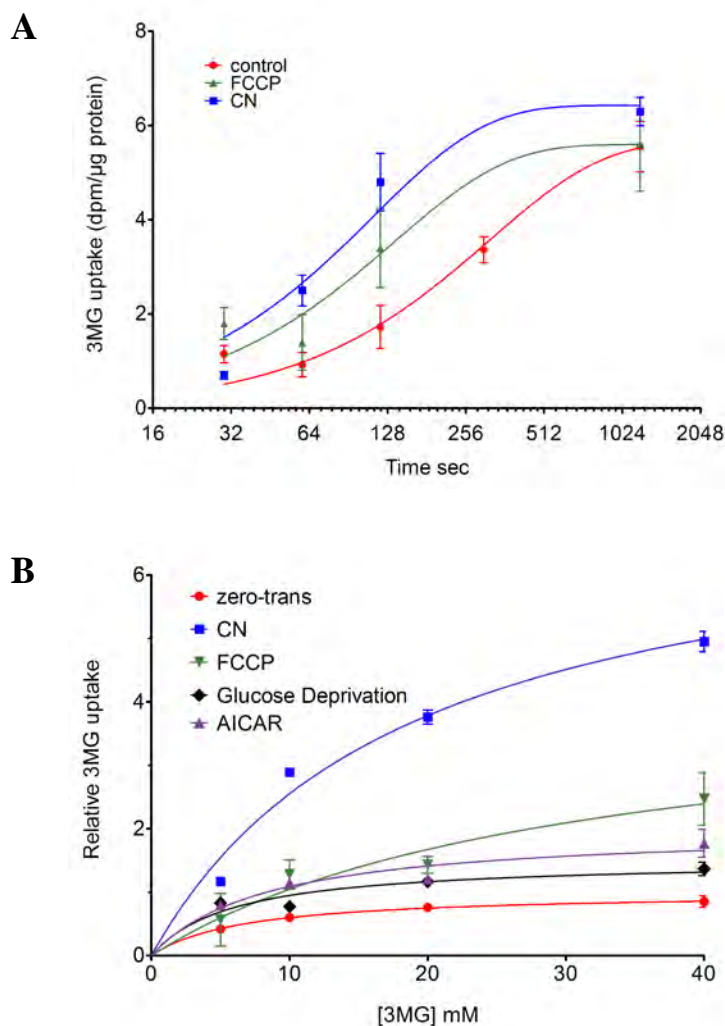


Figure 3.4: Sugar uptake at 4 °C in bEnd.3 cells.

A, Time course of 20 mM 3-OMG uptake in control cells (●) or in cells exposed to 5mM KCN (■) or to 8 µg/ml FCCP (▲) for 15 min at 37 °C prior to cooling, glucose depletion, and transport initiation. *Ordinate*, 3-OMG uptake (dpm/µg total cell protein); *Abscissa*, time in seconds (note the log₂ scale). Data points represent the mean ± S.E. of three separate experiments. Curves drawn through the points were computed by nonlinear regression assuming monoexponential 3-OMG uptake. B, concentration dependence of zero-trans 3-OMG uptake in control cells (●), cells exposed to 5mM KCN (■), 8 µg/ml FCCP (▲), 0 glucose (◆), or to 2mM AICAR (●) for 15 min at 37 °C. *Ordinate*, relative rate of unidirectional 3-OMG uptake; *Abscissa*, [3-OMG] in mM. Curves were computed by nonlinear regression using equation 1, and the resulting V_{max} and $K_{m(app)}$ values are summarized in Table 1. Each point represents the mean ± S.E. of three to eight separate experiments.

^a zero-trans uptake^b Equilibrium exchange uptake

	^c K _m	^c 95% confidence intervals	^c relative V _{max}	^c 95% confidence intervals	^d n	K _m	^c 95% confidence intervals	^c relative V _{max}	^c 95% confidence intervals	^d n
Control	6.7 ± 0.4	5.1 to 8.4	1	0.9 to 1.1	12	14.9 ± 12.6	-62.2 to 99.9	^e 3.17 ± 0.46	-3.1 to 9.5	3
KCN	18.7 ± 6.7	-10.5 to 47.9	^{e,f} 7.32 ± 1.2	2.1 to 12.6	6	18.4 ± 13.9	-41.4 to 78.3	^e 10.0 ± 3.5	-4.8 to 24.9	3
FCCP	30.1 ± 18.4	-48.9 to 109.2	4.26 ± 1.4	-1.8 to 10.2	6	35.9 ± 27.8	-83.9 to 155.8	^e 14.6 ± 6.5	-13.5 to 42.6	3
-Glc	29.4 ± 11.0	-17.8 to 76.4	^e 1.7 ± 0.3	0.2 to 3.2	3	N/D				
AICAR	3.9 ± 1.9	-20.1 to 27.8	^e 1.5 ± 0.2	-1.1 to 4.1	3	N/D				

Table 3.1: Summary of bEnd. 3-OMG Transport^a unidirectional sugar uptake into cells depleted of sugar at 4°C for 15 min^b unidirectional sugar uptake into cells where [3MG]_I = [3MG]_o^c the concentration dependence of sugar uptake was analyzed by non-linear regression assuming Michaelis-Menten kinetics to obtain K_m and V_{max}. All V_{max} values are expressed relative to V_{max} for zero-trans uptake in matched control cells. Control zero-trans 3MG uptake V_{max} = 180 pmol/μg/min. Results are shown as mean ± SEM and the 95% confidence intervals for the analysis are indicated.^d number of separate experiments in which 3MG transport was measured at least 4 different [3MG]^e V_{max} is significantly greater than control V_{max} for zero-trans uptake (p < 0.05)^f KCN stimulation of 3MG V_{max} for zero-trans uptake is 3.18 ± 0.92 fold greater than FCCP stimulation of uptake.

N/D: values not determined

Michaelis-Menten equation. Control bEnd.3 cell zero-trans 3-OMG uptake is characterized by a V_{\max} of 180 ± 10 pmol/ μ g total cell protein/min and $K_{m(\text{app})}$ of 6.7 ± 0.4 mM (Figure 3.4B; Table 3.1). KCN and FCCP increase V_{\max} for 3-OMG uptake by (7.2 ± 1.2) and (4.3 ± 1.4) fold respectively. K_m for zero-trans 3-OMG uptake increases in metabolically stressed cells. Transport stimulation by KCN is rapidly reversed upon washout of KCN at 37°C (Figure 3.5).

Equilibrium Exchange 3-OMG Uptake

Under physiological conditions, endothelial cells are bathed in serum and interstitial glucose, and therefore rarely experience situations where intracellular glucose is zero. We therefore sought to measure sugar uptake in bEnd.3 cells under equilibrium exchange conditions which more closely resemble those experienced *in vivo*. In equilibrium exchange, the concentrations of intracellular and extracellular 3-OMG are identical and unidirectional sugar transport is measured using [^3H]-3-OMG. Equilibrium exchange 3-OMG uptake was measured in the absence and presence of either 5 mM KCN or 8 μ g/ml FCCP. Equilibrium 3-OMG uptake in control cells is characterized by a V_{\max} of 571 ± 83 pmol/ μ g total cell protein/min and $K_{m(\text{app})}$ of 14.9 ± 12.6 mM (Figure 3.6; Table 1). This suggests that as with transport in erythrocytes, unidirectional sugar uptake displays trans-acceleration (214). KCN and FCCP increase V_{\max} for exchange 3-OMG uptake by (3.2 ± 1.1) - and (4.6 ± 2.1) -fold respectively. Poisoning has no significant affect on K_m for exchange 3-OMG uptake.

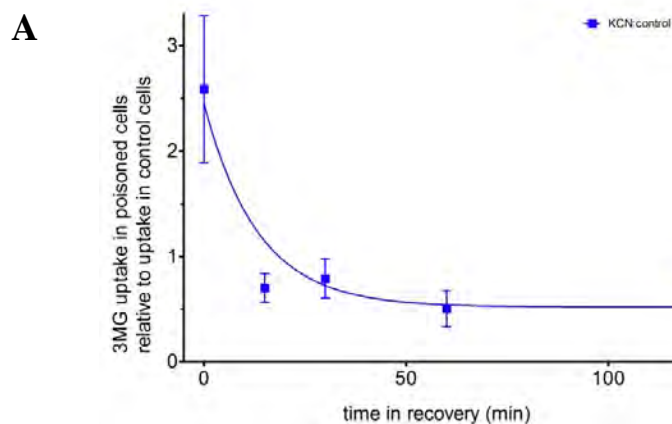


Figure 3.5: Time Course of Recovery from KCN Poisoning

Cells were treated with 5 mM KCN for 15 min at 37 °C then replaced with KCN-free medium containing glucose for the times shown on the *abscissa*. The cells were cooled to 4 °C and zero-trans 3-OMG uptake was measured at 20 mM 3-OMG. Curve was calculated by nonlinear regression assuming a monoexponential decay in transport rates. Each point represents the mean \pm S.E. of three separate experiments.

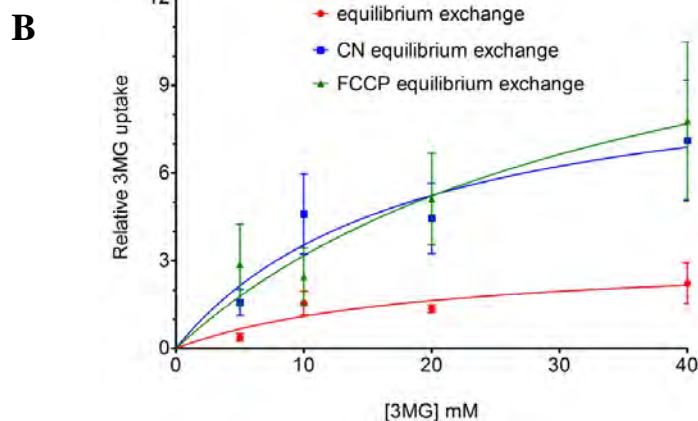


Figure 3.6: bEnd.3 Equilibrium Exchange Transport

Cells were pre-loaded with increasing amounts of 3-OMG (from 5 to 40 mM) and allowed to equilibrate before treating for 10 min with control medium (●), 5mM KCN (■), or 8 μ g/ml FCCP (▲) each containing the preloading [3-OMG] at 37 °C. The cells were cooled, and unidirectional 3-OMG uptake was measured at 4 °C. *Ordinate*, relative rate of unidirectional 3-OMG uptake; *Abscissa*, [3-OMG] in mM. Curves were computed using Equation 1, and the resulting V_{max} and $K_{m(app)}$ values are summarized in Table 1. Each point represents the mean \pm S.E. for three separate experiments

KCN and FCCP depletion of cellular [ATP] (Figure 3.2A and B) and stimulation of 3-OMG uptake (Figure 3.7A and B) are dose dependent with $K_{0.5}$ for transport stimulation of 0.04 ± 0.03 mM KCN and < 1 ng/mL FCCP. Zero-trans and exchange 3-OMG transport are equally sensitive to FCCP (Figure 3.7B).

Quantitation of GLUT 1 mRNA using RT-PCR

In order to examine whether increases in zero-trans and equilibrium exchange sugar transport capacity are caused by up-regulation of GLUT1 expression (or any other GLUT), we first measured bEnd.3 GLUT1 mRNA levels using endpoint reverse transcriptase PCR (RT-PCR) in the absence and presence of either 5 mM KCN or 8 μ g/ml FCCP. While endpoint RT-PCR is not quantitative, the primer sets and total mRNA template concentrations used for each sample were the same. Our results obtained indicate that there are no changes in total GLUT1, mRNA levels in the presence of either KCN or FCCP (Figure 3.8A and B),

We previously detected GLUT8 and GLUT9 mRNA in bEnd.3 cells. In order to obtain a more quantitative analysis of expression, we used quantitative RT-PCR (qPCR) to probe for changes in GLUT1, GLUT8, and GLUT9 mRNA levels in the presence of 5 mM KCN or 8 μ g/ml FCCP. Four separate mRNA samples were prepared in the absence or presence of either 5 mM KCN or 8 μ g/ml FCCP, and each template was used to run the qPCR. The results were analyzed using the $\Delta\Delta C_t$ method, averaged and compared for relative mRNA expression. As with the endpoint RT-PCR, our results show no

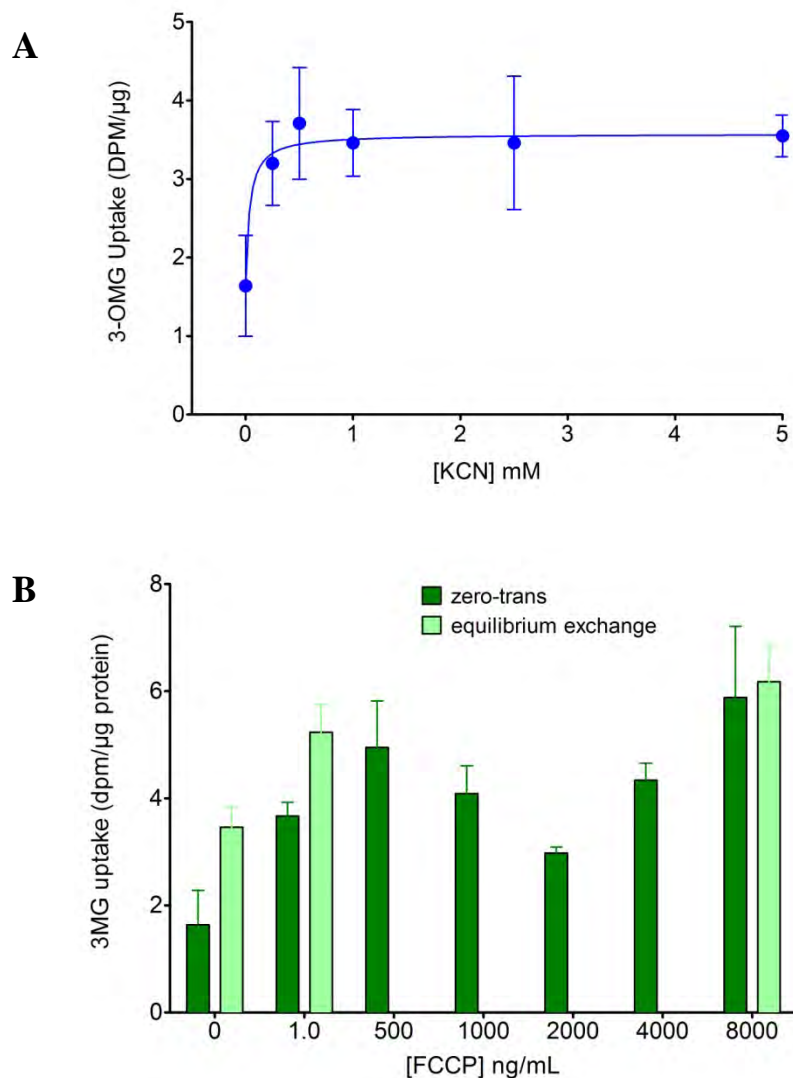


Figure 3.7: Concentration Dependence of Transport Stimulation by Poison

Cells were exposed to varying [KCN] *A*, or [FCCP] *B*, for 10 min at 37 °C and then cooled, and 10 mM 3-OMG uptake was measured as previously described.

Ordinates, 3-OMG uptake in dpm/μg protein; *Abscissas*, [poison].

Results are shown as mean \pm S.E of at least three determinations. The *curve* in *A* was computed by nonlinear regression assuming that sugar uptake increases in a saturable manner with [poison]. $K_{0.5}$ for transport stimulation by KCN is 0.04 ± 0.03 mM.

FCCP stimulation of zero-trans (■) and equilibrium exchange (□) transport are shown.

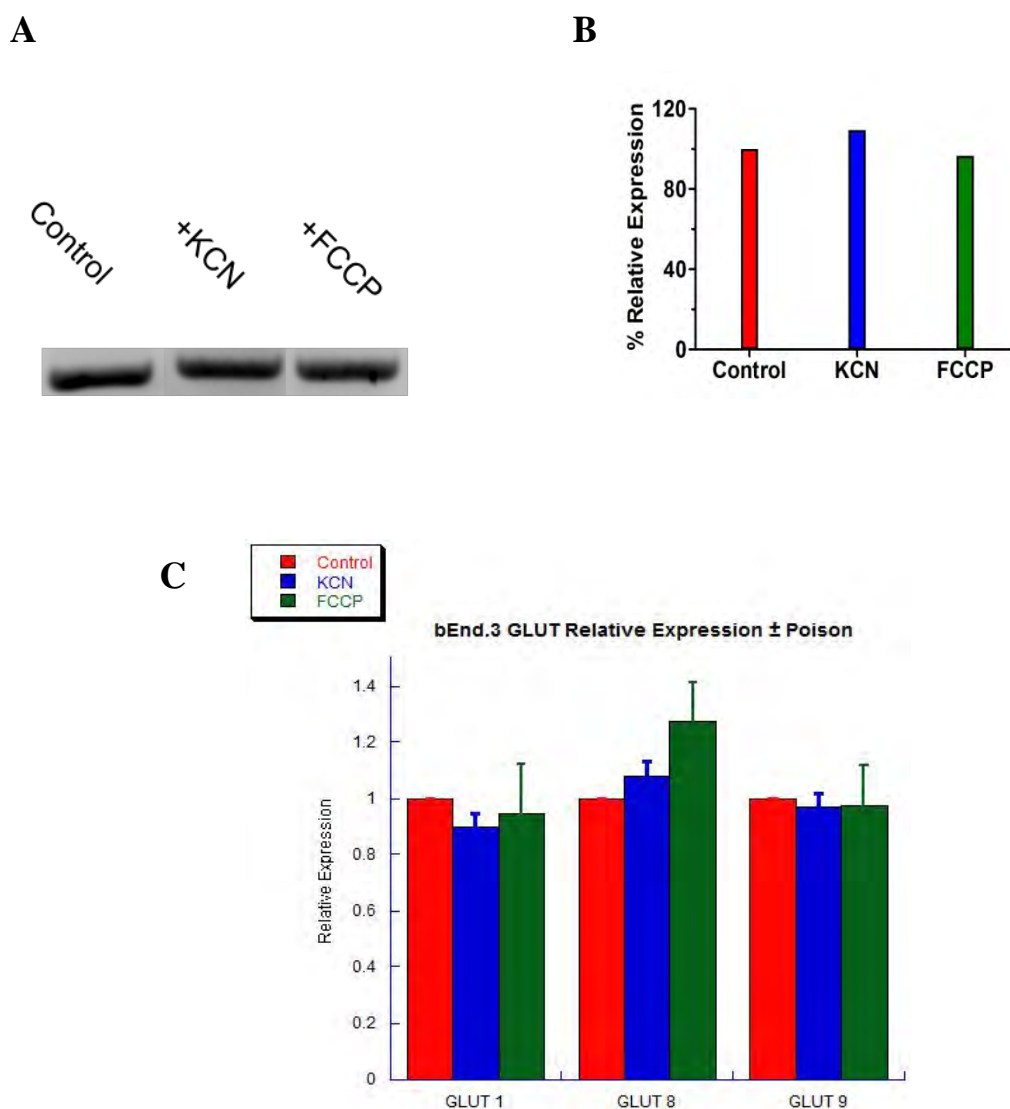


Figure 3.8: RT-PCR of bEnd.3 Cells

A, end point reverse transcriptase-PCR of bEnd.3 cells using a GLUT1 primer. Cells were incubated for 10 min in either PBS, PBS + 5mM KCN, or PBS + 8 μ g/ml FCCP before isolating total RNA, and reverse transcriptase-PCR was carried out using a GLUT1 primer. Samples were run on a 1.5% agarose gel. *B*, Quantitation of GLUT1 band densities from end point RT-PCR. *Ordinate*, relative expression (%). Experimental conditions (control PBS (■), PBS + KCN (■), and PBS + FCCP(■)) are shown below the *abscissa*. *C*, Quantitative RT-PCR of bEnd.3 cells. *Ordinate* Relative expression, GLUT protein screened is indicated below the *abscissa* Cells were processed as in *A* and 100 ng of total RNA was used for each reaction, which was run twice with four replicates for each condition. Results are shown as mean \pm S.E. Primers specific to GLUT1, GLUT8, and GLUT9 were used in each reaction.

significant change in GLUT1, GLUT8, or GLUT9 mRNA levels during KCN- or FCCP-induced ATP depletion (Figure 3.8C).

Plasma Membrane Biotinylation of bEnd.3 GLUT1

ATP depletion of bEnd.3 cells does not alter GLUT1 message levels. However, increased translation of pre-synthesized GLUT1 mRNA could increase levels of plasma membrane resident protein, resulting in increased zero-trans and exchange sugar transport capacity. To test for this possibility, cells were incubated for 10 minutes in the absence or presence of 5 mM KCN or 8 μ g/ml FCCP, lysed, and analyzed by Western blot. (Figure 3.9A). Two GLUT1 C-terminal antibody reactive bands are observed: a 48 kDa species and a more abundant and broadly mobile species of 55 kDa. Treatment of membranes with PNGase F causes both species to collapse to a 42 kDa GLUT1 C-terminal antibody reactive species (Figure 3.9C). Densitometric analysis indicates that neither the 48 kDa nor the 55 kDa species is significantly increased by KCN or FCCP (Figure 3.9B). This result combined with the qPCR results indicates that increases in zero-trans and exchange V_{\max} are not explained by either increased GLUT1 message or protein in bEnd.3 cells.

We next asked whether cell surface recruitment of intracellular GLUT1 was responsible for increased sugar transport. Cells were incubated for 10 minutes in PBS in the absence or presence of 5 mM KCN or 8 μ g/ml FCCP, washed, and then cooled to 4°C. Cells were then treated with a membrane-impermeable, amine-reactive biotin (Sulfo-NHS-SS-Biotin), the reaction was quenched and the cells lysed in detergent-containing lysis buffer. Biotinylated proteins were precipitated with streptavidin beads,

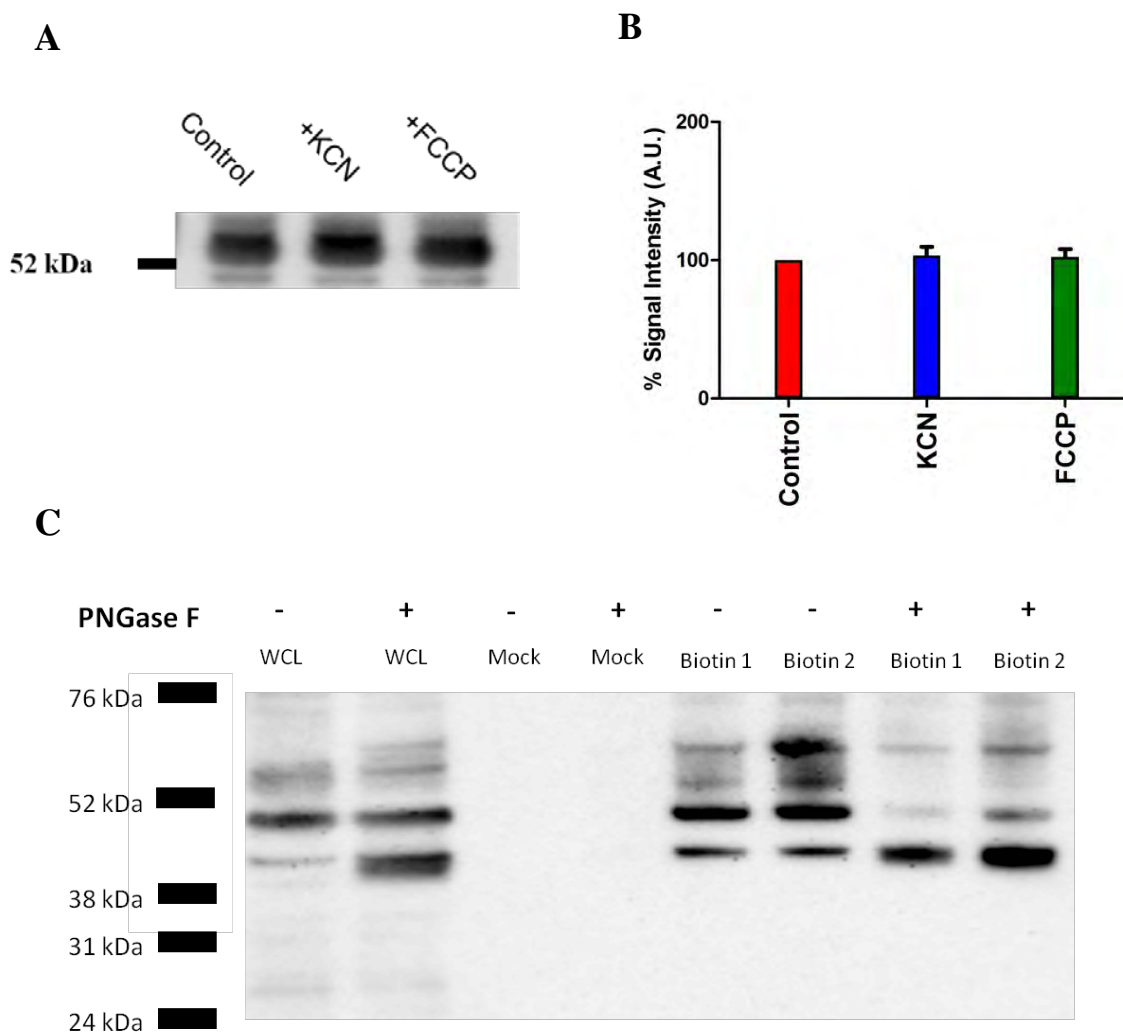


Figure 3.9: Western Blot of bEnd3 Cells During Poisoning

A, representative Western blot of whole cell lysates of bEnd.3 cells in the absence or presence of either 5mM KCN or 8 μ g/ml of FCCP for 10 min. Total protein (20 μ g) was loaded into each lane and probed with GLUT1 C-terminal antibody. *B*, quantitation of Western blot band density. *Ordinate*, relative expression (%); *Abscissa*, experimental condition: PBS, PBS + KCN, and PBS + FCCP. *C*. Effect of PNGase F on GLUT1 C-terminal antibody-reactive protein mobility. Whole cell lysates (WCL) and cell surface biotinylated proteins (see Fig 3.10 for details) were treated with (+) or without (-) PNGase F (10,000 units for 1 hour at 37 $^{\circ}$ C). Peptides were resolved by SDS-PAGE and subjected to immunoblot analysis using GLUT1 C-terminal antibody. The mobility of molecular weight standards is indicated to the left of the autoradiograph. Two biotinylation experiments (Biotin 1 and Biotin 2) and 1 mock biotinylation (Mock) were carried out on bEnd.3 cells. PNGase F enriches a 42 kDa species at the expense of 55 and 48 kDa species.

analyzed by Western blot (Figure 3.10A and C) and band densities were quantitated (Figure 3.10B and D). The blots indicate that ATP depletion of bEnd.3 cells increases cell surface GLUT1 C-terminal antibody reactive species by at least two-fold whereas surface Na^+, K^+ ATPase levels are unaffected by metabolic stress. Interestingly, cell surface expression of the 48 kDa GLUT1 C-terminal antibody reactive species is unchanged by metabolic depletion whereas expression of the 55 kDa species is increased by 3 to 5 fold (Figure 3.10A and B). These results mirror the 2-7 fold increase in 3-OMG transport capacity produced by metabolic poisons.

AMP-activated protein kinase (AMPK) is a key regulator of cellular glucose transport and glycolysis in muscle and heart (179,202). AICAR (an AMPK agonist) enters cells via nucleoside transporters, is transformed to ZMP and then allosterically activates AMPK (218). AICAR (2 mM) treatment of bEND.3 cells for 2 hours increases V_{\max} for zero-trans 3-OMG uptake (Figure 3.4B; Table 3.1) Glucose-depletion, KCN, FCCP or AICAR treatment of bEnd.3 cells increases AMPK phosphorylation as judged by immunoblot analyses using AMPK and phospho- AMPK-directed antibodies (Figure 3.11).

Discussion

This study examines the hypothesis that brain microvasculature endothelial cells respond acutely to cellular metabolic stress with increased sugar transport capacity resulting from recruitment of intracellular GLUT1 stores to the plasma membrane.

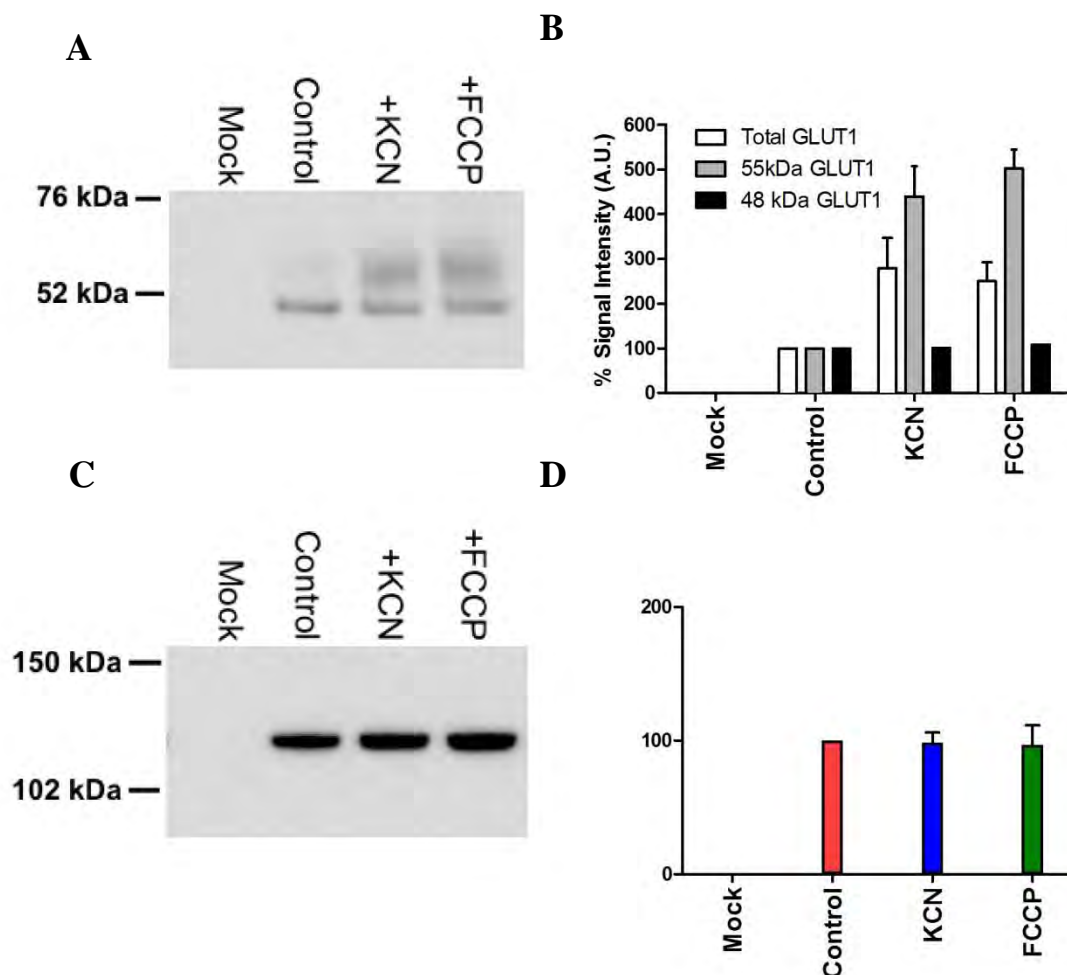


Figure 3.10: Surface Biotinylation of bEnd.3 GLUT1

A and C. Representative Western blots of cell surface biotinylated bEnd.3 cell proteins obtained in the absence and presence of either 5 mM KCN or 8 $\mu\text{g/ml}$ FCCP. Cells were poisoned at 37 $^{\circ}\text{C}$ for 10 minutes before cooling to 4 $^{\circ}\text{C}$ and biotinylation. 30 μg of total streptavidin-pull down protein was loaded onto each gel and blotted with either GLUT1 C-Ab (A) or antibody raised against $\text{Na}^+\text{K}^+\text{ATPase}$ (C). Band densities were quantitated and shown in B (GLUT1) and D ($\text{Na}^+\text{K}^+\text{ATPase}$). *Ordinate*, relative expression (%); *Abcissa*, experimental condition: PBS, PBS + KCN, and PBS + FCCP. In D, results are shown for total C-terminal antibody-reactive species (open bars), for 55 kDa C-terminal antibody-reactive species (gray bars) and for 48 kDa C-terminal antibody-reactive species (black bars). Each experiment was repeated at least three times and the results of quantitations (B and D) are shown as mean \pm SEM.

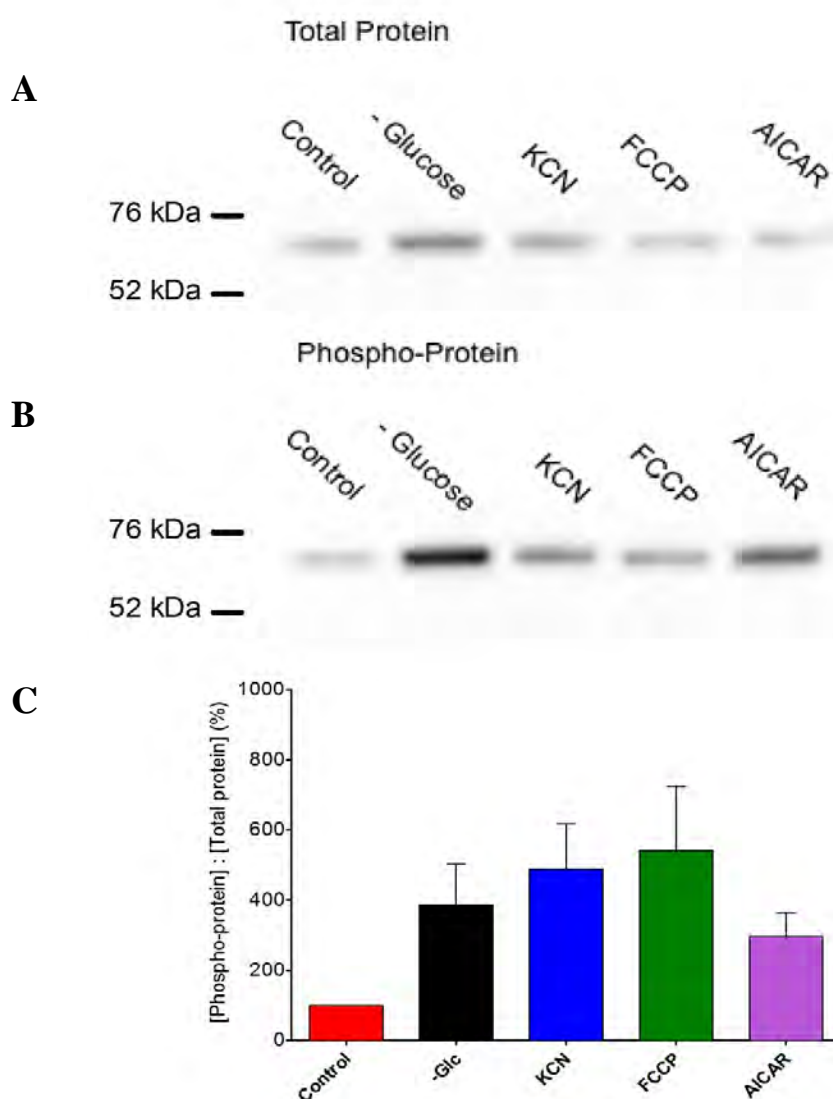


Figure 3.11: AMPK Phosphorylation During Metabolic Stress

Immunoblot analysis of bEnd.3 cell AMPK and phosphorylated AMPK content. *A* and *B* Whole cell lysates (20 μ g protein) were resolved by SDS PAGE and immunoblotted using AMPK (*A*) and phosphorylated AMPK (*B*) directed antibodies. Prior to lysis, cells were treated for 15 min at 37 $^{\circ}$ C with 5 M glucose (control), 0 glucose, 5 mM KCN, 8 μ g/mL FCCP or 2 mM AICAR. The mobilities of 76 and 52 kDa molecular weight standards are indicated. *C*. Quantitation of band densities. *Ordinate*: ratio of immunoreactive phosphorylated AMPK to AMPK in extracts. *Abscissa*: Experimental conditions (control PBS, 0 glucose, PBS + KCN, PBS + FCCP and PBS + AICAR). Results are shown as mean \pm S.E.M of 3 separate experiments.

Previous studies have used the metabolic poisons KCN and FCCP to induce acute metabolic stress in cardiomyocytes, skeletal muscle and nucleated erythrocytes.

Metabolic depletion rapidly stimulates sugar transport in these tissues (183,219,220). In the present study, we demonstrate rapid depletion of ATP in bEnd.3 cells using metabolic poisons. ATP levels recover within 60 minutes of removal of KCN; however, the effect of FCCP treatment is irreversible. We also show that KCN or FCCP treatment induces a 3.2 to 7.2 fold increase in V_{\max} for zero-trans and equilibrium exchange sugar uptake in bEnd.3 cells.

Acute glucose depletion (15 minutes at 37°C) also rapidly reduces bEnd.3 cell ATP content but only by 50%. This treatment increases V_{\max} for sugar uptake suggesting that sugar transport in blood-brain barrier endothelial cells is, like transport in cardiomyocytes and skeletal muscle, acutely sensitive to cellular metabolic status (179,221). AMP-activated protein kinase (AMPK) is a key regulator of cellular metabolism. Upon elevation of cytoplasmic AMP levels, AMPK is phosphorylated and acts as a metabolic master switch, stimulating important metabolic processes such as fatty acid oxidation and glycolysis (180,181). Activated AMPK stimulates glycolysis in hypoxic cardiomyocytes and monocytes by activating 6-phosphofructo-2-kinase (179,202). Activated AMPK further supports increased anaerobic metabolism in heart and skeletal muscle by promoting recruitment of GLUT4 and GLUT1 to the cell membrane (203,222) thereby increasing sugar uptake and metabolism.

This mechanism may also be active in brain microvasculature endothelial cells because bEnd.3 cells acutely respond to metabolic poison, glucose-depletion and to the

AMPK agonist AICAR with increased AMPK phosphorylation as well as increased sugar transport rates.

Quantitative PCR and Western blot analyses of whole cell lysates show no significant changes in either GLUT1 mRNA levels or total protein expression in ATP-depleted cells. PCR data also indicates that GLUT1 appears to be the only GLUT isoform expressed at significant levels in bEnd.3 cells. Plasma membrane protein biotinylation studies show that GLUT1 levels are increased at the plasma membrane by 2-2.5 fold within ten minutes of treatment with either KCN or FCCP. These findings suggest that metabolic depletion of brain microvasculature endothelial cells results in AMPK activation, which in turn may induce net GLUT1 translocation to the cell membrane.

Immunoblot analysis of the GLUT1 content of bEnd.3 cell total lysates and streptavidin pull-downs of biotinylated membrane proteins indicates that two GLUT1 C-terminal antibody reactive species are present: a minor 48 kDa protein and a more broadly mobile 55 kDa species. Both species collapse into a 42 kDa species upon treatment with the glycosidase PNGase F suggesting that each corresponds to a differentially glycosylated form of GLUT1. It is likely that the 42 kDa species seen in the PNGase F-treated cells represents the non-glycosylated form of GLUT1 that would be seen in the endoplasmic reticulum prior to modification by oligosaccharyltransferase. The 48 kDa species, on the other hand, may potentially represent GLUT1 that is incompletely glycosylated but trafficked to the plasma membrane nonetheless, while the 55 kDa species represents the completely glycosylated form of GLUT1. Similar behavior is observed for human red cell GLUT1 (110,223) and rat brain microvascular endothelial

cells (224). Interestingly, cell surface levels of the 48 kDa species are unaffected by metabolic depletion whereas surface levels of the 55 kDa species are significantly increased giving rise to an approximate 2 to 3-fold increase in total cell surface GLUT1.

It is interesting to compare our findings using cultured bEnd.3 cells with transport studies in polarized endothelial cells. Rat blood-brain barrier glucose transport is acutely stimulated during seizure and immunohistochemical analysis suggests that this results from recruitment of intracellular GLUT1 to both luminal and abluminal endothelial cell membranes (201). This being the case, our demonstration of GLUT1 recruitment in an unpolarized endothelial cell is not only representative of recruitment in a polarized bEND cell *in vivo* but may also uniquely provide the tools for detailed biochemical analysis of this phenomenon.

Earlier immunohistochemical analyses of GLUT1 expression in rat bEND cells *in situ* suggesting an asymmetric (1:4) distribution of GLUT1 between luminal and abluminal membranes (185,217) appear to be incorrect. Rather, GLUT1 is equally distributed between luminal and abluminal membranes (26). If stimulation of trans-capillary transport involves GLUT1 recruitment to luminal and abluminal endothelial membranes, polarized GLUT1 expression in bEND cells would significantly impact net transport stimulation.

Our analysis (13,23) indicates that starting from an equal distribution of carriers in luminal and abluminal membranes, increasing abluminal or luminal [GLUT1] in the absence of a commensurate increase at the trans-membrane would be without impact on net trans-endothelial cell sugar transport because the transport capacity of the membrane

containing the fewest number of transporters remains rate-limiting. Polarized GLUT1 expression in the BBB endothelium only makes sense if one membrane (e.g. the luminal membrane) contains many more transporters than the abluminal membrane and regulation involves up-regulation at the abluminal membrane. The available evidence argues against this (26).

It has previously been shown that between 30-50% of GLUT1 resides in intracellular pools in endothelial cells (13,186). While this may partially explain the 2-3 fold increases in biotinylated GLUT1 seen during metabolic poisoning, it does not explain the 3-7 fold increases in V_{max} for transport seen in the 3-OMG uptake measurements. Therefore, based on our analysis, there are two possible explanations for this increase: 1. the amount of intracellular GLUT1 has been underestimated and there is a much higher percentage of GLUT1 inside the cell than at the plasma membrane, or 2. the catalytic activity of GLUT1 is being modified to allow increased transport in addition to the translocation of GLUT1 to the plasma membrane. Further studies measuring the intracellular GLUT1 content would give a clearer picture as to the distribution of GLUT1 under control and metabolically stressed conditions.

There are a number of steps in intracellular vesicular trafficking that require ATP to function. For example, the formation of clathrin-coated pits and the dissociation of clathrin from internalized vesicles are well known steps of endocytosis that require energy to function (225). Similarly, in exocytosis, steps such as the movement of vesicles along actin filaments and the disassociation of SNARE complexes are all ATP dependent processes (226,227). Therefore, it is safe to assume that severe ATP depletion of bEnd.3

cells by KCN and FCCP would effectively shut down intracellular trafficking. In order for GLUT1 to increase at the plasma membrane upon ATP depletion, its trafficking to the cell surface must be occurring rapidly in bEnd.3 cells before ATP is depleted too severely for trafficking to continue. Our data show that ATP depletion is occurring within 10-15 minutes of exposure to poison, so GLUT1 translocation must also be occurring within this window. However, further studies are required to determine the time frame of GLUT1 trafficking after initial poison treatment, the amount of ATP depletion required to cause the translocation of GLUT1 to the plasma membrane, and the point at which ATP is too low for trafficking to continue.

In summary, acute metabolic depletion of murine bEnd.3 cells results in AMPK phosphorylation, GLUT1 recruitment to the cell membrane and increased sugar transport. This may allow endothelial cells to respond rapidly with increased blood-brain barrier sugar transport in locally hypoxic or metabolically-stressed regions of the brain. The exact nature of the involvement of AMPK in GLUT1 regulation in bEnd.3 cells requires further investigation.

CHAPTER IV

AMP KINASE REGULATION OF SUGAR TRANSPORT IN BRAIN CAPILLARY ENDOTHELIAL CELLS DURING ACUTE METABOLIC STRESS

Abstract

AMP-dependent kinase (AMPK) and GLUT1-mediated sugar transport in blood-brain barrier endothelial cells are activated during acute cellular metabolic stress. Using murine brain microvasculature endothelium bEnd.3 cells, we demonstrate that AMPK modulates endothelial cell glucose uptake by causing the net transfer of GLUT1 from intracellular pools to the plasma membrane. AMPK phosphorylation and stimulation of 3-O-methylglucose transport by the AMPK agonist AICAR are inhibited in a dose-dependent manner by the AMPK antagonist Compound C. Compound C also reduces AMPK phosphorylation and 3-O-methylglucose transport stimulation induced by cellular glucose-depletion, by potassium cyanide (KCN) or by carbonyl cyanide-p-trifluoromethoxy-phenylhydrazone (FCCP). Phosphorylation of the downstream AMPK-target, acetyl-CoA carboxylase, is blocked by Compound C. Cell-surface biotinylation studies reveal that plasma membrane GLUT1 levels are increased 2-3 fold by cellular glucose depletion, AICAR- or KCN-treatment, and that these increases are prevented by Compound C. These results support the hypothesis that AMPK activation in blood-brain barrier derived endothelial cells directs the trafficking of GLUT1 from intracellular pools to the plasma membrane, thereby increasing endothelial sugar transport capacity.

Introduction

The mammalian brain normally uses glucose as its primary energy source. While brain function and development require a constant glucose supply, diffusional exchange of glucose between blood and brain is severely restricted by the blood-brain barrier. This barrier comprises a non-fenestrated endothelium formed by capillary endothelial cells connected by tight junctions. Glucose that enters the brain must therefore cross the endothelium by protein-mediated trans-cellular transport. In the mammalian brain, this is catalyzed by the glucose transport protein GLUT1, which is expressed in luminal and abluminal membranes of endothelial cells and is essential for brain metabolic homeostasis (34,38,39,73,228).

Under resting conditions and at physiologic blood glucose levels, GLUT1-mediated glucose transport across the blood-brain barrier barely exceeds brain glucose utilization (13). When glucose consumption exceeds glucose supply, for example during hypoglycemia, hypoxia or intense neuronal activation, blood-brain barrier glucose transport responds by two different mechanisms. During chronic metabolic stress (e.g. hypoxia (194) and hypoglycemia (213,229)), GLUT1 gene and protein expression increase *in vitro* (215) and *in vivo* (216), thereby increasing blood-brain barrier sugar transport capacity. In contrast, acute metabolic stress (e.g. short-lived hypoglycemia, hypoxia, metabolic poisoning (187), or seizures (75,200)), is without effect on GLUT1 expression but promotes recruitment of intracellular GLUT1 to the plasma membrane (186), thereby increasing blood-brain barrier sugar transport (230). The signals that regulate blood-brain barrier sugar transport during acute metabolic stress are not known.

Phosphorylated AMP-activated kinase (AMPK) plays a key role in maintaining energy homeostasis in skeletal muscle (221,231), heart (202,232), brain (233,234), and endothelial cells (235) by switching cellular metabolism to lowered ATP consumption and increased ATP production. AMPK regulates glycolysis, fatty acid oxidation, and glucose transport (180,181,236). AMPK directs plasma membrane trafficking of GLUT1 (222,237) and the insulin-sensitive glucose transporter GLUT4 in heart and muscle (238).

We recently demonstrated that several forms of acute metabolic stress, including glucose starvation, KCN or FCCP treatment, induce AMPK-phosphorylation (205) in the cultured brain microvascular endothelial cell line bEnd.3 (239). However, it is unclear whether AMPK activation is directly responsible for increased GLUT1-mediated sugar uptake. The results of the present study strongly suggest that AMPK directs the trafficking of GLUT1 between the endothelial cell membrane and intracellular pools, and thereby regulates blood-brain barrier endothelial cell sugar transport.

Experimental Procedures

Tissue Culture

bEnd.3 cells were obtained from ATCC and maintained in Dulbecco's Modified Eagle Medium (DMEM) from Gibco supplemented with 10% fetal bovine serum (FBS) from Hyclone and 1% Penicillin/Streptomycin (Pen/Strep) solution (Gibco) at 37°C in a humidified 5% CO₂ incubator as described previously (187).

Antibodies

A custom, affinity-purified rabbit polyclonal antibody raised against a synthetic peptide corresponding to GLUT1 amino acids 480-492 was produced by New England Peptide. Rabbit polyclonal and monoclonal antibodies against AMPK, phosphorylated AMPK (P-Thr172), ACC, and phosphorylated ACC (P-Ser-79) were obtained from Cell Signaling Technology. HRP conjugated Goat anti-rabbit secondary antibody was obtained from Jackson ImmunoResearch.

Buffers

Cell lysis buffer consisted of 5 mM HEPES, 5 mM MgCl₂, 150 mM NaCl, 50 μM EDTA, and 1% SDS. Uptake stop solution included 10 μM cytochalasin B (CCB, Sigma) and 100 μM phloretin (Sigma) in DPBS. TBS was composed of 20 mM Tris base and 135 mM NaCl, pH 7.6. TBST comprised TBS buffer with 0.2% Tween-20. Biotin quench solution was composed of 250 mM Tris base. Biotin lysis buffer contained TBS with 0.5% Triton-X-100.

Western Blotting of bEnd.3 Cells

Confluent 100 mm dishes of bEnd.3 cells were treated with 2 mM AICAR (ThermoFisher) or 2 mM AICAR plus 1, 2, 5, 10, or 20 μM Compound C (Tocris Bioscience) for two hours; Cells were then washed twice with DPBS, lysed, and analyzed for total protein concentration using a micro BCA kit (Pierce). Western blots were performed as previously described (187) using a 1:1,000 dilution of either rabbit AMPK

P-Thr172 or rabbit ACC P-Ser 79 antibody. Samples were run in duplicate, and band densities were quantitated using ImageJ software.

3-OMG Uptake Measurements in bEnd.3 cells

Uptake was measured for 30 sec at 4 °C as previously described (187) using 20 mM 3-O-methylglucose (3-OMG) containing 2.5 $\mu\text{Ci/ml}$ [^3H]-3-O-methylglucose ([^3H]-3-OMG) in DPBS. Sugar uptake measurements in AICAR-treated cells were performed as described above with the following modifications: on the day of the assay, cells were placed in serum-free DMEM or serum-free DMEM containing either 0 or 2 mM AICAR or 2 mM AICAR plus 1, 2, 10, or 20 μM Compound C for 2 hours at 37°C. Cells were washed with 1 ml of either glucose-free DPBS, DPBS containing 2 mM AICAR, or DPBS containing 2 mM AICAR plus Compound C, and sugar uptake was measured.

Sugar uptake in metabolically-poisoned and glucose-depleted cells was measured as described above with the following modifications: cells were placed in serum-free DMEM \pm 10 μM Compound C, serum-free DMEM containing 2 mM AICAR \pm 10 μM Compound C for 2 hours, or serum-free DMEM \pm 10 μM Compound C for 1.5 hours followed by serum-free glucose-free DMEM \pm 10 μM Compound C for 30 minutes. Cells were washed with 1 ml of either glucose-free DPBS, or glucose-free DPBS plus the appropriate poison (AICAR, KCN, or FCCP) \pm 10 μM Compound C at which point uptake was measured.

Biotinylation of bEnd.3 cells

Biotinylation was carried out as previously described (187) with the following modifications: 150 cm² plates of confluent bEnd.3 cells were placed in serum-free DMEM with 2 mM AICAR ± 10 μM Compound C for 2 hours, 2 mM AICAR ± 10 μM Compound C for 1.5 hours followed by serum-free, glucose-free DMEM ± 10 μM Compound C for 30 minutes, or 5 mM KCN ± 10 μM Compound C for 10 minutes at 37°C prior to proceeding with biotinylation.

Results

Compound C Inhibits AICAR-dependent AMPK Phosphorylation

Phosphorylation of AMPK threonine 172 activates AMPK (181). In order to analyze Compound C inhibition of AMPK activity, we treated bEnd.3 cells with 2 mM AICAR to activate AMPK in the absence or presence of increasing concentrations of Compound C. Thr₁₇₂ phosphorylation was analyzed by using an AMPK-phospho-Thr₁₇₂-specific antibody (Figure 4.1A). AICAR-promoted AMPK phosphorylation decreases with increasing concentrations of Compound C and is suppressed at 10 μM inhibitor. $K_{i(\text{app})}$ ($5.5 \pm 2.2 \mu\text{M}$) for inhibition of AMPK was computed by non-linear regression analysis of the concentration dependence of Compound C-inhibition of AICAR-dependent AMPK phosphorylation by assuming simple Michaelis-Menten inhibition (Figure 4.1B).

We also examined phosphorylation of acetyl co-A carboxylase (ACC), a direct downstream target of AMPK (239). Using an antibody specific to phosphorylated Ser₇₉

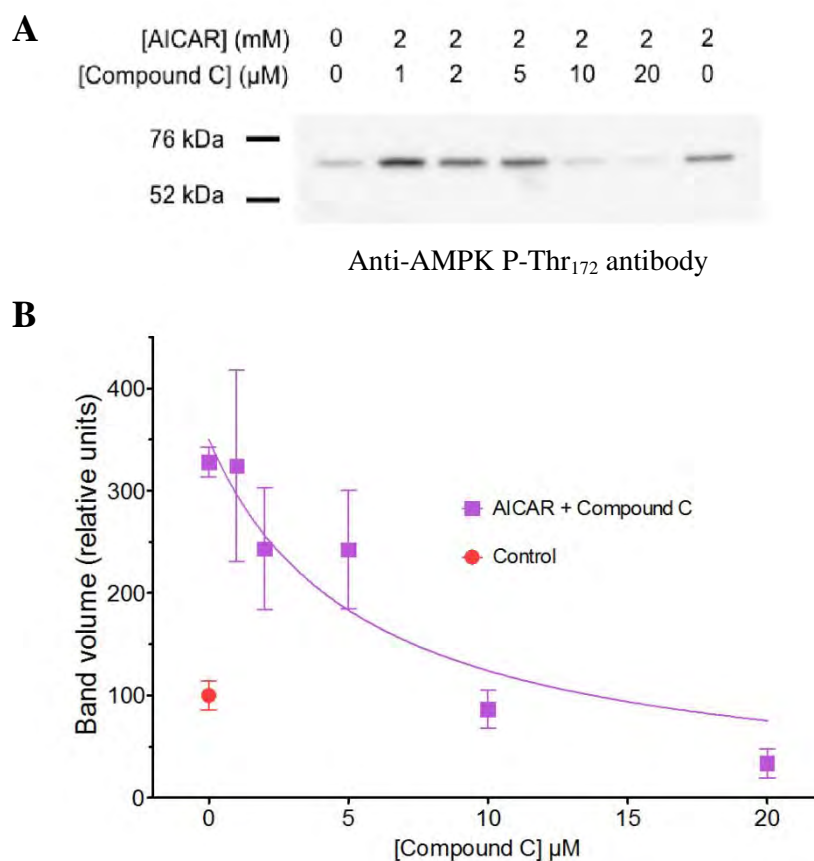


Figure 4.1: Inhibition of AMPK Phosphorylation by Compound C

Inhibition of AMPK by Compound C. *A*. Representative Western blot of whole cell bEnd.3 lysates in the absence or presence of AICAR and Compound C (concentrations indicated above the blots). Cell lysate (30 μ g total protein) was loaded into each lane and probed with AMPK P-Thr 172 antibody. The mobility of molecular weight standards is indicated. *B*, Quantitation of Western blot band volumes from *A* and *C* respectively. *Ordinate*: relative band volume (%); *Abscissa*: Concentration of Compound C (μ M). Data are shown for control cells (●) and AICAR-treated cells exposed to Compound C (■). Curves drawn through the Compound C data were computed by non-linear regression assuming simple competitive inhibition and provide K_{iapp} for Compound C inhibition of phosphorylation. Data points represent the mean \pm S.E.M. for two separate experiments.

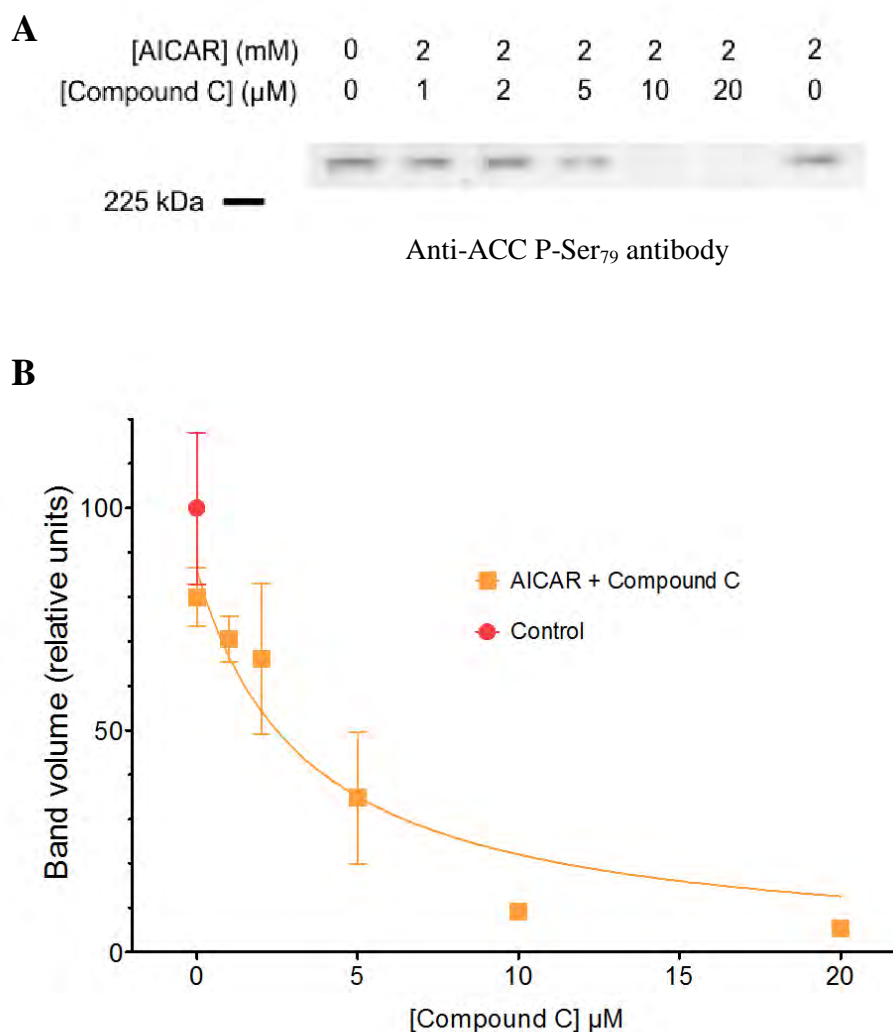


Figure 4.2: Inhibition of ACC Phosphorylation by Compound C

A. Representative Western blot of whole cell bEnd.3 lysates in the absence or presence of AICAR and Compound C (concentrations indicated above the blots). Cell lysate (30 μ g total protein) was loaded into each lane and probed with ACC P-Ser 79 antibody. The mobility of molecular weight standards is indicated. **B.** Quantitation of Western blot band volumes from **A**. *Ordinate:* relative band volume (%); *Abscissa:* Concentration of Compound C (μ M). Data are shown for control cells (●) and AICAR-treated cells exposed to Compound C (■). Curves drawn through the Compound C data were computed by non-linear regression assuming simple competitive inhibition and provide K_{iapp} for Compound C inhibition of phosphorylation. Data points represent the mean \pm S.E.M. for two separate experiments.

on ACC, we measured ACC phosphorylation in the presence of increasing [Compound C] (Figure 4.2A, 4.2B). Compound C reduces ACC phosphorylation in a dose-dependent manner with $K_{i(\text{app})} = 3.4 \pm 1.2 \mu\text{M}$. We also observe significant ACC phosphorylation in the absence of AICAR and Compound C, suggesting that basal AMPK activity is sufficient to phosphorylate ACC in untreated cells.

Compound C Inhibits AICAR-stimulated 3-OMG Uptake

The facilitative glucose transport protein GLUT1 mediates sugar transport in control and AICAR-treated bEnd.3 cells, where AICAR increases V_{max} for 3-OMG net uptake by 2-fold (187). We therefore asked if AICAR-stimulation of transport is suppressed by Compound C.

bEnd.3 cells were treated with 2 mM AICAR plus increasing concentrations of compound C and uptake of 20 mM 3-OMG was measured over 30 seconds at 4°C (Figure 4.3). 3-OMG is a non-metabolizable GLUT1 substrate whose net uptake proceeds until intracellular [3-OMG] = extracellular [3-OMG] and unidirectional 3-OMG uptake and exit are quantitatively identical. Net uptake at 30 seconds achieves only 9 and 20% equilibration in control and FCCP-treated cells respectively (187), indicating that transport determinations at 30 sec underestimate steady-state transport rates by less than 7%. In the present study, AICAR stimulates sugar uptake approximately 2.5-fold over control cells. Addition of Compound C inhibits bEnd.3 sugar uptake in a dose-dependent manner. $K_{i(\text{app})}$ for Compound C inhibition of AICAR-activated sugar uptake is $1.1 \pm 0.2 \mu\text{M}$. The 95% confidence interval for $K_{i(\text{app})}$ for transport inhibition (0.1 - 2.1 μM)

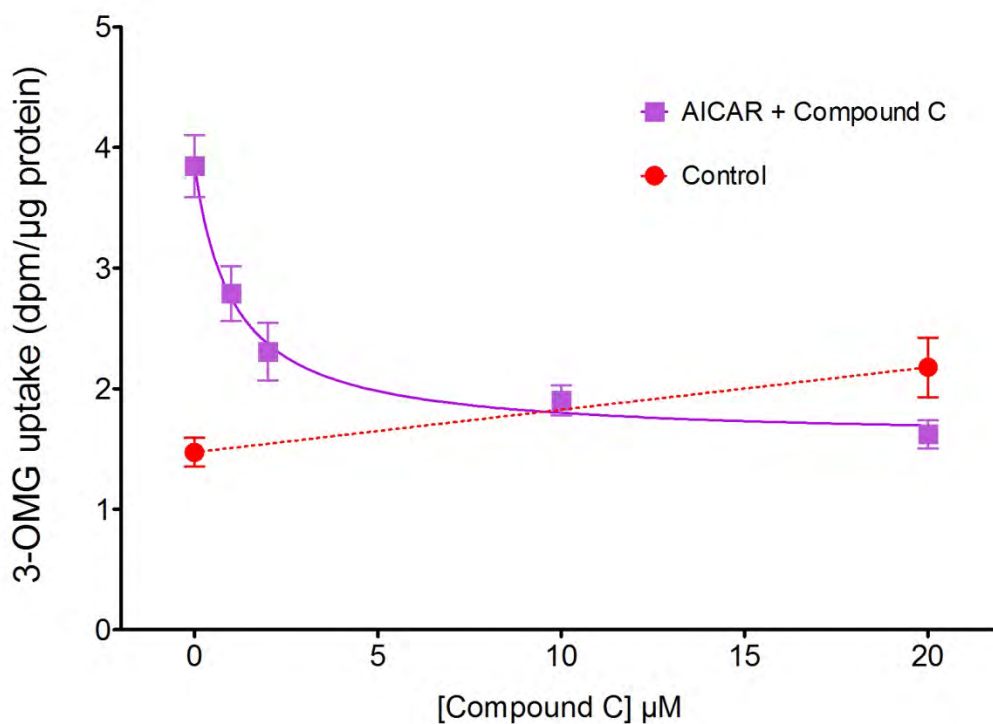


Figure 4.3: Inhibition of Stimulation of Sugar Uptake by Compound C

Sugar uptake at 4°C in bEnd.3 Cells in Response to Compound C. 20 mM 3-OMG uptake was measured for 30 seconds in untreated cells (●) or in cells exposed 2 mM AICAR and increasing [Compound C] (■) for 2 hours at 37°C prior to cooling, glucose depletion and transport initiation. *Ordinate*: 3-OMG uptake (dpm per μg total cell protein); *Abscissa*: [Compound C] in μM. The curve drawn through the AICAR-treated cell data was computed by non-linear regression assuming simple saturable inhibition of uptake by Compound C but that uptake inhibition is incomplete. This permits calculation of $K_{i(app)}$ for transport inhibition. Each point represents the mean ± S.E.M of three separate experiments.

overlaps with the confidence intervals for $K_{i(\text{app})}$ for Compound C inhibition of AMPK phosphorylation (0 - 11 μM) and ACC phosphorylation (0.1 - 6.8 μM ; Figures 4.1A, 4.2A). Transport in the absence of AICAR is stimulated by Compound C, demonstrating that inhibition of AICAR-stimulated transport is not a direct action of the inhibitor on GLUT1.

Compound C Inhibits AMPK Phosphorylation During Acute Metabolic Stress

AMPK phosphorylation increases, while total AMPK protein remains unchanged during acute metabolic stress (187). We therefore asked whether Compound C inhibits acute metabolic stress-induced AMPK activation in endothelial cells. We subjected bEnd.3 cells to AICAR treatment, glucose starvation (30 minutes), 5 mM KCN (10 minutes), or 8 $\mu\text{g/ml}$ FCCP (10 minutes) in the absence or presence of Compound C, and assayed AMPK phosphorylation by Western blot. An untreated control was measured for basal AMPK phosphorylation (Figure 4.4A). Quantitation of phosphorylation (Figure 4.4B) indicates that all stress conditions and AICAR treatment increase AMPK phosphorylation by 4- to 10-fold. Cells treated only with Compound C show no significant increase in phosphorylation over controls. Compound C treatment causes stress-induced AMPK phosphorylation to decrease by 36% in glucose-starved cells, 56% in AICAR-treated cells, 69% in KCN-treated cells, and 61% in FCCP-treated cells. Although AMPK phosphorylation was reduced in the presence of Compound C, complete phosphorylation inhibition was not observed.

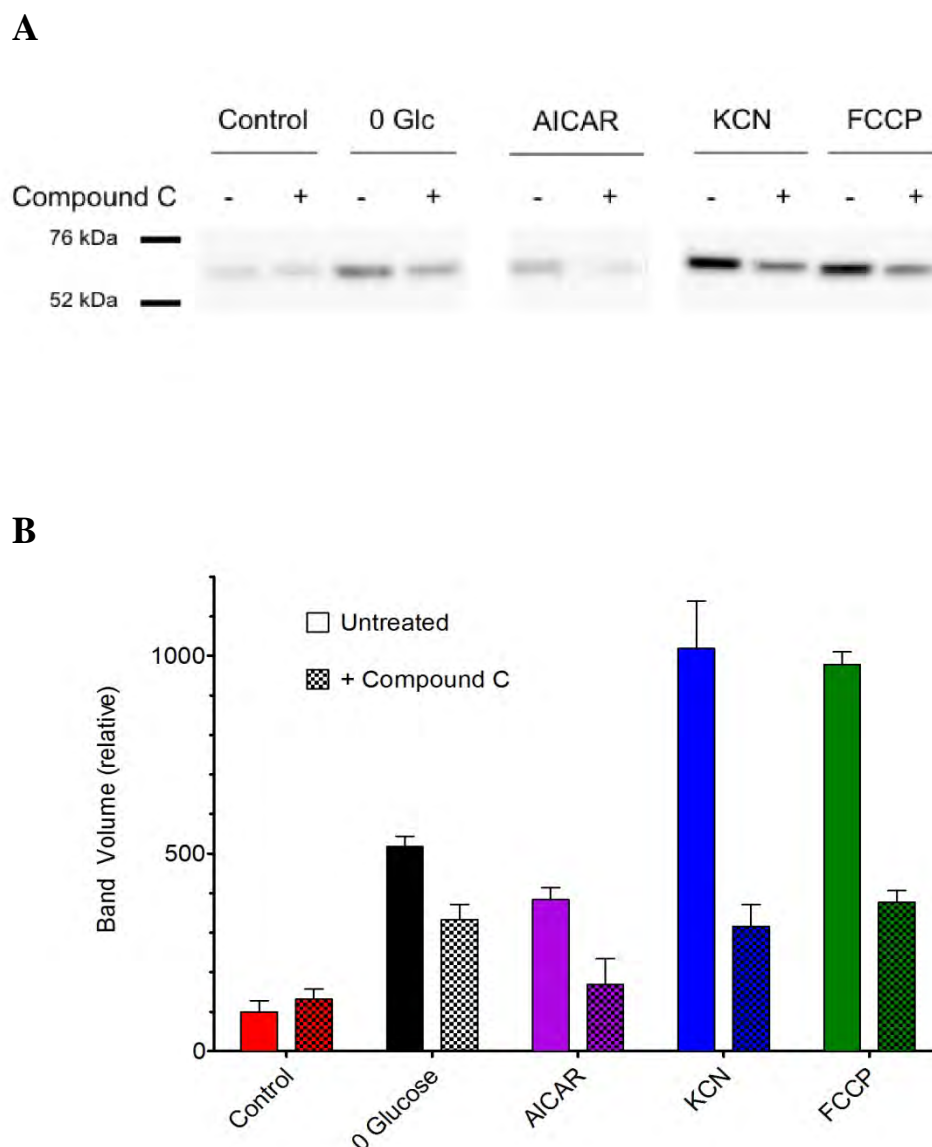


Figure 4.4: Inhibition of AMPK Phosphorylation During Stress

Compound C inhibition of AMPK phosphorylation during metabolic stress. *A.* Representative Western blot of whole cell bEnd.3 lysates in the absence or presence of glucose, KCN, FCCP, AICAR and Compound C. Prior to lysis, cells were treated for 15 min at 37 °C with 5 mM glucose (control), 0 glucose, 5 mM KCN, 8 μ g/mL FCCP or for 2 hours with 2 mM AICAR in the absence or presence of 10 μ M Compound C. Cell lysate (30 μ g total protein) was loaded into each lane and probed with AMPK P-Thr 172 antibody and band volumes were quantitated. *B.* *Ordinate:* relative band volume (%); *Abcissa:* experimental condition. Data represent the mean \pm S.E.M of three separate experiments.

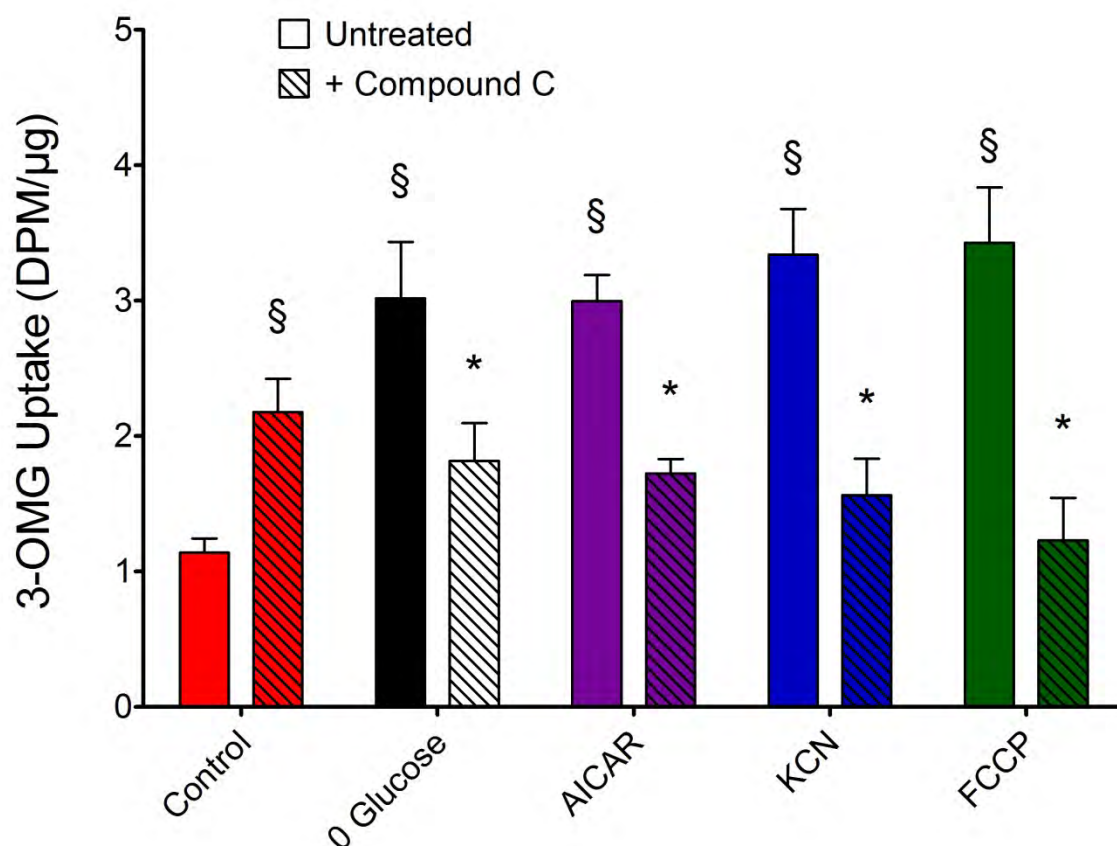


Figure 4.5: Inhibition of Metabolic Stress-Stimulated Transport

Compound C inhibition of stimulated 3-OMG uptake. Prior to cooling to 4°C, glucose depletion and transport initiation, cells were treated for 15 min at 37 °C with 5 mM glucose (control), 0 glucose, 5 mM KCN, 8 μg/mL FCCP or for 2 hours with 2 mM AICAR in the absence or presence of 10 μM Compound C. Uptake of 20 mM 3-OMG was then measured for 30 seconds in each condition. *Ordinate*: 3-OMG uptake (dpm per μg total cell protein). *Abscissa*: experimental condition. Data represent the mean ± S.E.M of three separate experiments. The symbol (*) represents a significant decrease in each data point versus its –Compound C control (p= 0.001). The symbol (§) represents a significant increase in each data point versus untreated control (p=0.000001). P values were obtained from a 1 tailed t-test assuming 2 sample equal variance.

Compound C Inhibits Metabolic Stress-Induced 3-OMG Uptake Stimulation

We next asked whether inhibition of AMPK phosphorylation suppresses sugar uptake stimulation during metabolic stress. 3-OMG uptake was measured in bEnd.3 cells in the absence and presence of 10 μ M Compound C in cells that were glucose-starved, treated with 2 mM AICAR, treated with 5 mM KCN, or treated with 8 μ g/ml FCCP, as described above. 3-OMG uptake (Figure 4.5) is stimulated 2.6-fold in glucose starved cells, 2.6-fold in AICAR treated cells, 2.9-fold in KCN treated cells, and 3.0-fold in FCCP treated cells. Glucose transport in control cells is also stimulated 1.9-fold by 10 μ M Compound C. Compound C inhibits 3-OMG uptake by 40% in glucose starved cells, 42% in AICAR treated cells, by 54% in KCN treated cells, and by 64% in FCCP treated cells (Figure 4.5).

Compound C Inhibition of GLUT1 Recruitment During Acute Metabolic Stress

bEnd.3 sugar transport stimulation during acute metabolic stress is mediated by recruitment of intracellular GLUT1 to the plasma membrane (187). The role of AMPK in mediating this process was evaluated by examining the effects of Compound C on GLUT1 recruitment. Cells were treated with 2 mM AICAR, glucose-starved or KCN-treated as described above in the absence or presence of 10 μ M Compound C. Cells were then washed, cooled to 4°C, and treated with the membrane-impermeant Sulfo-NHS-SS-Biotin to label exposed primary amines (lysine side-chains). The reaction was quenched, the cells lysed in lysis buffer containing detergent, and biotinylated proteins were precipitated with streptavidin beads. Precipitated proteins were analyzed by Western blot

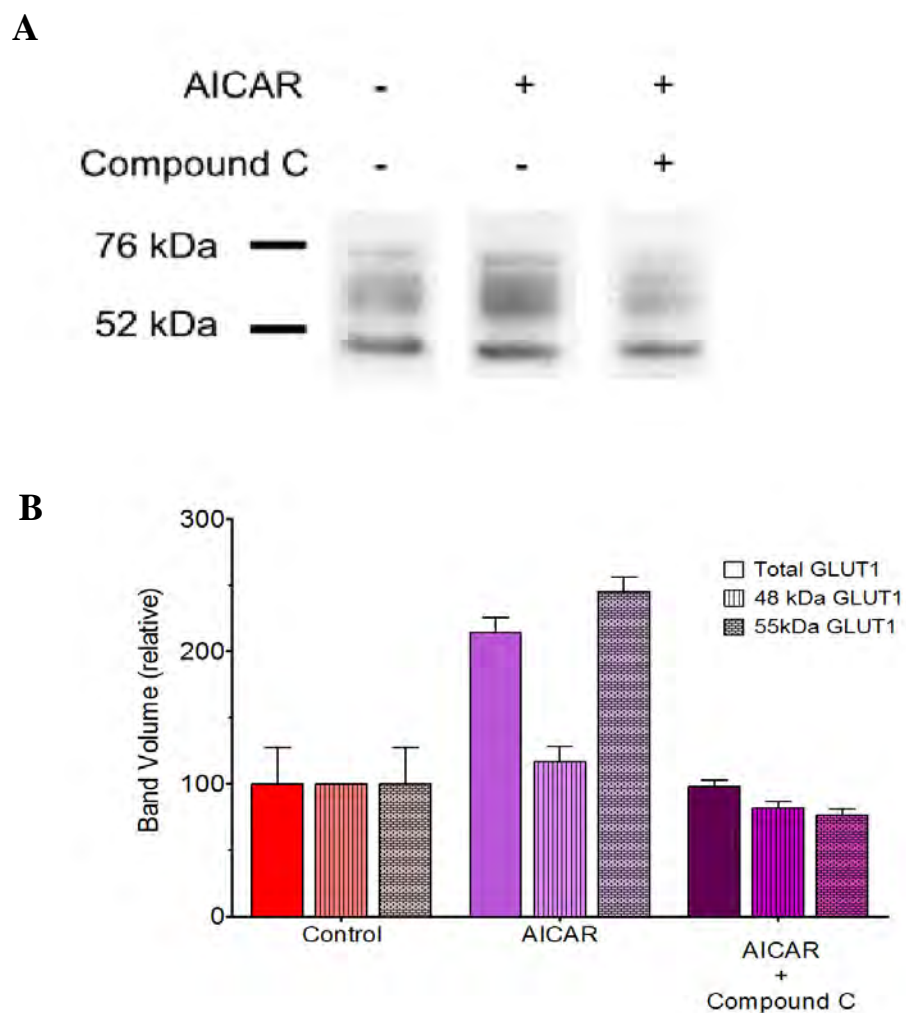


Figure 4.6: Inhibition of AMPK Induced GLUT1 Recruitment By Compound C

Inhibition of plasma membrane GLUT1 recruitment by Compound C. *A*. Representative Western blot of cell surface biotinylated bEnd.3 cell proteins obtained in the absence and presence of 2 mM AICAR and 10 μ M Compound C. Three C-terminal antibody-reactive species are observed with $M_{r(\text{app})}$ 42 kDa, 48 kDa, and 55 kDa, respectively. Cells were treated for 2 hours with AICAR at 37 °C before cooling to 4 °C and biotinylation. 80 μ g of total protein was loaded into each lane and blotted with GLUT1 C-Ab. Band densities were quantitated as total, 48 kDa, and 55 kDa GLUT1 species and are shown in *B*. *Ordinate*: Relative band volume %. *Abscissa*: Experimental condition. Quantitations are shown as mean \pm SEM of at least two experiments.

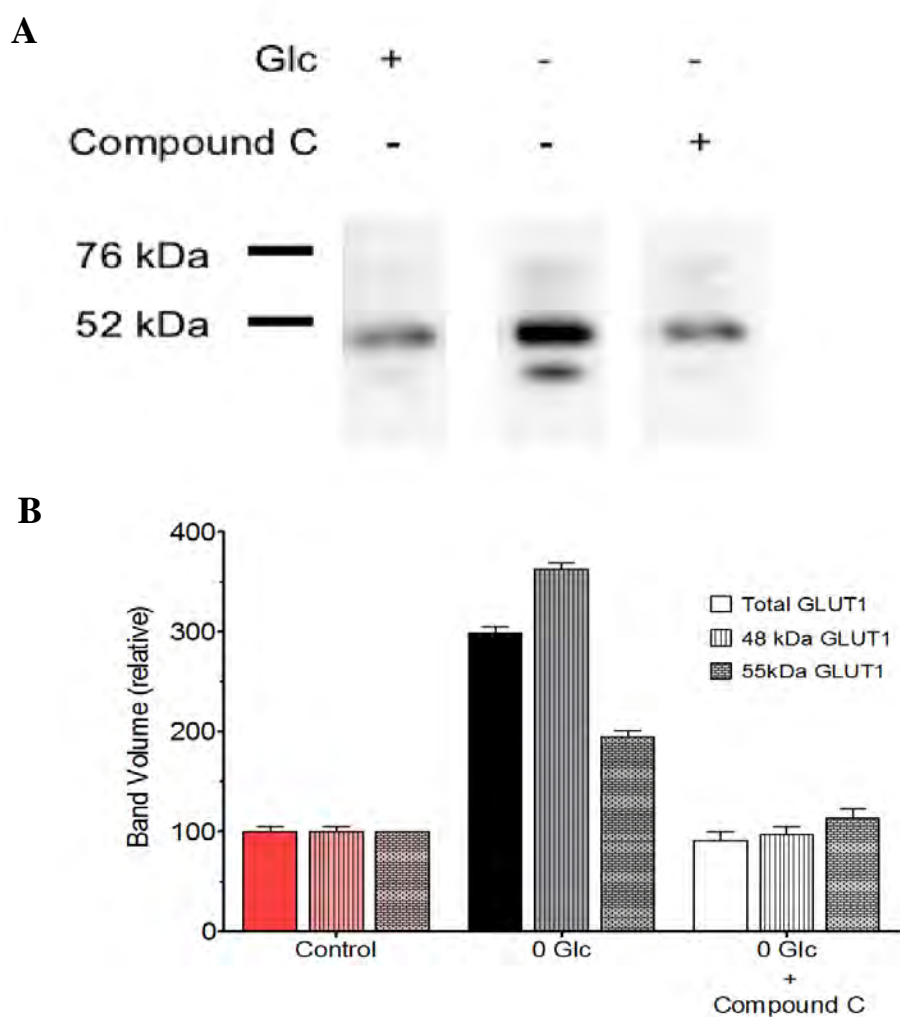


Figure 4.7: Inhibition of GLUT1 Recruitment Upon Glucose Depletion

A. Representative Western blots of cell-surface biotinylated bEnd.3 cell proteins obtained in the absence and presence of 5 mM Glucose and 10 μ M Compound C. Three C-terminal antibody-reactive species are observed with $M_{r(\text{app})}$ 42 kDa, 48 kDa, and 55 kDa. Cells were glucose-depleted for 15 minutes at 37 $^{\circ}$ C before cooling to 4 $^{\circ}$ C and biotinylation. Total streptavidin-pull down protein (80 μ g) was loaded into each lane and blotted with GLUT1 C-Ab. Band densities were quantitated as total, 48 kDa, and 55 kDa GLUT1 species and are shown in B. *Ordinate*: Relative band volume %. *Abscissa*: Experimental condition. Each experiment was repeated at least twice and the results of quantitations are shown as mean \pm SEM.

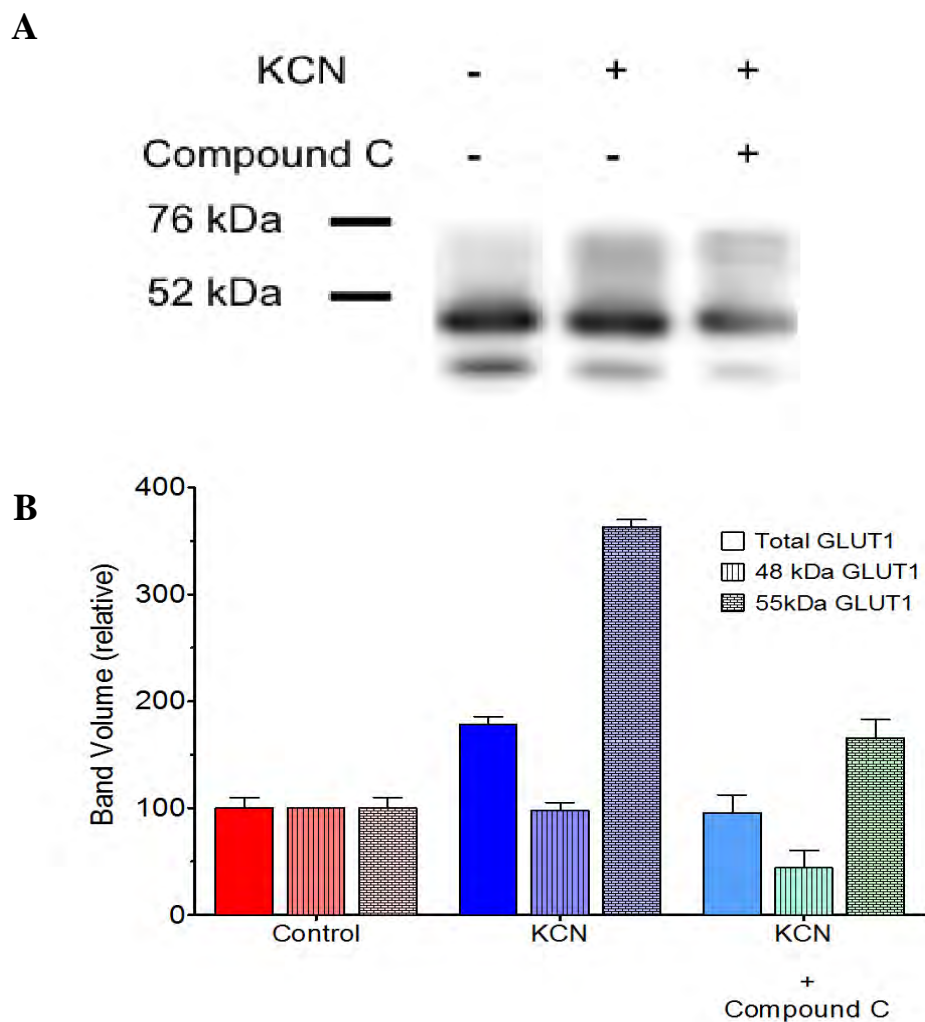


Figure 4.8: Inhibition of KCN Recruitment of GLUT1 by Compound C

A. Representative Western blots of cell surface biotinylated bEnd.3 cell proteins obtained in the absence and presence of 5 mM KCN and 10 μ M Compound C. Three C-terminal antibody-reactive species are observed with $M_{r(\text{app})}$ 42 kDa, 48 kDa, and 55 kDa. Cells were KCN-treated for 15 minutes at 37 $^{\circ}$ C before cooling to 4 $^{\circ}$ C and biotinylation. Total protein (80 μ g) was loaded into each lane and blotted with GLUT1 C-Ab. Band densities were quantitated as total, 48 kDa, and 55 kDa GLUT1 species and are shown in B.

Ordinate: Relative band volume %. *Abscissa:* Experimental condition. Each experiment was repeated at least twice and the results of quantitations are shown as mean \pm SEM.

using anti-GLUT1 C-terminal IgGs (Figures 4.6A, 4.7A, and 4.8A) and band densities were quantitated (Figures 4.6B, 4.7B, and 4.8B). As recently reported (187), biotinylated, C-terminal-reactive GLUT1 is revealed as a 48 kDa species plus a broadly mobile 55 kDa species. Occasionally a 42 kDa species is also observed (Figures 4.7A, 4.8A). Treatment of membranes with peptide: *N*-glycosidase F causes all species to collapse to a 40-42 kDa GLUT1 species (187). Cell-surface expression of the 48-kDa GLUT1 C-terminal antibody-reactive species is unchanged by AICAR or KCN, whereas expression of the 55-kDa species is increased by 2–3-fold (Fig. 5, *B* and *F*). Glucose depletion appears to enhance cell-surface expression of the 48 and 55 kDa species by 4- and 2-fold, respectively. AICAR treatment increases total plasma membrane GLUT1 by approximately 2.1-fold, glucose depletion by approximately 3.0-fold, and KCN treatment by approximately 1.8-fold over controls. In contrast, Compound C-treated cells show no significant increase in plasma membrane GLUT1 (Figure 4.6B, 4.7B and 4.8B). These results mirror the increases in 3-OMG transport capacity produced by metabolic poisons.

Discussion

This study examines the hypothesis that AMPK modulates GLUT1-mediated sugar uptake in brain microvascular endothelial cells by regulating plasma membrane GLUT1 levels during acute metabolic stress. We show that endothelial cell AMPK is phosphorylated during metabolic stress and that this is inhibited in a dose-dependent manner by the AMPK antagonist, Compound C. AMPK activation by the AMPK agonist AICAR or by metabolic stress is associated with stimulation of GLUT1-mediated sugar uptake; but transport stimulation is inhibited in a dose-dependent manner by Compound

C. Transport stimulation appears to be caused by recruitment of intracellular GLUT1 to the cell surface, because Compound C blocks AICAR- and metabolic stress-induced GLUT1 recruitment.

Compound C is a high affinity ligand that competes with AMP and ATP for binding to AMPK (240). ATP- and Compound C-liganded AMPK are catalytically inactive but AMP-binding promotes AMPK phosphorylation, resulting in activation (180,181). ZMP, an AICAR metabolite, also binds at the AMP-binding site to activate the kinase (181,187). Compound C and ZMP-binding are thus mutually exclusive, thereby explaining Compound C-inhibition of AMPK activation by AICAR. Our studies confirm that AMPK phosphorylation in bEnd.3 cells is blocked by Compound C in a dose-dependent manner. The observed $K_{i(\text{app})}$ (1 - 5 μM) is significantly greater than the reported $K_{d(\text{app})}$ (120 nM) for Compound C interaction with AMPK (241). This discrepancy most likely results from competition between Compound C and intracellular ZMP for binding to AMPK. At $[\text{ZMP}] \leq 2 \text{ mM}$ and $K_{d(\text{app})}$ for ZMP binding to AMPK = 90 μM (242), $K_{i(\text{app})}$ for Compound C inhibition of AMPK ($K_{d\text{Compound C}}(1 + [\text{ZMP}]/K_{d\text{ZMP}})) \leq 2.8 \mu\text{M}$.

Our previous work shows that acute metabolic stress induced by ATP depletion and mimicked by AICAR application to bEnd.3 cells increases sugar uptake and promotes AMPK phosphorylation (187). While a link between AMPK activation and sugar transport stimulation can be inferred, these findings do not establish causality. The present study demonstrates that AMPK activation and stimulation of sugar transport are both inhibited by the AMPK inhibitor Compound C.

Compound C does not inhibit sugar transport directly. Rather, bEnd.3 cell 3-OMG uptake is stimulated 1.9-fold by Compound C. This may result from a well-characterized, independent regulatory mechanism (113,154,214,243-245) in which GLUT1-adenine nucleotide interactions allosterically modify sugar transport activity. ATP binding to GLUT1 reduces V_{\max} and K_m for sugar uptake, while AMP displaces ATP from GLUT1, converting the protein to a high-capacity, low-affinity transporter. Compound C may compete with intracellular ATP for binding to GLUT1, thereby reversing allosteric inhibition of transport and increasing sugar uptake. It would be interesting to examine whether Compound C directly binds GLUT1 and can displace ATP and stimulate sugar uptake using a cell system without AMPK, such as red blood cells.

Stimulation of sugar uptake and AMPK phosphorylation by metabolic stress are significantly attenuated by Compound C. Cell-surface GLUT1 recruitment is completely blocked by Compound C. Phosphorylation of acetyl-CoA carboxylase (a GLUT1-independent, AMPK downstream target (240)) is also inhibited by Compound C. These data, in conjunction with our previous findings (187), strengthen the hypothesis that AMPK-activation mediates bEnd.3 cell sugar transport stimulation during metabolic stress. Past studies have suggested that metabolic stress, and consequently AMPK, may play a role in changing the lipid environment in the plasma membrane, causing the masking and unmasking of glucose transporters at the cell surface (156,246). When GLUT1 resides in lipid raft domains, its accessibility and activity are limited. However, during times of metabolic stress, GLUT1 would move out of lipid raft domains via AMPK activity, thus increasing glucose uptake into the cell. This unmasking of GLUT1

could explain both the increased biotin labeling and increased GLUT1-mediated transport we saw in our studies. However, further studies have been done demonstrating that lipid rafts are an artifact of Triton-X100 treatment of biological membranes (247,248). Therefore, it is not feasible that AMPK modulation of lipid rafts is affecting GLUT1 surface labeling by biotin, or its transport activity.

Chronic metabolic stress (hours to days) causes increased GLUT1 expression and increased sugar transport in brain microvascular endothelial cells (194,196,197,213,216,229). In contrast, acute metabolic stress (seconds to minutes) is without effect on GLUT1 expression, but increases cellular sugar transport capacity via recruitment of GLUT1 to the plasma membrane (187,200,201). The work presented here supports the hypothesis that AMPK modulates GLUT1 trafficking to the plasma membrane. AMPK-inhibition prevents stress-induced GLUT1 recruitment to the cell surface and ablates transport stimulation. AMPK is the primary sensor in cellular energy homeostasis (180,181), targeting and controlling numerous downstream processes such as gene expression and protein synthesis (249,250), glycolysis (179,251) and fatty acid oxidation (231,252,253). AMPK regulates GLUT1- and GLUT4-mediated sugar transport in muscle and adipose through control of gene expression or protein trafficking to the plasma membrane (237,238,250,254). AMPK therefore plays a dual role of initiating primary responses to acute changes in metabolic state and long-term responses to chronic alterations in cellular metabolism.

This dual role may be important in regulating the flow of metabolic substrates across the blood-brain barrier. Tight junctions connecting the endothelial cells of the blood-brain

barrier (255) prevent the diffusional exchange of small polar molecules between serum and brain. Metabolites needed for brain function must be transported across the endothelial cell barrier before they can be utilized (34-36,256). Glucose is a primary energy source for the brain and its transport across the blood-brain barrier is rate-limiting for brain glucose utilization under conditions of metabolic stress (13,23). When a region of the brain becomes significantly activated or when blood glucose levels fall, local blood-flow and glucose uptake are activated to maintain brain glucose availability (196,197,213,216,229,257). Our previous work (187) in combination with the present study reveal the underlying mechanism of blood-brain barrier sugar transport regulation during acute metabolic stress. Elevated intracellular AMP interacts with AMPK, causing AMPK phosphorylation and activation. Activated AMPK promotes the trafficking of intracellular GLUT1 to endothelial cell luminal and abluminal membranes, thereby enhancing glucose transport across the blood-brain barrier and glucose utilization by the brain. The downstream targets regulating GLUT1 trafficking and the trafficking steps (endocytosis, exocytosis) regulated by AMPK are unknown and warrant further study.

CHAPTER V

CONCLUSIONS AND FUTURE DIRECTIONS

It has long been assumed that increased glucose transport at the blood-brain barrier during acute metabolic stress is a result of increases in GLUT1 intrinsic activity, likely through loss of ATP binding to GLUT1 (155,214,243). Unlike chronic metabolic stress, acute stress has not been shown to increase GLUT1 expression (178,200). However, there have been few studies that have either confirmed this hypothesis or definitively characterized how glucose transport is increased during acute stress. The data presented in this thesis demonstrate a model for acute regulation of GLUT1-mediated sugar uptake in blood-brain barrier endothelial cells which is only in partial agreement with current assessments of acute stress effects on glucose transport. We have shown that GLUT1-mediated uptake is increased within 10 minutes of ATP depletion through translocation of intracellular stores to the plasma membrane without increases in GLUT1 expression. We have also demonstrated that the AMP-dependent protein kinase AMPK is a key modulator of GLUT1 trafficking under conditions where ATP is rapidly depleted.

Perhaps one of the most pressing questions raised in studies of acute metabolic stress at the blood-brain barrier involves its relevance to *in vivo* metabolism. It could be argued that acute depletions of intracellular ATP are rare outside of individuals with metabolic disorders. Certainly, the cases of almost total ATP depletion seen in KCN and FCCP treated bEnd.3 cells are highly unlikely to occur unless the affected organism were

poisoned by these compounds. However, acute hypoglycemia can occur through a number of different means that are quite common to a variety of mammals, especially humans. Many patients with both type-1 and type-2 diabetes battle with acute hypoglycemia on a regular basis that results from poor blood sugar control and rapid insulin release into the bloodstream (258). In non-diabetics, sudden drops in blood glucose can be caused simply by exercise without sufficient food intake, particularly in athletes (259). The use of aspirin has long been known to decrease blood glucose, raising the potential for sudden hypoglycemia, especially if misused (260). In addition, the increase in anti-depressant prescriptions, particularly monoamine oxidase inhibitors (MAOI), has been prevalent in recent years. There is evidence that certain classes of these drugs can cause rapid decreases in blood glucose, especially if mixed with other medications and even certain foods (261). Therefore, our studies provide relevant insight into a regulatory mechanism that is necessary for maintaining brain function in a variety of pathological and normal physiological situations. Particularly, acute glucose deprivation of bEnd.3 cells, which only reduces ATP by only 50%, has the most relevance to the situations mentioned above. Admittedly, the complete, rapid depletion of intracellular ATP by KCN and FCCP in bEnd.3 cells is an extreme condition to study the acute stress response in bEnd.3 cells. However, studies using KCN and FCCP provide useful and relevant insight into the mechanisms of blood-brain barrier glucose transport regulation for many reasons.

The use of KCN and FCCP allow changes in ATP levels to be induced and visualized on a very short time scale without inducing apoptosis, as demonstrated by the KCN

washout experiments. Rapid ATP depletion means that glucose uptake can be measured after very short time points, which offers more accurate insight into how quickly endothelial cells are able to sense, and then respond to, perturbations in energy supply. In addition, both compounds affect ATP depletion and sugar uptake in a dose-dependent manner, allowing for more sensitive attenuation of the metabolic stress condition that simply cannot be achieved with glucose depletion. Finally, the use of KCN and FCCP allowed us to directly test the hypothesis that intrinsic changes in GLUT1 activity as a result of loss of ATP binding was the cause of increased GLUT1-mediated transport. Since ATP levels were depleted close to zero in KCN and FCCP-treated bEnd.3 cells, GLUT1-mediated transport would have increased without changes in protein expression or localization, and without interference of intracellular ATP. However, based on our findings, GLUT1 translocation to the plasma membrane appears to be the primary cause of increased glucose uptake in blood-brain barrier endothelial cells, with allosteric regulation by ATP only playing a minor role. Regardless of the severity of ATP depletion by KCN and FCCP, the transport and GLUT1 localization results are in agreement with the data generated from the much less drastic glucose starvation and AMPK stimulation experiments.

Translocation of GLUT1 to the plasma membrane in response to outside signals, while not unique to endothelial cells, does provide a dynamic adaptive mechanism for maintaining energy homeostasis. In most cases, increased GLUT1 at the plasma membrane resulting from growth factor or stress molecule signaling is caused by direct upregulation of GLUT1 expression. Increased GLUT1 synthesis leads to increased

cellular protein that eventually ends up at the plasma membrane (156,165,166,262). However, since approximately 50% of GLUT1 resides in intracellular pools at the blood-brain barrier (186), by default, mobilization of those carriers to the plasma membrane would allow a doubling of transport capacity into the cell. Not only do our data support this view, but the rapid response to metabolic stresses is comparable to that seen in the insulin-response by GLUT4 in adipocytes. While the sugar uptake capacity in insulin-responsive cells is much more dramatic, some similarities exist based on the rapid, reversible transport response to stress/insulin seen in bEnd.3 cells and insulin-sensitive tissue, respectively (263). The most striking difference in the bEnd.3 response to acute metabolic stress is that, unlike in insulin stimulated cells, GLUT1 trafficking to the plasma membrane is not a result of increased constitutive recycling, as evidenced by the lack of Na⁺K⁺ATPase recruitment upon acute stress. Instead, it would appear that regulation of GLUT1 trafficking is via a more specific mechanism that allows for its rapid recruitment to the plasma membrane in response to decreasing ATP.

AMPK has long been considered the master switch in maintaining cellular metabolic homeostasis in cells. Its ability to increase fatty acid oxidation, glycolysis, and glucose uptake and decrease lipogenesis, gluconeogenesis, and glycogen synthesis are well documented in a variety of tissue types (181,236). As a result, there are a number of downstream targets for AMPK that allow it to control everything from protein synthesis and gene expression to protein trafficking. Its activity is tied directly to AMP binding its catalytic α subunit, inducing phosphorylation and activation of the enzyme, so it should

be no surprise that increased AMP generated by ATP depletion through glucose starvation and KCN or FCCP treatment would activate AMPK in bEnd.3 cells. All of these stresses were shown to activate AMPK, and specific inhibition of AMPK by Compound C ablates its phosphorylation, regardless of the stress condition monitored. In addition, AMPK activation through the agonist AICAR, as well as activation through metabolic stress, increases GLUT1-mediated sugar uptake and recruitment to the plasma membrane. What is surprising and unique is that Compound C inactivation of AMPK ablates both stimulation of sugar uptake and GLUT1 recruitment to the plasma membrane, regardless of the stress condition tested. This indicates that AMPK activation is both necessary and sufficient for increased GLUT1-mediated transport and GLUT1 translocation to the plasma membrane. It will be important to confirm these results by knocking down AMPK in bEnd.3 cells to eliminate the possibility of non-specific side effects from Compound C treatment. Although there are a number of other stress-activated signaling molecules that can regulate GLUT1-mediated transport, such as p38 and ERK1/2, based on our studies it would appear that they play little to no role in regulation of endothelial cell glucose transport during acute stress (264,265).

HIF1 α is also a known regulator of GLUT1-mediated transport, and is primarily responsible for the upregulation of GLUT1 expression seen at the blood-brain barrier during chronic stress (177,178). Interestingly, HIF1 α is also a downstream target of AMPK, which can be regulated through the mTOR signaling pathway (266). Therefore, it is possible that HIF1 α could be a downstream modulator of AMPK's effect on GLUT1

during acute metabolic stress. Based on our preliminary studies, no conclusions can be drawn about HIF1 α and its role as a downstream target of AMPK regulation of bEnd.3 cell glucose transport. However, future studies could be performed to assess the role HIF1 α plays in regulating bEnd.3 GLUT1 during metabolic stress.

Changes in GLUT1 trafficking to the plasma membrane can occur by three possible mechanisms: changes in endocytosis, changes in exocytosis, or changes in both processes. The increased cell surface GLUT1 seen in bEnd.3 cells could arise from either a decrease in endocytosis, an increase in exocytosis, or a combination of the two during metabolic stress. Since AMPK is involved in regulating GLUT1 trafficking in bEnd.3 cells, considerations should be made as to its mode of action on GLUT1 recycling, even though AMPK does not directly phosphorylate GLUT1 itself (150). Studies in muscle cells have shown that AMPK activation can induce an increase in GLUT4-mediated sugar uptake that is insulin independent. Furthermore, stimulation of these cells with insulin in conjunction with activation of AMPK shows additive increases to GLUT4-mediated glucose uptake. It has been shown that insulin primarily regulates GLUT4 trafficking by accelerating exocytosis of the protein to the plasma membrane. However, AMPK activity in insulin-sensitive cells has the opposite effect, decreasing endocytosis of GLUT4 from the plasma membrane. Thus, the addition of both stimuli causes an increase in exocytosis, a decrease in endocytosis, and an additive increase in GLUT4-mediated sugar uptake (267). In terms of GLUT1, AMPK's activity in insulin-sensitive muscle cells may give insight into its mode of action in bEnd.3 cells. Based on these

studies, GLUT1 recruitment to the plasma membrane could be a result of AMPK-decreased endocytosis. Certainly, AMPK activation has a direct effect on GLUT1 trafficking. However, further study is needed to determine which aspects of trafficking are regulated by AMPK and through which pathway, since PKC and PI3K have both been shown to control GLUT1 translocation to the plasma membrane in a variety of cell types, including insulin-sensitive tissue (166,268). In addition, there could be other as yet unknown factors that regulate GLUT1 trafficking. For example, it is possible that GLUT1 trafficking could be directed based on the whether ATP or AMP is bound to the transporter. If ATP is bound to GLUT1, then energy supplies in the cell are high, so higher levels of transporter are unnecessary at the plasma membrane. As a result, GLUT1 may be directed to reside inside the cell. In contrast, when ATP drops and AMP binds GLUT1, it is possible that some factor (possibly AMPK or a downstream target) could recognize AMP-GLUT1 and induce translocation to the plasma membrane. Although there is no data to currently support this model, it is possible that the nucleotide bound to GLUT1 may play a role in not only its transport activity, but its localization. While there are also a few potential downstream targets to investigate, such as HIF1 α , many of the signaling factors involved in GLUT1 trafficking, and protein trafficking in general, remain elusive at this time. Therefore, much work needs to be done to identify and characterize these targets in the context of modulation of endothelial cell glucose transport. Our attempts to measure the changes to GLUT1 endocytosis and exocytosis have thus far been unsuccessful. However, transfection of a tagged GLUT1 construct

could provide useful information about changes in GLUT1 localization, as well as changes in the kinetics of internalization and externalization during metabolic stress.

When considering GLUT1-mediated transport at the blood-brain barrier, the role of the brain in regulating endothelial cell transport must be included. While our data suggest that the blood-brain barrier is able to sense and respond to changes in energy levels through the activity of AMPK, it remains a possibility that the brain itself would play a role in maintaining its own energy supply. Intracellular glucose concentration in neurons and astrocytes tends to be lower than endothelial glucose, even under normal metabolic conditions (13). Therefore, decreases in glucose supply across the blood-brain barrier would also be sensed by neurons and astrocytes rather quickly. There is evidence to suggest that astrocyte-endothelial cell communication is a common phenomenon at the blood-brain barrier. Astrocyte feet rest on the blood vessels comprising the endothelium, so cell-to-cell signaling could be achieved relatively quickly and easily. It has been shown that astrocytes are able to rapidly communicate with neurons and each other, increasing glucose transport during metabolic activity (20,269). In addition, two-way communication between astrocytes and the blood-brain barrier have been shown to affect both astrocyte differentiation and blood-brain barrier permeability (270). However, what is most interesting is that astrocytes have not only been shown to induce blood-brain barrier-like properties in non blood-brain barrier endothelial cells when co-cultured, but chronically glucose-deprived astrocytes can influence glucose transporter expression and glucose uptake in brain microvessels (257,271,272). These studies indicate that there is a mechanism for brain-endothelial communication, but the factors involved in coordinating

glucose uptake across the blood-brain barrier are unclear. It is possible that ATP depletion could lead to activation of AMPK in neurons, astrocytes, or both. This activation of AMPK could also activate GLUT1-mediated transport at the blood-brain barrier through a secretory signaling mechanism. Furthermore, the studies on brain-endothelial communication give no insight as to how rapid changes in energy affect brain metabolism. It is possible that brain cells respond in a similar manner to blood-brain barrier endothelial cells, though there is no evidence to date in support of this. Perhaps the endothelium is responsible for maintaining brain glucose homeostasis during acute stress, while brain cells are able to induce the blood-brain barrier to increase transport capacity under more chronic stress conditions. Unfortunately, our studies have not provided sufficient data at this time to reach any such conclusions, but it is clear that there is much to be learned about regulation of glucose uptake by the brain.

In conclusion, the data presented in this thesis provide a preliminary model for how blood-brain barrier endothelial cell glucose transport is modulated during acute metabolic stress. There have been numerous studies demonstrating the changes to localized cerebral blood flow during times of metabolic stress and brain injury (14-16). It has been presumed that increased blood flow allows the delivery of essential metabolites to the area under stress, most importantly glucose and oxygen. However, without a mechanism to accommodate this localized influx of nutrients, the extra volume of blood would do no good due to the impermeability of the blood-brain barrier. Our studies have further defined the mechanism of how the blood-brain barrier endothelial cells may respond to metabolic stress by rapidly increasing local glucose transport capacity as needed. During

metabolic stress, AMPK is activated, causing translocation of intracellular GLUT1 to the plasma membrane. By increasing GLUT1 at the endothelial cell surface, the blood-brain barrier is at least doubling the capacity for glucose uptake into the brain, providing much needed metabolic substrate during times when acute stress leaves energy demand high or energy supply low. Thus, by exerting localized control over both the vasculature and endothelium, the brain is able to regulate glucose supplies in order to compensate for rapid changes in its metabolic state, ensuring continued function and survival of the organ and organism.

While it is clear that GLUT1 translocation, mediated by AMPK, is responsible for increased glucose transport rate, there are a number of questions that still remain as a result of this work. For example: what are some of the other downstream signaling factors that modulate GLUT1 trafficking through AMPK? Do these unknown factors regulate GLUT1 endocytosis, exocytosis, or both? Is this trafficking effect truly GLUT1-specific, or are there other proteins that follow the same pathway? What is the role of neurons and astrocytes in modulating endothelial GLUT1 during acute stress, if any? Does acute metabolic stress in brain cells produce the same effect on transport at the blood-brain barrier? Seeking the answers to these questions will not only provide the groundwork for many future studies, but will contribute significantly to a more complete understanding of how the brain, and the barrier that protects it, modulate glucose uptake and energy homeostasis.

BIBLIOGRAPHY

1. Anil, M. H., and Forbes, J. M. (1987) Neural Control and Neurosensory Functions of the Liver *Proc Nutr Soc.* **46**, 125-133
2. Bell, F. R. (1971) Hypothalamic Control of Food Intake *Proc Nutr Soc.* **30**, 103-109
3. Heinrichs, M., von Dawans, B., and Domes, G. (2009) Oxytocin, Vasopressin, and Human Social Behavior *Front Neuroendocrin.* **30**, 548-557
4. McNeilly, A. S. (1980) Prolactin and the Control of Gonadotrophin Secretion in the Female *J Reprod Fertil.* **58**, 537-549
5. Ross, H. E., and Young, L. J. (2009) Oxytocin and the Neural Mechanisms Regulating Social Cognition and Affiliative Behavior *Front Neuroendocrin.* **30**, 534-547
6. Salo, L. M., Campos, R. R., and McAllen, R. M. (2006) Differential Control of Cardiac Functions by the Brain *Clin Exp Pharmacol Physiol.* **33**, 1255-1258
7. Greengard, P., and Straub, R. W. (1962) Metabolic Studies on the Hyperpolarization Following Activity in Mammalian Non-Myelinated Nerve Fibres *J Physiol.* **161**, 414-423
8. Stewart, M. A., Passonneau, J. V., and Lowry, O. H. (1965) Substrate Changes in Peripheral Nerve During Ischemia and Wallerian Degeneration *J Neurochem.* **12**, 719-727
9. Bak, L. K., Schousboe, A., Sonnewald, U., and Waagepetersen, H. S. (2006) Glucose Is Necessary to Maintain Neurotransmitter Homeostasis During Synaptic Activity in Cultured Glutamatergic Neurons *J Cereb Blood Flow Metab.* **26**, 1285-1297
10. den Hertog, A., Greengard, P., and Ritchie, J. M. (1969) On the Metabolic Basis of Nervous Activity *J Physiol.* **204**, 511-521
11. Castro, M. A., Beltrán, F. A., Brauchi, S., and Concha, I. I. (2009) A Metabolic Switch in Brain: Glucose and Lactate Metabolism Modulation by Ascorbic Acid *J Neurochem.* **110**, 423-440
12. Hertz, L., and Dienel, G. A. (2005) Lactate Transport and Transporters: General Principles and Functional Roles in Brain Cells *J Neurosci Res.* **79**, 11-18
13. Simpson, I. A., Carruthers, A., and Vannucci, S. J. (2007) Supply and Demand in Cerebral Energy Metabolism: The Role of Nutrient Transporters *J Cereb Blood Flow Metab.* **27**, 1766-1791
14. Berntman, L., and Siesjou, B. K. (1978) Cerebral Metabolic and Circulatory Changes Induced by Hypoxia in Starved Rats. *J Neurochem.* **31**, 1265-1276
15. Fox, P. T., and Raichle, M. E. (1986) Focal Physiological Uncoupling of Cerebral Blood Flow and Oxidative Metabolism During Somatosensory Stimulation in Human Subjects *Proc Natl Acad Sci U S A.* **83**, 1140-1144
16. Abdul-Rahman, A., Dahlgren, N., Ingvar, M., Rehncrona, S., and Siesjo, B. K. (1979) Local Versus Regional Cerebral Blood Flow in the Rat at High (Hypoxia) and Low (Phenobarbital Anesthesia) Flow Rates *Acta Physiol Scand.* **106**, 53-60

17. Pierre, K., and Pellerin, L. (2005) Monocarboxylate Transporters in the Central Nervous System: Distribution, Regulation and Function *J Neurochem.* **94**, 1-14
18. Fillenz, M. (2005) The Role of Lactate in Brain Metabolism *Neurochem Int.* **47**, 413-417
19. Fox, P. T., Raichle, M. E., Mintun, M. A., and Dence, C. (1988) Nonoxidative Glucose Consumption During Focal Physiologic Neural Activity *Science.* **241**, 462-464
20. Gjedde, A., Marrett, S., and Vafaee, M. (2002) Oxidative and Nonoxidative Metabolism of Excited Neurons and Astrocytes *J Cereb Blood Flow Metab.* **22**, 1-14
21. Prichard, J., Rothman, D., Novotny, E., Petroff, O., Kuwabara, T., Avison, M., Howseman, A., Hanstock, C., and Shulman, R. (1991) Lactate Rise Detected by ¹H Nmr in Human Visual Cortex During Physiologic Stimulation *Proc Natl Acad Sci U S A.* **88**, 5829-5831
22. Pellerin, L., and Magistretti, P. J. (1994) Glutamate Uptake into Astrocytes Stimulates Aerobic Glycolysis: A Mechanism Coupling Neuronal Activity to Glucose Utilization *Proc Natl Acad Sci U S A.* **91**, 10625-10629
23. Mangia, S., Simpson, I. A., Vannucci, S. J., and Carruthers, A. (2009) The in Vivo Neuron-to-Astrocyte Lactate Shuttle in Human Brain: Evidence from Modeling of Measured Lactate Levels During Visual Stimulation *J Neurochem.* **109 Suppl 1**, 55-62
24. Coomber, B. L., and Stewart, P. A. (1985) Morphometric Analysis of Cns Microvascular Endothelium *Microvasc Res.* **30**, 99-115
25. Oldendorf, W. H., Cornford, M. E., and Brown, W. J. (1977) The Large Apparent Work Capability of the Blood-Brain Barrier: A Study of the Mitochondrial Content of Capillary Endothelial Cells in Brain and Other Tissues of the Rat *Ann Neurol.* **1**, 409-417
26. Dejana, E. (2004) Endothelial Cell-Cell Junctions: Happy Together *Nat Rev Mol Cell Biol.* **5**, 261-270
27. Betz, A. L., and Goldstein, G. W. (1986) Specialized Properties and Solute Transport in Brain Capillaries *Ann Rev Physiol.* **48**, 241-250
28. Brightman, M. W., and Reese, T. S. (1969) Junctions between Intimately Apposed Cell Membranes in the Vertebrate Brain *J Cell Biol.* **40**, 648-677
29. Brightman, M. W., Klatzo, I., Olsson, Y., and Reese, T. S. (1970) The Blood-Brain Barrier to Proteins under Normal and Pathological Conditions *J Neurol Sci.* **10**, 215-239
30. Dainty, J., and Krnjevia, K. (1955) The Rate of Exchange of ²⁴Na in Cat Nerves *J Physiol.* **128**, 489-503
31. Krnjevic, K. (1955) The Distribution of Na and K in Cat Nerves *J Physiol.* **128**, 473-488
32. Welch, K., and Davson, H. (1972) The Permeability of Capillaries of the Sciatic Nerve of the Rabbit to Several Materials *J Neurosurg.* **36**, 21-26
33. Fishman, R. A. (1964) Carrier Transport of Glucose between Blood and Cerebrospinal Fluid *Am J Physiol.* **206**, 836-844

34. Crone, C. (1965) Facilitated Transfer of Glucose from Blood into Brain Tissue *J Physiol.* **181**, 103-113
35. Eidelberg, E., Fishman, J., and Hams, M. L. (1967) Penetration of Sugars across the Blood-Brain Barrier *J Physiol.* **191**, 47-57
36. Buschiazzo, P. M., Terrell, E. B., and Regen, D. M. (1970) Sugar Transport across the Blood-Brain Barrier *Am J Physiol.* **219**, 1505-1513
37. Cutler, R. W., and Sipe, J. C. (1971) Mediated Transport of Glucose between Blood and Brain in the Cat *Am J Physiol.* **220**, 1182-1186
38. Lund-Andersen, H. (1979) Transport of Glucose from Blood to Brain *Physiol Rev.* **59**, 305-352
39. Pardridge, W. M., Boado, R. J., and Farrell, C. R. (1990) Brain-Type Glucose Transporter (Glut-1) Is Selectively Localized to the Blood-Brain Barrier. Studies with Quantitative Western Blotting and in Situ Hybridization *J Biol Chem.* **265**, 18035-18040
40. Agre, P., King, L. S., Yasui, M., Guggino, W. B., Ottersen, O. P., Fujiyoshi, Y., Engel, A., and Nielsen, S. (2002) Aquaporin Water Channels--from Atomic Structure to Clinical Medicine *J Physiol.* **542**, 3-16
41. Ahern, C. A., and Kobertz, W. R. (2008) Chemical Tools for K⁺ Channel Biology *Biochemistry.* **48**, 517-526
42. Carruthers, A. (1990) Facilitated Diffusion of Glucose *Physiol Rev.* **70**, 1135-1176
43. Widdas, W. F. (1952) Inability of Diffusion to Account for Placental Glucose Transfer in the Sheep and Consideration of the Kinetics of a Possible Carrier Transfer *J Physiol.* **118**, 23-39
44. Faller, L. D. (2008) Mechanistic Studies of Sodium Pump *Arch Biochem Biophys.* **476**, 12-21
45. Kimura, J., Ono, T., Sakamoto, K., Ito, E., Watanabe, S., Maeda, S., Shikama, Y., Yatabe, M. S., and Matsuoka, I. (2009) Na⁺ & Ndash; Ca²⁺ Exchanger Expression and Its Modulation *Biol Pharm Bull.* **32**, 325-331
46. Wright, E. M. (2001) Renal Na⁺-Glucose Cotransporters *Am J Physiol Renal Physiol.* **280**, F10-18
47. Pao, S. S., Paulsen, I. T., and Saier, M. H., Jr. (1998) Major Facilitator Superfamily *Microbiol Mol Biol Rev.* **62**, 1-34
48. Marger, M. D., and Saier Jr, M. H. (1993) A Major Superfamily of Transmembrane Facilitators That Catalyse Uniport, Symport and Antiport *Trends Biochem Sci.* **18**, 13-20
49. Saier, M. H., Jr., Beatty, J. T., Goffeau, A., Harley, K. T., Heijne, W. H., Huang, S. C., Jack, D. L., Jahn, P. S., Lew, K., Liu, J., Pao, S. S., Paulsen, I. T., Tseng, T. T., and Virk, P. S. (1999) The Major Facilitator Superfamily *J Mol Microbiol Biotechnol.* **1**, 257-279
50. Lemieux, M. J., Jinmei, S., Myong Jin, K., Yafei, H., Anthony, V., Manfred, A., Xiao-Dan, L., and Da-Neng, W. (2003) Three-Dimensional Crystallization of the *Escherichia Coli* Glycerol-3-Phosphate Transporter: A Member of the Major Facilitator Superfamily *Protein Sci.* **12**, 2748-2756

51. Abramson, J., Smirnova, I., Kasho, V., Verner, G., Kaback, H. R., and Iwata, S. (2003) Structure and Mechanism of the Lactose Permease of *Escherichia Coli* *Science* **301**, 610-615
52. Yin, Y., He, X., Szewczyk, P., Nguyen, T., and Chang, G. (2006) Structure of the Multidrug Transporter Emrd from *Escherichia Coli* *Science* **312**, 741-744
53. Hirai, T., Heymann, J. A. W., Shi, D., Sarker, R., Maloney, P. C., and Subramaniam, S. (2002) Three-Dimensional Structure of a Bacterial Oxalate Transporter *Nat Struct Mol Biol.* **9**, 597-600
54. Uldry, M., and Thorens, B. (2004) The Slc2 Family of Facilitated Hexose and Polyol Transporters *Pflügers Archiv.* **447**, 480-489
55. Wu, X., and Freeze, H. H. (2002) Glut14, a Duplicon of Glut3, Is Specifically Expressed in Testis as Alternative Splice Forms *Genomics* **80**, 553-557
56. Joost, H.-G., Bell, G. I., Best, J. D., Birnbaum, M. J., Charron, M. J., Chen, Y. T., Doege, H., James, D. E., Lodish, H. F., Moley, K. H., Moley, J. F., Mueckler, M., Rogers, S., Schurmann, A., Seino, S., and Thorens, B. (2002) Nomenclature of the Glut/Slc2a Family of Sugar/Polyol Transport Facilitators *Am J Physiol Endocrinol Metab.* **282**, E974-976
57. Joost, H.G., and Thorens, B. (2001) The Extended Glut-Family of Sugar/Polyol Transport Facilitators: Nomenclature, Sequence Characteristics, and Potential Function of Its Novel Members *Mol Membr Biol.* **18**, 247-256
58. Dwyer, D. S. (2001) Model of the 3-D Structure of the Glut3 Glucose Transporter and Molecular Dynamics Simulation of Glucose Transport *Proteins* **42**, 531-541
59. Salas-Burgos, A., Iserovich, P., Zuniga, F., Vera, J. C., and Fischbarg, J. (2004) Predicting the Three-Dimensional Structure of the Human Facilitative Glucose Transporter Glut1 by a Novel Evolutionary Homology Strategy: Insights on the Molecular Mechanism of Substrate Migration, and Binding Sites for Glucose and Inhibitory Molecules *Biophys J.* **87**, 2990-2999
60. Henderson, P. J. F. (1990) The Homologous Glucose Transport Proteins of Prokaryotes and Eukaryotes *Res Microbiol.* **141**, 316-328
61. Henderson, P. J. F., and Maiden, M. C. J. (1990) Homologous Sugar Transport Proteins in *Escherichia Coli* and Their Relatives in Both Prokaryotes and Eukaryotes *Philos Trans R Soc Lond B Biol Sci.* **326**, 391-410
62. Sato, M., and Mueckler, M. (1999) A Conserved Amino Acid Motif (R-X-G-R-R) in the Glut1 Glucose Transporter Is an Important Determinant of Membrane Topology *J Biol Chem.* **274**, 24721-24725
63. Zhao, F. Q., and Keating, A. F. (2007) Functional Properties and Genomics of Glucose Transporters *Curr Genomics.* **8**, 113-128
64. Haber, R., Weinstein, S., O'Boyle, E., and Morgello, S. (1993) Tissue Distribution of the Human Glut3 Glucose Transporter *Endocrinology.* **132**, 2538-2543
65. Hellwig, B., and Joost, H. G. (1991) Differentiation of Erythrocyte-(Glut1), Liver-(Glut2), and Adipocyte-Type (Glut4) Glucose Transporters by Binding of the Inhibitory Ligands Cytochalasin B, Forskolin, Dipyrindamole, and Isobutylmethylxanthine *Mol Pharmacol.* **40**, 383-389

66. Lachaal, M., Rampal, A. L., Ryu, J., Lee, W., Hah, J.-S., and Jung, C. Y. (2000) Characterization and Partial Purification of Liver Glucose Transporter Glut2 *Biochim Biophys Acta*. **1466**, 379-389
67. Agus, D. B., Gambhir, S. S., Pardridge, W. M., Spielholz, C., Baselga, J., Vera, J. C., and Golde, D. W. (1997) Vitamin C Crosses the Blood-Brain Barrier in the Oxidized Form through the Glucose Transporters *J Clin Invest*. **100**, 2842-2848
68. Rivas, C., Zúñiga, F., Salas-Burgos, A., Mardones, L., Ormazabal, V., and Vera, J. (2008) Vitamin C Transporters *J Physiol Biochem*. **64**, 357-375
69. Vera, J. C., Rivas, C. I., Fischbarg, J., and Golde, D. W. (1993) Mammalian Facilitative Hexose Transporters Mediate the Transport of Dehydroascorbic Acid *Nature*. **364**, 79-82
70. Mueckler, M., Caruso, C., Baldwin, S., Panico, M., Blench, I., Morris, H., Allard, W., Lienhard, G., and Lodish, H. (1985) Sequence and Structure of a Human Glucose Transporter *Science*. **229**, 941-945
71. Mann, G. E., Yudilevich, D. L., and Sobrevia, L. (2003) Regulation of Amino Acid and Glucose Transporters in Endothelial and Smooth Muscle Cells *Physiol Rev*. **83**, 183-252
72. Harik, S. I., Kalaria, R. N., Andersson, L., Lundahl, P., and Perry, G. (1990) Immunocytochemical Localization of the Erythroid Glucose Transporter: Abundance in Tissues with Barrier Functions *J Neurosci*. **10**, 3862-3872
73. Takata, K., Kasahara, T., Kasahara, M., Ezaki, O., and Hirano, H. (1990) Erythrocyte/Hepg2-Type Glucose Transporter Is Concentrated in Cells of Blood-Tissue Barriers *Biochim Biophys Acta*. **173**, 67-73
74. Drewes, L. R., Horton, R. W., Betz, A. L., and Gilboe, D. D. (1977) Cytochalasin B Inhibition of Brain Glucose Transport and the Influence of Blood Components on Inhibitor Concentration *Biochim Biophys Acta*. **471**, 477-486
75. Pardridge, W. M. (1983) Brain Metabolism: A Perspective from the Blood-Brain Barrier *Physiol Rev*. **63**, 1481-1535
76. Thorens, B., Sarkar, H. K., Kaback, H. R., and Lodish, H. F. (1988) Cloning and Functional Expression in Bacteria of a Novel Glucose Transporter Present in Liver, Intestine, Kidney, and ²-Pancreatic Islet Cells *Cell*. **55**, 281-290
77. Hebert, D. N., and Carruthers, A. (1991) Uniporters and Anion Antiporters *Curr Opin Cell Biol*. **3**, 702-709
78. Simpson, I. A., Dwyer, D., Malide, D., Moley, K. H., Travis, A., and Vannucci, S. J. (2008) The Facilitative Glucose Transporter Glut3: 20 Years of Distinction *Am J Physiol Endocrinol Metab*. **295**, E242-253
79. Haney, P. M., Levy, M. A., Strube, M. S., and Mueckler, M. (1995) Insulin-Sensitive Targeting of the Glut4 Glucose Transporter in L6 Myoblasts Is Conferred by Its CooH-Terminal Cytoplasmic Tail *J Cell Biol*. **129**, 641-658
80. Shewan, A. M., Marsh, B. J., Melvin, D. R., Martin, S., Gould, G. W., and James, D. E. (2000) The Cytosolic C-Terminus of the Glucose Transporter Glut4 Contains an Acidic Cluster Endosomal Targeting Motif Distal to the Dilucine Signal *Biochem J*. **350**, 99-107

81. Augustin, R., Carayannopoulos, M. O., Dowd, L. O., Phay, J. E., Moley, J. F., and Moley, K. H. (2004) Identification and Characterization of Human Glucose Transporter-Like Protein-9 (Glut9): Alternative Splicing Alters Trafficking *J Biol Chem.* **279**, 16229-16236
82. Burant, C. F., Takeda, J., Brot-Laroche, E., Bell, G. I., and Davidson, N. O. (1992) Fructose Transporter in Human Spermatozoa and Small Intestine Is Glut5 *J Biol Chem.* **267**, 14523-14526
83. Cheeseman, C. (2008) Glut7: A New Intestinal Facilitated Hexose Transporter *Am J Physiol Endocrinol Metab.* **295**, E238-241
84. Doege, H., Bocianski, A., Scheepers, A., Axer, H., Eckel, J., Joost, H. G., and Schurmann, A. (2001) Characterization of Human Glucose Transporter (Glut) 11 (Encoded by Slc2a11), a Novel Sugar-Transport Facilitator Specifically Expressed in Heart and Skeletal Muscle *Biochem J.* **359**, 443-449
85. Li, Q., Manolescu, A., Ritzel, M., Yao, S., Slugoski, M., Young, J. D., Chen, X. Z., and Cheeseman, C. I. (2004) Cloning and Functional Characterization of the Human Glut7 Isoform Slc2a7 from the Small Intestine *Am J Physiol Gastrointest Liver Physiol.* **287**, G236-242
86. Darakhshan, F., Hajduch, E., Kristiansen, S., Richter, E. A., and Hundal, H. S. (1998) Biochemical and Functional Characterization of the Glut5 Fructose Transporter in Rat Skeletal Muscle *Biochem J.* **336 (Pt 2)**, 361-366
87. Schurmann, A. (2008) Insight into the "Odd" Hexose Transporters Glut3, Glut5, and Glut7 *Am J Physiol Endocrinol Metab.* **295**, E225-226
88. Carayannopoulos, M. O., Schlein, A., Wyman, A., Chi, M., Keembiyehetty, C., and Moley, K. H. (2004) Glut9 Is Differentially Expressed and Targeted in the Preimplantation Embryo *Endocrinology.* **145**, 1435-1443
89. Doblado, M., and Moley, K. H. (2009) Facilitative Glucose Transporter 9, a Unique Hexose and Urate Transporter *Am J Physiol Endocrinol Metab.* **297**, E831-835
90. Matsuo, H., Chiba, T., Nagamori, S., Nakayama, A., Domoto, H., Phetdee, K., Wiriyasermkul, P., Kikuchi, Y., Oda, T., Nishiyama, J., Nakamura, T., Morimoto, Y., Kamakura, K., Sakurai, Y., Nonoyama, S., Kanai, Y., and Shinomiya, N. (2008) Mutations in Glucose Transporter 9 Gene Slc2a9 Cause Renal Hypouricemia *Amer J Hum Genet.* **83**, 744-751
91. Preitner, F., Bonny, O., Laverrière, A., Rotman, S., Firsov, D., Da Costa, A., Metref, S., and Thorens, B. (2009) Glut9 Is a Major Regulator of Urate Homeostasis and Its Genetic Inactivation Induces Hyperuricosuria and Urate Nephropathy *Proc Natl Acad Sci U S A.* **106**, 15501-15506
92. Caulfield, M. J., Munroe, P. B., O'Neill, D., Witkowska, K., Charchar, F. J., Doblado, M., Evans, S., Eyheramendy, S., Onipinla, A., Howard, P., Shaw-Hawkins, S., Dobson, R. J., Wallace, C., Newhouse, S. J., Brown, M., Connell, J. M., Dominiczak, A., Farrall, M., Lathrop, G. M., Samani, N. J., Kumari, M., Marmot, M., Brunner, E., Chambers, J., Elliott, P., Kooner, J., Laan, M., Org, E., Veldre, G., Viigimaa, M., Cappuccio, F. P., Ji, C., Iacone, R., Strazzullo, P.,

- Moley, K. H., and Cheeseman, C. (2008) Slc2a9 Is a High-Capacity Urate Transporter in Humans *PLoS Med.* **5**, e197
93. Wu, X., Li, W., Sharma, V., Godzik, A., and Freeze, H. H. (2002) Cloning and Characterization of Glucose Transporter 11, a Novel Sugar Transporter That Is Alternatively Spliced in Various Tissues *Mol Genet Metab.* **76**, 37-45
 94. Doege, H., Bocianski, A., Joost, H. G., and Schurmann, A. (2000) Activity and Genomic Organization of Human Glucose Transporter 9 (Glut9), (Glut6) a Novel Member of the Family of Sugar-Transport Facilitators Predominantly Expressed in Brain and Leucocytes *Biochem J.* **350 Pt 3**, 771-776
 95. Lisinski, I., Schurmann, A., Joost, H. G., Cushman, S. W., and Al-Hasani, H. (2001) Targeting of Glut6 (Formerly Glut9) and Glut8 in Rat Adipose Cells *Biochem J.* **358**, 517-522
 96. Ibberson, M., Uldry, M., and Thorens, B. (2000) Glutx1 (Glut8), a Novel Mammalian Glucose Transporter Expressed in the Central Nervous System and Insulin-Sensitive Tissues *J Biol Chem.* **275**, 4607-4612
 97. Doege, H., Schurmann, A., Bahrenberg, G., Brauers, A., and Joost, H. G. (2000) Glut8, a Novel Member of the Sugar Transport Facilitator Family with Glucose Transport Activity *J Biol Chem.* **275**, 16275-16280
 98. Carayannopoulos, M. O., Chi, M. M.-Y., Cui, Y., Pingsterhaus, J. M., McKnight, R. A., Mueckler, M., Devaskar, S. U., and Moley, K. H. (2000) Glut8 Is a Glucose Transporter Responsible for Insulin-Stimulated Glucose Uptake in the Blastocyst *Proc Natl Acad Sci U S A.* **97**, 7313-7318
 99. Schmidt, S., Joost, H.-G., and Schurmann, A. (2009) Glut8, the Enigmatic Intracellular Hexose Transporter *Am J Physiol Endocrinol Metab.* **296**, E614-618
 100. Widmer, M., Uldry, M., and Thorens, B. (2005) Glut8 Subcellular Localization and Absence of Translocation to the Plasma Membrane in Pc12 Cells and Hippocampal Neurons *Endocrinology.* **146**, 4727-4736
 101. McVie-Wylie, A. J., Lamson, D. R., and Chen, Y. T. (2001) Molecular Cloning of a Novel Member of the Glut Family of Transporters, Slc2a10 (Glut10), Localized on Chromosome 20q13.1: A Candidate Gene for Niddm Susceptibility *Genomics.* **72**, 113-117
 102. Dawson, P. A., Mychaleckyj, J. C., Fossey, S. C., Mihic, S. J., Craddock, A. L., and Bowden, D. W. (2001) Sequence and Functional Analysis of Glut10: A Glucose Transporter in the Type 2 Diabetes-Linked Region of Chromosome 20q12-13.1 *Mol Genet Metab.* **74**, 186-199
 103. Coucke, P. J., Willaert, A., Wessels, M. W., Callewaert, B., Zoppi, N., De Backer, J., Fox, J. E., Mancini, G. M. S., Kambouris, M., Gardella, R., Facchetti, F., Willems, P. J., Forsyth, R., Dietz, H. C., Barlati, S., Colombi, M., Loeyes, B., and De Paepe, A. (2006) Mutations in the Facilitative Glucose Transporter Glut10 Alter Angiogenesis and Cause Arterial Tortuosity Syndrome *Nat Genet.* **38**, 452-457
 104. Rogers, S., Chandler, J. D., Clarke, A. L., Petrou, S., and Best, J. D. (2003) Glucose Transporter Glut12-Functional Characterization in *Xenopus Laevis* Oocytes *Biochem Biophys Res Commun.* **308**, 422-426

105. Rogers, S., Macheda, M. L., Docherty, S. E., Carty, M. D., Henderson, M. A., Soeller, W. C., Gibbs, E. M., James, D. E., and Best, J. D. (2002) Identification of a Novel Glucose Transporter-Like Protein---Glut-12 *Am J Physiol Endocrinol Metab.* **282**, E733-738
106. Stuart, C. A., Howell, M. E. A., Zhang, Y., and Yin, D. (2009) Insulin-Stimulated Translocation of Glucose Transporter (Glut) 12 Parallels That of Glut4 in Normal Muscle *J Clin Endocrinol Metab.* **94**, 3535-3542
107. Wilson-O'Brien, A. L., DeHaan, C. L., and Rogers, S. (2008) Mitogen-Stimulated and Rapamycin-Sensitive Glucose Transporter 12 Targeting and Functional Glucose Transport in Renal Epithelial Cells *Endocrinology.* **149**, 917-924
108. Katz, E. B., Stenbit, A. E., Hatton, K., DePinhot, R., and Charron, M. J. (1995) Cardiac and Adipose Tissue Abnormalities but Not Diabetes in Mice Deficient in Glut4 *Nature.* **377**, 151-155
109. Uldry, M., Ibberson, M., Horisberger, J. D., Chatton, J. Y., Riederer, B. M., and Thorens, B. (2001) Identification of a Mammalian H(+)-Myo-Inositol Symporter Expressed Predominantly in the Brain *EMBO J.* **20**, 4467-4477
110. Gorga, F. R., Baldwin, S. A., and Lienhard, G. E. (1979) The Monosaccharide Transporter from Human Erythrocytes Is Heterogeneously Glycosylated *Biochem Biophys Res Commun.* **91**, 955-961
111. Asano, T., Katagiri, H., Takata, K., Lin, J. L., Ishihara, H., Inukai, K., Tsukuda, K., Kikuchi, M., Hirano, H., and Yazaki, Y. (1991) The Role of N-Glycosylation of Glut1 for Glucose Transport Activity *J Biol Chem.* **266**, 24632-24636
112. Fry, D. C., Kuby, S. A., and Mildvan, A. S. (1986) Atp-Binding Site of Adenylate Kinase: Mechanistic Implications of Its Homology with Ras-Encoded P21, F1-Atpase, and Other Nucleotide-Binding Proteins *Proc Natl Acad Sci U S A.* **83**, 907-911
113. Levine, K. B., Cloherty, E. K., Fidyk, N. J., and Carruthers, A. (1998) Structural and Physiologic Determinants of Human Erythrocyte Sugar Transport Regulation by Adenosine Triphosphate *Biochemistry.* **37**, 12221-12232
114. Levine, K. B., Hamill, S., Cloherty, E. K., and Carruthers, A. (2001) Alanine Scanning Mutagenesis of the Human Erythrocyte Glucose Transporter Putative Atp Binding Domain *Blood Cells Mol Dis.* **27**, 139-142
115. Helgerson, A. L., and Carruthers, A. (1989) The Human Erythrocyte Sugar Transporter Is Also a Nucleotide Binding Protein *Biochemistry.* **28**, 8337-8346
116. Helgerson, A. L., Hebert, D. N., Naderi, S., and Carruthers, A. (1989) Characterization of Two Independent Modes of Action of Atp on Human Erythrocyte Sugar Transport *Biochemistry.* **28**, 6410-6417
117. Heard, K. S., Fidyk, N., and Carruthers, A. (2000) Atp-Dependent Substrate Occlusion by the Human Erythrocyte Sugar Transporter *Biochemistry.* **39**, 3005-3014
118. Oka, Y., Asano, T., Shibasaki, Y., Lin, J. L., Tsukuda, K., Katagiri, H., Akanuma, Y., and Takaku, F. (1990) C-Terminal Truncated Glucose Transporter Is Locked into an Inward-Facing Form without Transport Activity *Nature.* **345**, 550-553

119. Alvarez, J., Lee, D. C., Baldwin, S. A., and Chapman, D. (1987) Fourier Transform Infrared Spectroscopic Study of the Structure and Conformational Changes of the Human Erythrocyte Glucose Transporter *J Biol Chem.* **262**, 3502-3509
120. Chin, J. J., Jung, E. K., Chen, V., and Jung, C. Y. (1987) Structural Basis of Human Erythrocyte Glucose Transporter Function in Proteoliposome Vesicles: Circular Dichroism Measurements *Proc Natl Acad Sci U S A.* **84**, 4113-4116
121. Chin, J. J., Jung, E. K., and Jung, C. Y. (1986) Structural Basis of Human Erythrocyte Glucose Transporter Function in Reconstituted Vesicles *J Biol Chem.* **261**, 7101-7104
122. Pawagi, A. B., and Deber, C. M. (1987) D-Glucose Binding Increases Secondary Structure of Human Erythrocyte Monosaccharide Transport Protein *Biochem Biophys Res Commun.* **145**, 1087-1091
123. Blodgett, D. M., Graybill, C., and Carruthers, A. (2008) Analysis of Glucose Transporter Topology and Structural Dynamics *J Biol Chem.* **283**, 36416-36424
124. Mueckler, M., and Makepeace, C. (2006) Transmembrane Segment 12 of the Glut1 Glucose Transporter Is an Outer Helix and Is Not Directly Involved in the Transport Mechanism *J Biol Chem.* **281**, 36993-36998
125. Clark, A. E., and Holman, G. D. (1990) Exofacial Photolabelling of the Human Erythrocyte Glucose Transporter with an Azitri-fluoroethylbenzoyl-Substituted Bismannose *Biochem J.* **269**, 615-622
126. Holyoake, J., Caulfeild, V., Baldwin, S. A., and Sansom, M. S. P. (2006) Modeling, Docking, and Simulation of the Major Facilitator Superfamily *Biophys J.* **91**, L84-L86
127. Maiden, M. C., Davis, E. O., Baldwin, S. A., Moore, D. C., and Henderson, P. J. (1987) Mammalian and Bacterial Sugar Transport Proteins Are Homologous *Nature.* **325**, 641-643
128. Cope, D. L., Holman, G. D., Baldwin, S. A., and Wolstenholme, A. J. (1994) Domain Assembly of the Glut1 Glucose Transporter *Biochem J.* **300** (Pt 2), 291-294
129. Helgerson, A. L., and Carruthers, A. (1987) Equilibrium Ligand Binding to the Human Erythrocyte Sugar Transporter. Evidence for Two Sugar-Binding Sites Per Carrier *J Biol Chem.* **262**, 5464-5475
130. Kasahara, M., and Hinkle, P. C. (1977) Reconstitution and Purification of the D-Glucose Transporter from Human Erythrocytes *J Biol Chem.* **252**, 7384-7390
131. Hebert, D. N., and Carruthers, A. (1991) Cholate-Solubilized Erythrocyte Glucose Transporters Exist as a Mixture of Homodimers and Homotetramers *Biochemistry.* **30**, 4654-4658
132. Pessino, A., Hebert, D. N., Woon, C. W., Harrison, S. A., Clancy, B. M., Buxton, J. M., Carruthers, A., and Czech, M. P. (1991) Evidence That Functional Erythrocyte-Type Glucose Transporters Are Oligomers *J Biol Chem.* **266**, 20213-20217
133. Graybill, C., van Hoek, A. N., Desai, D., Carruthers, A. M., and Carruthers, A. (2006) Ultrastructure of Human Erythrocyte Glut1 *Biochemistry.* **45**, 8096-8107

134. Carruthers, A., and Melchior, D. L. (1985) Transport of Alpha- and Beta-D-Glucose by the Intact Human Red Cell *Biochemistry*. **24**, 4244-4250
135. Leitch, J. M., and Carruthers, A. (2009) Alpha- and Beta-Monosaccharide Transport in Human Erythrocytes *Am J Physiol Cell Physiol*. **296**, C151-161
136. Bachelard, H. S. (1972) Deoxyglucose and Brain Glycolysis *Biochem J*. **127**, 83P
137. Baker, G. F., Basketter, D. A., and Widdas, W. F. (1978) Asymmetry of the Hexose Transfer System in Human Erythrocytes. Experiments with Non-Transportable Inhibitors *J Physiol*. **278**, 377-388
138. Bloch, R. (1973) Inhibition of Glucose Transport in the Human Erythrocyte by Cytochalasin B *Biochemistry*. **12**, 4799-4801
139. Basketter, D. A., and Widdas, W. F. (1978) Asymmetry of the Hexose Transfer System in Human Erythrocytes. Comparison of the Effects of Cytochalasin B, Phloretin and Maltose as Competitive Inhibitors *J Physiol*. **278**, 389-401
140. Sergeant, S., and Kim, H. D. (1985) Inhibition of 3-O-Methylglucose Transport in Human Erythrocytes by Forskolin *J Biol Chem*. **260**, 14677-14682
141. Lieb, W. R., and Stein, W. D. (1974) Testing and Characterizing the Simple Carrier *Biochim Biophys Acta*. **373**, 178-196
142. Helgerson, A. L., and Carruthers, A. (1989) Analysis of Protein-Mediated 3-O-Methylglucose Transport in Rat Erythrocytes: Rejection of the Alternating Conformation Carrier Model for Sugar Transport *Biochemistry*. **28**, 4580-4594
143. Baker, G. F., and Widdas, W. F. (1973) The Asymmetry of the Facilitated Transfer System for Hexoses in Human Red Cells and the Simple Kinetics of a Two Component Model *J Physiol*. **231**, 143-165
144. Hamill, S., Cloherty, E. K., and Carruthers, A. (1999) The Human Erythrocyte Sugar Transporter Presents Two Sugar Import Sites *Biochemistry*. **38**, 16974-16983
145. Sultzman, L. A., and Carruthers, A. (1999) Stop-Flow Analysis of Cooperative Interactions between Glut1 Sugar Import and Export Sites *Biochemistry*. **38**, 6640-6650
146. Levine, K. B., Robichaud, T. K., Hamill, S., Sultzman, L. A., and Carruthers, A. (2005) Properties of the Human Erythrocyte Glucose Transport Protein Are Determined by Cellular Context *Biochemistry*. **44**, 5606-5616
147. Cloherty, E. K., Sultzman, L. A., Zottola, R. J., and Carruthers, A. (1995) Net Sugar Transport Is a Multistep Process. Evidence for Cytosolic Sugar Binding Sites in Erythrocytes *Biochemistry*. **34**, 15395-15406
148. Blodgett, D. M., and Carruthers, A. (2004) Conventional Transport Assays Underestimate Sugar Transport Rates in Human Red Cells *Blood Cells Mol Dis*. **32**, 401-407
149. Blodgett, D. M., and Carruthers, A. (2005) Quench-Flow Analysis Reveals Multiple Phases of Glut1-Mediated Sugar Transport *Biochemistry*. **44**, 2650-2660
150. Cloherty, E. K., Diamond, D. L., Heard, K. S., and Carruthers, A. (1996) Regulation of Glut1-Mediated Sugar Transport by an Antiport/Uniport Switch Mechanism *Biochemistry*. **35**, 13231-13239

151. Carruthers, A. (1986) Atp Regulation of the Human Red Cell Sugar Transporter *J Biol Chem.* **261**, 11028-11037
152. Carruthers, A. (1986) Anomalous Asymmetric Kinetics of Human Red Cell Hexose Transfer: Role of Cytosolic Adenosine 5'-Triphosphate *Biochemistry.* **25**, 3592-3602
153. Hebert, D. N., and Carruthers, A. (1986) Direct Evidence for Atp Modulation of Sugar Transport in Human Erythrocyte Ghosts *J Biol Chem.* **261**, 10093-10099
154. Cloherty, E. K., Levine, K. B., Graybill, C., and Carruthers, A. (2002) Cooperative Nucleotide Binding to the Human Erythrocyte Sugar Transporter *Biochemistry.* **41**, 12639-12651
155. Blodgett, D. M., De Zutter, J. K., Levine, K. B., Karim, P., and Carruthers, A. (2007) Structural Basis of Glut1 Inhibition by Cytoplasmic Atp *J Gen Physiol.* **130**, 157-168
156. Kumar, A., Xiao, Y.-P., Laipis, P. J., Fletcher, B. S., and Frost, S. C. (2004) Glucose Deprivation Enhances Targeting of Glut1 to Lipid Rafts in 3t3-L1 Adipocytes *Am J Physiol Endocrinol Metab.* **286**, E568-576
157. Montel-Hagen, A., Kinet, S., Manel, N., Mongellaz, C., Prohaska, R., Battini, J.-L., Delaunay, J., Sitbon, M., and Taylor, N. (2008) Erythrocyte Glut1 Triggers Dehydroascorbic Acid Uptake in Mammals Unable to Synthesize Vitamin C *Cell.* **132**, 1039-1048
158. Honkanen, R. A., McBath, H., Kushmerick, C., Callender, G. E., Scarlata, S. F., Fenstermacher, J. D., and Haspel, H. C. (1995) Barbiturates Inhibit Hexose Transport in Cultured Mammalian Cells and Human Erythrocytes and Interact Directly with Purified Glut-1 *Biochemistry.* **34**, 535-544
159. Haspel, H. C., Stephenson, K. N., Davies-Hill, T., El-Barbary, A., Lobo, J. F., Croxen, R. L., Mougrabi, W., Koehler-Stec, E. M., Fenstermacher, J. D., and Simpson, I. A. (1999) Effects of Barbiturates on Facilitative Glucose Transporters Are Pharmacologically Specific and Isoform Selective *J Membr Biol.* **169**, 45-53
160. Ducluzeau, P. H., Fletcher, L. M., Vidal, H., Laville, M., and Tavaré, J. M. (2002) Molecular Mechanisms of Insulin-Stimulated Glucose Uptake in Adipocytes *Diabetes Metab.* **28**, 85-92
161. Young, A. T., Dahl, J., Hausdorff, S. F., Bauer, P. H., Birnbaum, M. J., and Benjamin, T. L. (1995) Phosphatidylinositol 3-Kinase Binding to Polyoma Virus Middle Tumor Antigen Mediates Elevation of Glucose Transport by Increasing Translocation of the Glut1 Transporter *Proc Natl Acad Sci U S A.* **92**, 11613-11617
162. Egert, S., Nguyen, N., and Schwaiger, M. (1999) Myocardial Glucose Transporter Glut1: Translocation Induced by Insulin and Ischemia *J Mol Cell Cardiol.* **31**, 1337-1344
163. Wang, L., Hayashi, H., and Ebina, Y. (1999) Transient Effect of Platelet-Derived Growth Factor on Glut4 Translocation in 3t3-L1 Adipocytes *J Biol Chem.* **274**, 19246-19253

164. Sone, H., Deo, B. K., and Kumagai, A. K. (2000) Enhancement of Glucose Transport by Vascular Endothelial Growth Factor in Retinal Endothelial Cells *Invest Ophthalmol Vis Sci.* **41**, 1876-1884
165. Moyers, J. S., Shiyanova, T. L., Mehrbod, F., Dunbar, J. D., Noblitt, T. W., Otto, K. A., Reifel-Miller, A., and Kharitonov, A. (2007) Molecular Determinants of Fgf-21 Activity—Synergy and Cross-Talk with Ppar γ Signaling *J Cell Physiol.* **210**, 1-6
166. Heo, J. S., and Han, H. J. (2006) Pkc and Mapks Pathways Mediate Egf-Induced Stimulation of 2-Deoxyglucose Uptake in Mouse Embryonic Stem Cells *Cell Physiol Biochem.* **17**, 145-158
167. Phillips, T., Ferraz, I., Bell, S., Clegg, P. D., Carter, S. D., and Mobasher, A. (2005) Differential Regulation of the Glut1 and Glut3 Glucose Transporters by Growth Factors and Pro-Inflammatory Cytokines in Equine Articular Chondrocytes *Vet J.* **169**, 216-222
168. Furuta, E., Okuda, H., Kobayashi, A., and Watabe, K. (2010) Metabolic Genes in Cancer: Their Roles in Tumor Progression and Clinical Implications *Biochim Biophys Acta.* **1805**, 141-152
169. Ayala, F. R. R., Rocha, R. M., Carvalho, K. C., Carvalho, A. L., da Cunha, I. W., Lourenço, S. V., and Soares, F. A. (2010) Glut1 and Glut3 as Potential Prognostic Markers for Oral Squamous Cell Carcinoma *Molecules* **15**, 2374-2387
170. Brown, R. S., Goodman, T. M., Zasadny, K. R., Greenson, J. K., and Wahl, R. L. (2002) Expression of Hexokinase II and Glut-1 in Untreated Human Breast Cancer *Nucl Med Biol.* **29**, 443-453
171. Cantuaria, G., Fagotti, A., Ferrandina, G., Magalhaes, A., Nadji, M., Angioli, R., Penalver, M., Mancuso, S., and Scambia, G. (2001) Glut-1 Expression in Ovarian Carcinoma *Cancer.* **92**, 1144-1150
172. Haber, R. S., Rathan, A., Weiser, K. R., Pritsker, A., Itzkowitz, S. H., Bodian, C., Slater, G., Weiss, A., and Burstein, D. E. (1998) Glut1 Glucose Transporter Expression in Colorectal Carcinoma *Cancer.* **83**, 34-40
173. Nagase, Y., Takata, K., Moriyama, N., Aso, Y., Murakami, T., and Hirano, H. (1995) Investigative Urology: Immunohistochemical Localization of Glucose Transporters in Human Renal Cell Carcinoma *J Urol.* **153**, 798-801
174. Nishioka, T., Oda, Y., Seino, Y., Yamamoto, T., Inagaki, N., Yano, H., Imura, H., Shigemoto, R., and Kikuchi, H. (1992) Distribution of the Glucose Transporters in Human Brain Tumors *Cancer Res.* **52**, 3972-3979
175. Ogawa, J. i., Inoue, H., and Koide, S. (1997) Glucose-Transporter-Type-I-Gene Amplification Correlates with Sialyl-Lewis-X Synthesis and Proliferation in Lung Cancer *Int J Cancer.* **74**, 189-192
176. Ganapathy, V., Thangaraju, M., and Prasad, P. D. (2009) Nutrient Transporters in Cancer: Relevance to Warburg Hypothesis and Beyond *Pharmacol Ther.* **121**, 29-40
177. Chen, C., Pore, N., Behrooz, A., Ismail-Beigi, F., and Maity, A. (2001) Regulation of Glut1 Mrna by Hypoxia-Inducible Factor-1. Interaction between H-Ras and Hypoxia *J Biol Chem.* **276**, 9519-9525

178. Boado, R. J., and Pardridge, W. M. (2002) Glucose Deprivation and Hypoxia Increase the Expression of the Glut1 Glucose Transporter Via a Specific Mrna <I>Cis</I>-Acting Regulatory Element *J Neurochem.* **80**, 552-554
179. Marsin, A.-S., Bouzin, C., Bertrand, L., and Hue, L. (2002) The Stimulation of Glycolysis by Hypoxia in Activated Monocytes Is Mediated by Amp-Activated Protein Kinase and Inducible 6-Phosphofructo-2-Kinase *J Biol Chem.* **277**:, 30778-30783.
180. Hardie, D. G., Scott, J. W., Pan, D. A., and Hudson, E. R. (2003) Management of Cellular Energy by the Amp-Activated Protein Kinase System *FEBS Lett.* **546**, 113-120
181. Hardie, D. G. (2004) Amp-Activated Protein Kinase: A Master Switch in Glucose and Lipid Metabolism *Rev Endocr Metab Disord.* **5**, 119-125
182. Barros, L. F., Barnes, K., Ingram, J. C., Castro, J., Porras, O. H., and Baldwin, S. A. (2001) Hyperosmotic Shock Induces Both Activation and Translocation of Glucose Transporters in Mammalian Cells *Pflugers Arch.* **442**, 614-621
183. Haworth, R. A., and Berkoff, H. A. (1986) The Control of Sugar Uptake by Metabolic Demand in Isolated Adult Rat Heart Cells *Circ Res.* **58**, 157-165
184. Shetty, M., Loeb, J. N., Vikstrom, K., and Ismail-Beigi, F. (1993) Rapid Activation of Glut-1 Glucose Transporter Following Inhibition of Oxidative Phosphorylation in Clone 9 Cells *J Biol Chem.* **268**, 17225-17232
185. Simpson, I. A., Vannucci, S. J., DeJoseph, M. R., and Hawkins, R. A. (2001) Glucose Transporter Asymmetries in the Bovine Blood-Brain Barrier *J Biol Chem.* **276**, 12725-12729
186. Farrell, C. L., and Pardridge, W. M. (1991) Blood-Brain Barrier Glucose Transporter Is Asymmetrically Distributed on Brain Capillary Endothelial Luminal and Abluminal Membranes: An Electron Microscopic Immunogold Study *Proc Natl Acad Sci U S A.* **88**, 5779-5783
187. Cura, A. J., and Carruthers, A. (2010) Acute Modulation of Sugar Transport in Brain Capillary Endothelial Cell Cultures During Activation of the Metabolic Stress Pathway *J Biol Chem.* **285**, 15430-15439
188. Klepper, J., and Voit, T. (2002) Facilitated Glucose Transporter Protein Type 1 (Glut1) Deficiency Syndrome: Impaired Glucose Transport into Brain - a Review *Eur J Pediatr.* **161**, 295-304
189. Gordon, N., and Newton, R. W. (2003) Glucose Transporter Type1 (Glut-1) Deficiency *Brain Dev.* **25**, 477-480
190. Wang, D., Kranz-Eble, P., and De Vivo, D. C. (2000) Mutational Analysis of Glut1 (Slc2a1) in Glut-1 Deficiency Syndrome *Human Mutation* **16**, 224-231
191. Klepper, J., Juan Carlos, V., and Darryl, C. d. V. (1998) Deficient Transport of Dehydroascorbic Acid in the Glucose Transporter Protein Syndrome *Ann Neurol.* **44**, 286-287
192. Wang, D., Pascual, J. M., Yang, H., Engelstad, K., Jhung, S., Sun, R. P., and De Vivo, D. C. (2005) Glut-1 Deficiency Syndrome: Clinical, Genetic, and Therapeutic Aspects *Ann Neurol.* **57**, 111-118

193. Klepper, J., Diefenbach, S., Kohlschütter, A., and Voit, T. (2004) Effects of the Ketogenic Diet in the Glucose Transporter 1 Deficiency Syndrome *Prostaglandins Leukot Essent Fatty Acids*. **70**, 321-327
194. Harik, S. I., Behmand, R. A., and LaManna, J. C. (1994) Hypoxia Increases Glucose Transport at Blood-Brain Barrier in Rats *J Appl Physiol*. **77**, 896-901
195. Loike, J. D., Cao, L., Brett, J., Ogawa, S., Silverstein, S. C., and Stern, D. (1992) Hypoxia Induces Glucose Transporter Expression in Endothelial Cells *Am J Physiol Cell Physiol*. **263**, C326-333
196. Kumagai, A. K., Kang, Y. S., Boado, R. J., and Pardridge, W. M. (1995) Upregulation of Blood-Brain Barrier Glut1 Glucose Transporter Protein and Mrna in Experimental Chronic Hypoglycemia *Diabetes*. **44**, 1399-1404
197. Simpson, I. A., Appel, N. M., Hokari, M., Oki, J., Holman, G. D., Maher, F., Koehler-Stec, E. M., Vannucci, S. J., and Smith, Q. R. (1999) Blood-Brain Barrier Glucose Transporter: Effects of Hypo- and Hyperglycemia Revisited *J Neurochem*. **72**, 238-247
198. Cornford, E. M., Hyman, S., Cornford, M. E., and Caron, M. J. (1996) Glut1 Glucose Transporter Activity in Human Brain Injury *J Neurotrauma*. **13**, 523-536
199. Vannucci, S. J., Reinhart, R., Maher, F., Bondy, C. A., Lee, W.-H., Vannucci, R. C., and Simpson, I. A. (1998) Alterations in Glut1 and Glut3 Glucose Transporter Gene Expression Following Unilateral Hypoxia-Ischemia in the Immature Rat Brain *Brain Res Dev Brain Res*. **107**, 255-264
200. Cornford, E. M., Nguyen, E. V., and Landaw, E. M. (2000) Acute Upregulation of Blood-Brain Barrier Glucose Transporter Activity in Seizures *Am J Physiol Heart Circ Physiol*. **279**, H1346-1354
201. Cornford, E. M., Hyman, S., Cornford, M. E., Landaw, E. M., and Delgado-Escueta, A. V. (1998) Interictal Seizure Resections Show Two Configurations of Endothelial Glut1 Glucose Transporter in the Human Blood-Brain Barrier *J Cereb Blood Flow Metab*. **18**, 26-42
202. Marsin, A. S., Bertrand, L., Rider, M. H., Deprez, J., Beauloye, C., Vincent, M. F., Van den Berghe, G., Carling, D., and Hue, L. (2000) Phosphorylation and Activation of Heart Pfk-2 by Ampk Has a Role in the Stimulation of Glycolysis During Ischaemia *Curr Biol*. **10**, 1247-1255
203. Mu, J., Brozinick Jr, J. T., Valladares, O., Bucan, M., and Birnbaum, M. J. (2001) A Role for Amp-Activated Protein Kinase in Contraction- and Hypoxia-Regulated Glucose Transport in Skeletal Muscle *Mol Cell*. **7**, 1085-1094
204. Gumbleton, M., and Audus, K. L. (2001) Progress and Limitations in the Use of in Vitro Cell Cultures to Serve as a Permeability Screen for the Blood-Brain Barrier *J Pharm Sci*. **90**, 1681-1698
205. Omid, Y., Campbell, L., Barar, J., Connell, D., Akhtar, S., and Gumbleton, M. (2003) Evaluation of the Immortalised Mouse Brain Capillary Endothelial Cell Line, B.End3, as an in Vitro Blood-Brain Barrier Model for Drug Uptake and Transport Studies *Brain Res*. **990**, 95-112
206. Souza-Menezes, J., Morales, M. M., Tukaye, D. N., Guggino, S. E., and Guggino, W. B. (2007) Absence of Clc5 in Knockout Mice Leads to Glycosuria, Impaired

- Renal Glucose Handling and Low Proximal Tubule Glut2 Protein Expression *Cell Physiol Biochem.* **20**, 455-464
207. Ohkawa, Y., Marfella, C. G., and Imbalzano, A. N. (2006) Skeletal Muscle Specification by Myogenin and Mef2d Via the Swi/Snf Atpase Brg1 *EMBO J.* **25**, 490-501
 208. Cloherty, E. K., Heard, K. S., and Carruthers, A. (1996) Human Erythrocyte Sugar Transport Is Incompatible with Available Carrier Models *Biochemistry.* **35**, 10411-10421
 209. Boado, R. J., Tsukamoto, H., and Pardridge, W. M. (1996) Evidence for Translational Control Elements within the 5'-Untranslated Region of Glut1 Glucose Transporter Mrna *J Neurochem.* **67**, 1335-1343
 210. Flier, J. S., Mueckler, M., McCall, A. L., and Lodish, H. F. (1987) Distribution of Glucose Transporter Messenger Rna Transcripts in Tissues of Rat and Man *J Clin Invest.* **79**, 657-661
 211. Gerhart, D. Z., LeVasseur, R. J., Broderius, M. A., and Drewes, L. R. (1989) Glucose Transporter Localization in Brain Using Light and Electron Immunocytochemistry *J Neurosci Res.* **22**, 464-472
 212. Kalaria, R. N., Gravina, S. A., Schmidley, J. W., Perry, G., and Harik, S. I. (1988) The Glucose Transporter of the Human Brain and Blood-Brain Barrier *Ann Neurol.* **24**, 757-764
 213. McCall, A. L., Fixman, L. B., Fleming, N., Tornheim, K., Chick, W., and Ruderman, N. B. (1986) Chronic Hypoglycemia Increases Brain Glucose Transport *Am J Physiol Endocrinol Metab.* **251**, E442-447
 214. Levine, K. B., Cloherty, E. K., Hamill, S., and Carruthers, A. (2002) Molecular Determinants of Sugar Transport Regulation by Atp *Biochemistry.* **41**, 12629-12638
 215. Boado, R. J. (1995) Brain-Derived Peptides Regulate the Steady State Levels and Increase Stability of the Blood-Brain Barrier Glut1 Glucose Transporter Mrna *Neurosci Lett.* **197**, 179-182
 216. Boado, R. J., Wu, D., and Windisch, M. (1999) In Vivo Upregulation of the Blood-Brain Barrier Glut1 Glucose Transporter by Brain-Derived Peptides *Neurosci Res.* **34**, 217-224
 217. Cornford, E. M., Hyman, S., and Pardridge, W. M. (1993) An Electron Microscopic Immunogold Analysis of Developmental up-Regulation of the Blood-Brain Barrier Glut1 Glucose Transporter *J Cereb Blood Flow Metab.* **13**, 841-854
 218. Corton, J. M., Gillespie, J. G., Hawley, S. A., and Hardie, D. G. (1995) 5-Aminoimidazole-4-Carboxamide Ribonucleoside. A Specific Method for Activating Amp-Activated Protein Kinase in Intact Cells? *Eur J Biochem.* **229**, 558-565
 219. Hayashi, T., Wojtaszewski, J. F., and Goodyear, L. J. (1997) Exercise Regulation of Glucose Transport in Skeletal Muscle *Am J Physiol.* **273**, E1039-1051
 220. Simons, T. J. (1983) Characterization of Sugar Transport in the Pigeon Red Blood Cell *J Physiol.* **338**, 477-499

221. Coven, D. L., Hu, X., Cong, L., Bergeron, R., Shulman, G. I., Hardie, D. G., and Young, L. H. (2003) Physiological Role of Amp-Activated Protein Kinase in the Heart: Graded Activation During Exercise *Am J Physiol Endocrinol Metab.* **285**, E629-636
222. Barnes, K., Ingram, J. C., Porras, O. H., Barros, L. F., Hudson, E. R., Fryer, L. G., Fougelle, F., Carling, D., Hardie, D. G., and Baldwin, S. A. (2002) Activation of Glut1 by Metabolic and Osmotic Stress: Potential Involvement of Amp-Activated Protein Kinase (Ampk) *J Cell Sci.* **115**, 2433-2442
223. Vannucci, S. J., Maher, F., and Simpson, I. A. (1997) Glucose Transporter Proteins in Brain: Delivery of Glucose to Neurons and Glia *Glia.* **21**, 2-21
224. Kumagai, A. K., Dwyer, K. J., and Pardridge, W. M. (1994) Differential Glycosylation of the Glut1 Glucose Transporter in Brain Capillaries and Choroid Plexus *Biochim Biophys Acta.* **1193**, 24-30
225. Eisenberg, E., and Greene, L. E. (2007) Multiple Roles of Auxilin and Hsc70 in Clathrin-Mediated Endocytosis *Traffic.* **8**, 640-646
226. Bandorowicz-Pikula, J., and Pikula, S. (1998) Annexins and Atp in Membrane Traffic: A Comparison with Membrane Fusion Machinery *Acta Biochim Pol.* **45**, 721-733
227. Endow, S. A. (2003) Kinesin Motors as Molecular Machines *BioEssays.* **25**, 1212-1219
228. Dick, A. P., Harik, S. I., Klip, A., and Walker, D. M. (1984) Identification and Characterization of the Glucose Transporter of the Blood-Brain Barrier by Cytochalasin B Binding and Immunological Reactivity *Proc Natl Acad Sci U S A.* **81**, 7233-7237
229. Boado, R. J., and Pardridge, W. M. (1993) Glucose Deprivation Causes Posttranscriptional Enhancement of Brain Capillary Endothelial Glucose Transporter Gene Expression Via Glut1 Mrna Stabilization *J Neurochem.* **60**, 2290-2296
230. Fujii, N., Hayashi, T., Hirshman, M. F., Smith, J. T., Habinowski, S. A., Kaijser, L., Mu, J., Ljungqvist, O., Birnbaum, M. J., Witters, L. A., Thorell, A., and Goodyear, L. J. (2000) Exercise Induces Isoform-Specific Increase in 5'amp-Activated Protein Kinase Activity in Human Skeletal Muscle *Biochem Biophys Res Commun.* **273**, 1150-1155
231. Winder, W. W., and Hardie, D. G. (1996) Inactivation of Acetyl-Coa Carboxylase and Activation of Amp-Activated Protein Kinase in Muscle During Exercise *Am J Physiol Endocrinol Metab.* **270**, E299-304
232. Li, J., and McCullough, L. D. (2010) Effects of Amp-Activated Protein Kinase in Cerebral Ischemia *J Cereb Blood Flow Metab.* **30**, 480-492
233. Poels, J., Spasi, M. R., Callaerts, P., and Norga, K. K. (2009) Expanding Roles for Amp-Activated Protein Kinase in Neuronal Survival and Autophagy *BioEssays.* **31**, 944-952
234. Ronnett, G., V. , Ramamurthy, S., Kleman, A., M. , Landree, L., E. , and Aja, S. (2009) Ampk in the Brain: Its Roles in Energy Balance and Neuroprotection *J Neurochem.* **109**, 17-23

235. Fisslthaler, B., and Fleming, I. (2009) Activation and Signaling by the Amp-Activated Protein Kinase in Endothelial Cells *Circ Res.* **105**, 114-127
236. Corton, J. M., Gillespie, J. G., and Hardie, D. G. (1994) Role of the Amp-Activated Protein Kinase in the Cellular Stress Response *Curr Biol.* **4**, 315-324
237. Abbud, W., Habinowski, S., Zhang, J.-Z., Kendrew, J., Elkairi, F. S., Kemp, B. E., Witters, L. A., and Ismail-Beigi, F. (2000) Stimulation of Amp-Activated Protein Kinase (Ampk) Is Associated with Enhancement of Glut1-Mediated Glucose Transport *Arch Biochem Biophys.* **380**, 347-352
238. Klip, A., Schertzer, J. D., Bilan, P. J., Thong, F., and Antonescu, C. (2009) Regulation of Glucose Transporter 4 Traffic by Energy Deprivation from Mitochondrial Compromise *Acta Physiol.* **196**, 27-35
239. Ha, J., Daniel, S., Broyles, S. S., and Kim, K. H. (1994) Critical Phosphorylation Sites for Acetyl-Coa Carboxylase Activity *J Biol Chem.* **269**, 22162-22168.
240. Zhou, G., Myers, R., Li, Y., Chen, Y., Shen, X., Fenyk-Melody, J., Wu, M., Ventre, J., Doebber, T., Fujii, N., Musi, N., Hirshman, M. F., Goodyear, L. J., and Moller, D. E. (2001) Role of Amp-Activated Protein Kinase in Mechanism of Metformin Action *J Clin Invest.* **108**, 1167-1174
241. Guigas, B., Sakamoto, K., Taleux, N., Reyna, S. M., Musi, N., Viollet, B., and Hue, L. (2009) Beyond Aica Riboside: In Search of New Specific Amp-Activated Protein Kinase Activators *IUBMB Life.* **61**, 18-26
242. Ramanathan, L., Sheth, P. R., Ogas, P., Xiao, L., and Le, H. V. (2010) Purification and Characterization of Truncated Human Ampk [Alpha]2[Beta]2[Gamma]3 Heterotrimer from Baculovirus-Infected Insect Cells *Protein Expr Purif.* **70**, 13-22
243. Cloherty, E. K., Hamill, S., Levine, K., and Carruthers, A. (2001) Sugar Transporter Regulation by Atp and Quaternary Structure *Blood Cells Mol Dis.* **27**, 102-107
244. Cloherty, E. K., Levine, K. B., and Carruthers, A. (2001) The Red Blood Cell Glucose Transporter Presents Multiple, Nucleotide-Sensitive Sugar Exit Sites *Biochemistry.* **40**, 15549-15561
245. Diamond, D. L., and Carruthers, A. (1993) Metabolic Control of Sugar Transport by Derepression of Cell Surface Glucose Transporters. An Insulin-Independent Recruitment-Independent Mechanism of Regulation *J Biol Chem* **268**, 6437-6444
246. Barnes, K., Ingram, J. C., Bennett, M. D. M., Stewart, G. W., and Baldwin, S. A. (2004) Methyl-Beta-Cyclodextrin Stimulates Glucose Uptake in Clone 9 Cells: A Possible Role for Lipid Rafts *Biochem J.* **378**, 343-351
247. Heerklotz, H. (2002) Triton Promotes Domain Formation in Lipid Raft Mixtures *Biophys J.* **83**, 2693-2701
248. Munro, S. (2003) Lipid Rafts: Elusive or Illusive? *Cell.* **115**, 377-388
249. Lochhead, P. A., Salt, I. P., Walker, K. S., Hardie, D. G., and Sutherland, C. (2000) 5-Aminoimidazole-4-Carboxamide Riboside Mimics the Effects of Insulin on the Expression of the 2 Key Gluconeogenic Genes Pepck and Glucose-6-Phosphatase *Diabetes.* **49**, 896-903

250. Zheng, D., MacLean, P. S., Pohnert, S. C., Knight, J. B., Olson, A. L., Winder, W. W., and Dohm, G. L. (2001) Regulation of Muscle Glut-4 Transcription by Amp-Activated Protein Kinase *J Appl Physiol.* **91**, 1073-1083
251. Young, M. E., Radda, G. K., and Leighton, B. (1996) Activation of Glycogen Phosphorylase and Glycogenolysis in Rat Skeletal Muscle by Aicar -- an Activator of Amp-Activated Protein Kinase *FEBS Letters.* **382**, 43-47
252. Dagher, Z., Ruderman, N., Tornheim, K., and Ido, Y. (1999) The Effect of Amp-Activated Protein Kinase and Its Activator Aicar on the Metabolism of Human Umbilical Vein Endothelial Cells *Biochem Biophys Res Comm.* **265**, 112-115
253. Gillespie, J. G., and Hardie, D. G. (1992) Phosphorylation and Inactivation of Hmg-Coa Reductase at the Amp-Activated Protein Kinase Site in Response to Fructose Treatment of Isolated Rat Hepatocytes *FEBS Letters.* **306**, 59-62
254. Fryer, L. G. D., Foufelle, F., Barnes, K., Baldwin, S. A., Woods, A., and Carling, D. (2002) Characterization of the Role of the Amp-Activated Protein Kinase in the Stimulation of Glucose Transport in Skeletal Muscle Cells *Biochem J.* **363**, 167-174
255. Bradbury, M. W. (1985) The Blood-Brain Barrier. Transport across the Cerebral Endothelium *Circ Res.* **57**, 213-222
256. Oldendorf, W. H. (1971) Brain Uptake of Radiolabeled Amino Acids, Amines, and Hexoses after Arterial Injection *Am J Physiol.* **221**, 1629-1639
257. Régina, A., Morchoisne, S., Borson, N. D., McCall, A. L., Drewes, L. R., and Roux, F. (2001) Factor(S) Released by Glucose-Deprived Astrocytes Enhance Glucose Transporter Expression and Activity in Rat Brain Endothelial Cells *Biochim Biophys Acta.* **1540**, 233-242
258. Raslova, K. (2010) An Update on the Treatment of Type 1 and Type 2 Diabetes Mellitus: Focus on Insulin Detemir, a Long-Acting Human Insulin Analog *Vasc Health Risk Manag.* **6**, 399-410
259. Mondazzi, L., and Arcelli, E. (2009) Glycemic Index in Sport Nutrition *J Am Coll Nutr.* **28**, 455S-463
260. Zarich, S. (2009) Potential of Glucose-Lowering Drugs to Reduce Cardiovascular Events *Curr Diab Rep.* **9**, 87-94
261. Ann Wilson, G., and Furman, B. L. (1982) Effects of Inhibitors of 5-Hydroxytryptamine Uptake on Plasma Glucose and Their Interaction with 5-Hydroxytryptophan in Producing Hypoglycaemia in Mice *Eur J Pharmacol.* **78**, 263-270
262. Semenza, G. L. (1999) Regulation of Mammalian O₂ Homeostasis by Hypoxia-Inducible Factor 1 *Annu Rev Cell Dev Biol.* **15**, 551-578
263. Yang, J., and Holman, G. D. (1993) Comparison of Glut4 and Glut1 Subcellular Trafficking in Basal and Insulin-Stimulated 3t3-L1 Cells *J Biol Chem.* **268**, 4600-4603
264. Fujishiro, M., Gotoh, Y., Katagiri, H., Sakoda, H., Ogihara, T., Anai, M., Onishi, Y., Ono, H., Abe, M., Shojima, N., Fukushima, Y., Kikuchi, M., Oka, Y., and Asano, T. (2003) Three Mitogen-Activated Protein Kinases Inhibit Insulin

- Signaling by Different Mechanisms in 3t3-L1 Adipocytes *Mol Endocrinol.* **17**, 487-497
265. Yamamoto, Y., Yoshimasa, Y., Koh, M., Suga, J., Masuzaki, H., Ogawa, Y., Hosoda, K., Nishimura, H., Watanabe, Y., Inoue, G., and Nakao, K. (2000) Constitutively Active Mitogen-Activated Protein Kinase Kinase Increases Glut1 Expression and Recruits Both Glut1 and Glut4 at the Cell Surface in 3t3-L1 Adipocytes *Diabetes.* **49**, 332-339
266. Wang, W., and Guan, K. L. (2009) Amp-Activated Protein Kinase and Cancer *Acta Physiol.* **196**, 55-63
267. Fazakerley, D. J., Holman, G. D., Marley, A., James, D. E., Stöckli, J., and Coster, A. C. F. (2010) Kinetic Evidence for Unique Regulation of Glut4 Trafficking by Insulin and Amp-Activated Protein Kinase Activators in L6 Myotubes *J Biol Chem.* **285**, 1653-1660
268. Wieman, H. L., Wofford, J. A., and Rathmell, J. C. (2007) Cytokine Stimulation Promotes Glucose Uptake Via Phosphatidylinositol-3 Kinase/Akt Regulation of Glut1 Activity and Trafficking *Mol Biol Cell.* **18**, 1437-1446
269. Dienel, G. A., and Cruz, N. F. (2003) Neighborly Interactions of Metabolically-Activated Astrocytes in Vivo *Neurochem Intl.* **43**, 339-354
270. Abbott, N. J. (2002) Astrocyte-Endothelial Interactions and Blood-Brain Barrier Permeability *J Anat.* **200**, 629-638
271. Hayashi, Y., Nomura, M., Yamagishi, S.-I., Harada, S.-I., Yamashita, J., and Yamamoto, H. (1997) Induction of Various Blood-Brain Barrier Properties in Non-Neural Endothelial Cells by Close Apposition to Co-Cultured Astrocytes *Glia.* **19**, 13-26
272. Kuchler-Bopp, S., Delaunoy, J. P., Artault, J. C., Zaepfel, M., and Dietrich, J. B. (1999) Astrocytes Induce Several Blood-Brain Barrier Properties in Non-Neural Endothelial Cells *Neuroreport.* **10**, 1347-1353